INVESTIGATION OF THE HEATING AND CURING RATE OF POLYMERIC MATERIALS WITH THERMAL ENERGY, CONTINUOUS AND PULSED MICROWAVE RADIATION

by

Esmaiel Jabbari

Thesis submitted to the faculty of the
Virginia Polytechnic Institute and State University
in partial fulfillment of the requirements for the degree of

MASTER OF SCIENCE

in

Chemistry

APPROVED:

Thomas C. Ward, Chairman

Jack D. Graybeal

Herve Marand

August, 1989

Blacksburg, Virginia

INVESTIGATION OF THE HEATING AND CURING RATE OF POLYMERIC MATERIALS WITH THERMAL ENERGY, CONTINUOUS AND PULSED MICROWAVE RADIATION

by

ESMAIEL JABBARI

Submitted to the Department of Chemistry
on June 28, 1989 in partial fulfillment of the requirements
for the degree of Master of Science in Chemistry

(ABSTRACT)

The purpose of this work was to study the heating and curing rate of polymers with continuous and pulsed microwave radiation and compare with conventional thermal energy. The heating rate of poly(ethylene glycol) and poly(propylene glycol) has been studied as a function of molecular weight with pulsed as well as continuous microwave radiation, at constant average power. The curing rate of poly(amic acids) have also been studied with thermal energy, continuous and pulsed microwave radiation to better understand the interaction between pulsing the microwave and the polymeric material.

Results from the heating rate studies indicate that the enhancement in heating rate with pulsed microwave radiation depends on the low frequency absorption spectrum (i.e., less than 10,000 Hz) of the polymer. The heating rate of poly(propylene glycol), which has a low frequency absorption, was enhanced by pulsing the microwave energy whereas the heating rate of

poly(ethylene glycol), which does not have a low frequency absorption, remained the same when compared to continuous wave. Also results from the curing rate studies with poly(amic acids) indicate that the enhancement in curing rate observed in samples cured by microwave radiation as opposed to those thermally cured may be partially due to microwave power distribution in the cavity. This has been tested by agitating the sample to reduce any temperature gradient arising from the power distribution in the cavity. According to the experimental results, as the agitation rate was increased, the rate of imidization of poly(amic acids) with microwave radiation approached the rate of thermal imidization, at constant temperature. However, more research is required to clarify this complex phenomenon.

Acknowledgement

The author would like to express his deepest thanks to professor , and for their support and guidance during the course of this research.

The author would also like to thank and for their assistance in constructing the experimental apparatus. In addition, the author would like to thank for providing unlimited supply of poly(amic acid) samples during the course of this investigation.

Finally, the author would like to thank his family and friends for their support and encouragement.

Table of Contents

Table of Contents

List Of Figures

List Of Tables

List Of Nomenclature

a	Radius of the cavity
A	Arrhenius equation front factor
A_a	Absorption of the amic acid group
A_I	absorption of the imide group
A_r	Absorption of the reference group
A_s	Surface area of the sample cell
C_a	Concentration of the amic acid group
C_{H2o}	Concentration of water in solution
C_I	Concentration of the imide group
C_p	Concentration of the polymer in solution
C_r	Concentration of the reference group
C_v	Constant volume heat capacity of the sample
d	Pathlength or thickness of the sample
ΔE	Activation energy for the relaxation of dipoles
E_0	Electric field averaged over one period in the empty, unperturbed, cavity
E^*_0	Complex conjugate of the electric field averaged over one period in the empty, unperturbed, cavity
E_{hybrid}	Electric field for the loaded cavity hybrid mode
f	relaxation frequency of the dipoles
f_p	Pulse repetition rate of the pulsed microwave radiation
$F(C_p)$	A function depending on the concentration or the fraction of polymer in solution
$F(\varepsilon'_r)$	Correction factor to relate the electric field in the sample to the electric field in the empty cavity if the perturbation theory is employed

h	Heat transfer coefficient between the sample and the surrounding
i	$(-1)^{1/2}$, denotes imaginary number
$J_n(X)$	Bessel function of the first kind with order n
$K=K_e$	Effective rate constant for solution imidization of poly(amic acids)
K_{inter}	intermolecular imidization rate constant
K_{intra}	intramolecular imidization rate constant
K_{inv}	Rate constant for the inverse reaction of water with the imide group
K_z	Thermal conductivity of the sample along the Z-direction
L	Length of the cavity when tuned to TE_{111} mode
MW_e	Molecular weight of the poly(ethylene glycol)
MW_p	Molecular weight of the poly(propylene glycol)
n_e	Number of repeat units for poly(ethylene glycol) with molecular weight MW_e
n_p	Number of repeat units for poly(propylene glycol) with molecular weight MW_p
P_{avg}	Average microwave power
P_d	Dissipated power distribution (i.e., density) in the sample
$P_{d,t}$	Total dissipated power inside the sample
$P_{e,fs}$	Stored electric power density for empty cavity tuned to TE_{111} mode
$P_{e,fs,n}$	Normalized electric field distribution (i.e., density) inside the empty cylindrical cavity tuned to TE_{111} mode
P_p	Pulse peak power of the pulsed microwave radiation
Q	Quality factor (i.e., ratio of the stored power divided by the dissipated power) for the perturbed cavity
r	Length along the radial direction
R	gas constant=1.987×10^{-3} Kcal/mole K
R_i	Rate of imidization reaction

t	time
T_0	Ambient temperature inside the cavity
T_{max}	Temperature corresponding to maximum heating rate of the polymer near the glass transition temperature
T_p	Pulse period of the pulsed microwave radiation
dT/dt	Heating rate of the polymeric sample
V_c	Volume of the cavity when tuned to TE_{111} mode
V_s	Volume of the sample
X'_{11}	Zero of the derivative of the bessel function=1.8412
Z	Length along the axial direction
α	Absorption peak in the dielectric spectra related to the melting point
α_a	Conversion of the poly(amic acid) as a function of time
β	Absorption peak in the dielectric spectra related to the glass transition
γ	Absorption peak in the dielectric spectra related to the side chain motion below the glass transition temperature
δ	Absorption peak in the dielectric spectra related to local motion of the chains
ε_0	Permittivity of the free space
$\varepsilon'_{0,r}$	Relative dielectric constant of the empty cavity
$\varepsilon''_{0,r}$	Relative dielectric loss of the empty cavity
ε'_r	Relative dielectric constant of the polymer sample
ε''_r	Relative dielectric loss of the polymer sample
ε^{*}_r	Complex permittivity of the polymer sample
ε_s	Static dielectric constant of the polymer sample
ε_∞	Dielectric constant of the sample at infinite frequency

θ	Azimuthal angle
λ	Absorption peak in the dielectric spectra associated with ionic conduction
ξ_a	Absorption coefficient of the amic acid group
ξ_i	Absorption coefficient of the imide group
ξ_r	Absorption coefficient of the reference group
π	3.1415.....
ρ	density of the polymer sample
σ	A measure of interaction between the dipoles for the Cole-Cole equation
τ	Relaxation time constant of dipoles at temperature T
τ_{pw}	Pulse width of the pulsed microwave radiation
ω	Resonant frequency of the perturbed cavity
ω_0	Resonant frequency of the empty, unperturbed, cavity

I. Introduction

Microwave processing of materials have been developed in the past few decades primarily to overcome the limitations of conventional processing techniques with thermal energy. With microwave radiation, the energy is directly deposited inside the material, whereas with thermal heating, the energy is transferred by conduction from the surface to the bulk of material, thus the heating rate depends on temperature gradients across the material from surface to bulk with subsequent non-uniform heating and curing of the specimen.

Microwave processing of materials has its limitations. Electromagnetic radiation in the microwave region, of 2.45 giga-hertz, has a wavelength of 12.6 centimeters, and therefore there is a spatial variation of microwave power inside the applicator. This power distribution, and the non-linear dependence of the dielectric loss of polymeric materials on temperature, causes the formation of hot spots [31,33], visible to the naked eye, with subsequent burning of the specimen. This has limited the use of microwave processing for materials such as polymers [57]. The formation of hot spots and temperature runaway can abruptly influence the mechanical properties of the cured materials. On the other hand, microwave radiation has been utilized commercially for drying of wet solids [44,48] where the effect of hot spot formation and temperature runaway are less severe due to high heat of evaporation of water.

The major difficulties impeding the commercialization of microwave processing of materials, specially polymers, have been the following: 1) non-uniform distribution of energy in the applicator with subsequent formation of hot spots [49], 2) non-linear dependence of dielectric loss of the polymeric material on temperature which causes temperature runaway [31], and 3) the chemistry of the curing process with microwave radiation has not been well understood [19].

In the past decade, research in the area of curing of polymers with microwave radiation has emerged at a rapid pace due to the increasing demand from industry [1-30]. Major areas of investigation have been the curing of natural and synthetic rubber, epoxies, and epoxy resin composites with microwave radiation. Results from these investigations indicate that the curing rate of polymers can be accelerated with microwave radiation as opposed to thermal oven curing. Moreover, these results suggest that the rate of curing with microwave radiation can be further enhanced by pulsing the microwave energy [4,14]. Although temperature was not controlled in most of these previous investigations, an order of magnitude reduction in curing time, from hours to minutes, suggested that the kinetics of curing might be distinctly different with microwave radiation.

Recently there has been a report in the literature [8] indicating that the rate of imidization of poly(amic acids) is accelerated by as much as thirty five times at constant temperature, when using microwave radiation as opposed to thermal energy. However, in this work, they did not show that the temperature was uniform throughout the volume of the sample either theoretically by studying the distribution of microwave power in the reaction cell or experimentally by agitating the cell to eliminate any temperature gradient. Consequently, their assumption of uniform temperature throughout the volume of sample seemed plausible.

The purpose of this work was to study the heating and curing rates of polymers with continuous as well as pulse microwave radiation and compare them with those observed using conventional thermal heating. The heating rates of poly(ethylene glycol) and poly(propylene glycol) are studied using pulsed as well as continuous microwave radiation to find out whether pulsing the microwave energy can enhance

the heating rate of polymeric materials as compared to that observed using continuous wave, both being at the same average power.

The curing rate of poly(amic acids) are studied with thermal energy, and with continuous, and pulsed microwave radiation to better understand the interaction of microwave radiation with the polymeric material. To ascertain whether microwave radiation has any special effect on the kinetics of the curing reaction of polymers as opposed to thermal energy, we have studied the rate of imidization of poly(amic acids) at constant temperature with microwave radiation and with agitation to eliminate any temperature gradients inside the reaction cell.

In the literature review that follows (chapter two), a more detailed discussion of microwave processing of materials, with specific emphasis on polymeric materials, is presented. Chapter three discusses the theory of microwave heating and the distribution of microwave power in a cylindrical cavity, as it pertains to the selection of sample size, sample geometry, and prediction of temperature gradients in the sample cell. Chapter three also discusses the mechanism of microwave absorption in order to predict the heating rate of polymers near the glass transition temperature. Finally, in the last part of chapter three, the kinetics of imidization of poly(amic acids) is presented.

Chapter four presents the experimental systems for continuous and pulse microwave radiation experiments. The experimental apparatus and experimental conditions for heating and curing rate studies are also presented in chapter four. A discussion of results is presented in chapter five, followed by conclusions, recommendations, future work, and references.

II. Literature Review

One of the early commercial applications of microwave processing was in the drying of wet solids. Drying of wet solids has become one of the classical applications of microwave processing of materials as opposed to conventional drying techniques with thermal heating, because it clearly illustrates the advantages of microwave radiation. Conventional drying techniques can use three modes of heat transfer, vis, radiation, convection, and conduction, to carry out heat to the bulk of the material. Therefore, the thermal conductivity characteristics of the wet solid controls the rate of heating of the mass. Once the outside layers of the solid have become dry, a diffusion limited, falling rate regime is established with its subsequent drastic reduction in speed and efficiency of drying.

In contrast, in microwave drying, the energy is deposited in the volume of the solid (e.g., volumetric heating) and is absorbed directly by the water, thus the rate of heating is independent of the thermal conductivity characteristics of the wet solid. Therefore, drying in microwave fields maintain a high drying rate down to very low moisture contents, as displayed schematically in Figure 2-1, thus indicating that the diffusion mechanism has been short-circuited by this form of heating. Figure 2-1 shows that the rate of microwave drying becomes very efficient specially at low moisture content of the solid due to the enhanced diffusion of moisture with microwave radiation.

Microwave processing of wet solids improves the rate of heating, drying, and diffusion of moisture to the surface, thus this technique has remained one of the most successful applications of microwave processing of materials. In fact, microwave drying is one of the few applications of microwave processing in which detailed

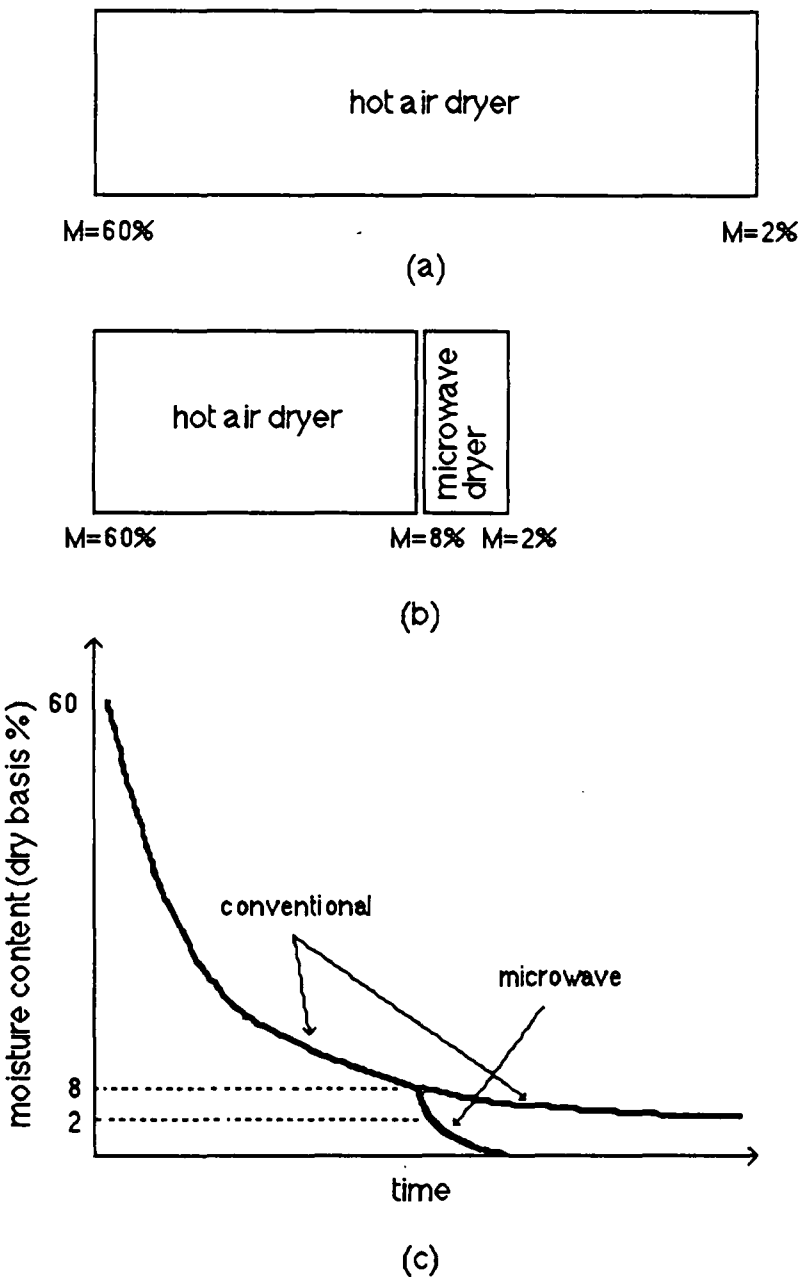

Figure 2-1: comparison of conventional versus microwave drying; a) conventional hot air drying, b) combination of hot air and microwave drying, and c) drying curves for cases (a) and (b); reproduced from reference [43].

theoretical models have been developed to predict the rate of heating, drying, and diffusion [44,48,55,56]. Other areas of interest, which are at the early stages of development, are microwave curing of concrete [17], heating and curing of foundry binders [25], heat-curing of denture based acrylic resins [20], and drying of cotton fabrics treated with water soluble resins [27].

Another area of application for microwave processing of materials, which has received considerable attention in the past few years and is still in the early stages of development, is sintering of ceramics, super-conductor materials, and metal oxides [9,10]. Some of the processing advantages of microwave energy in the ceramic area are its volumetric, rather than surface diffusion, heating (i.e., heat is generated throughout the material); instant on/off control (i.e., unlike conventional heating, energy can be applied or removed instantly); lack of thermal inertia; high energy transfer efficiency, and very high heating rates that can be precisely controlled. In particular, rapid heating rate of ceramics with microwave radiation can lead to a finer and more uniform microstructure, as displayed in Figure 2-2. This figure shows that the density of alumina is higher when sintered with microwave energy as opposed to conventional infrared process.

Figure 2-3 displays the temperature-time profile for iron oxide at different microwave power levels. The iron oxide powder (Fe_3O_4) reaches temperatures ranging 1000 degrees centigrade in less than one minute with microwave radiation which is very difficult to attain such fast heating rates with conventional thermal heating. Microwave radiation has been applied to sintering of mullite powder and boron carbide; metal oxides such as zinc oxide, iron oxide, chromium oxide, and silicone oxide; super-conductor materials such as calcined powders of yttrium oxide

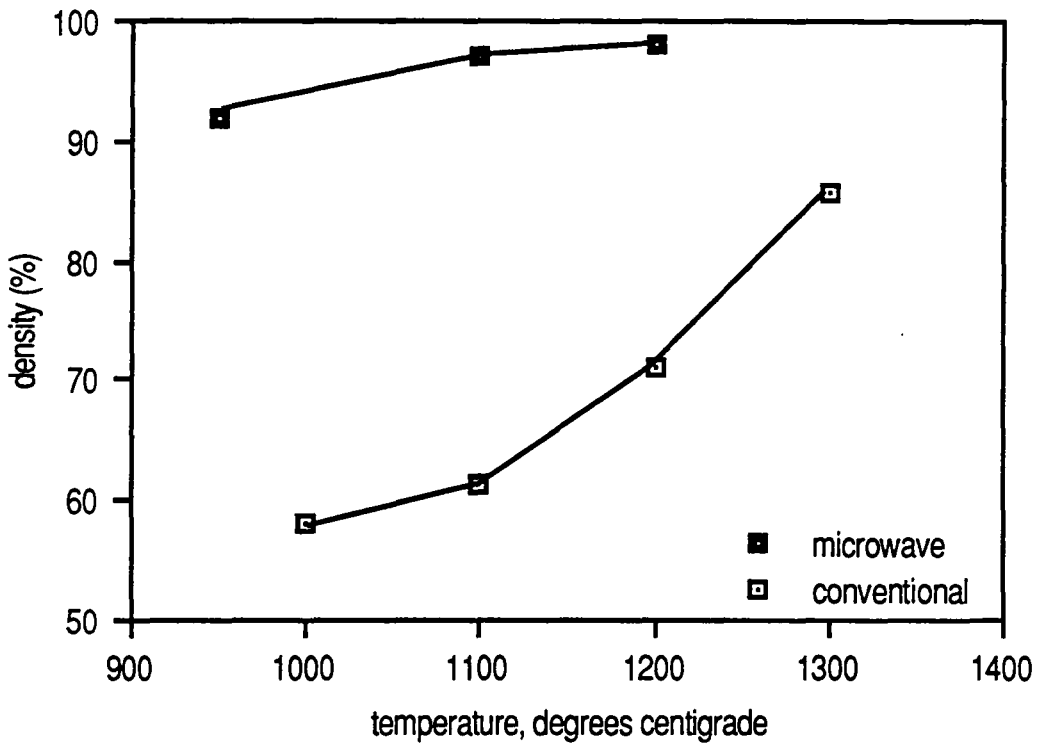

Figure 2-2: Microwave sintering of alumina increases densification when compared with the conventional infrared process; reproduced from reference [10].

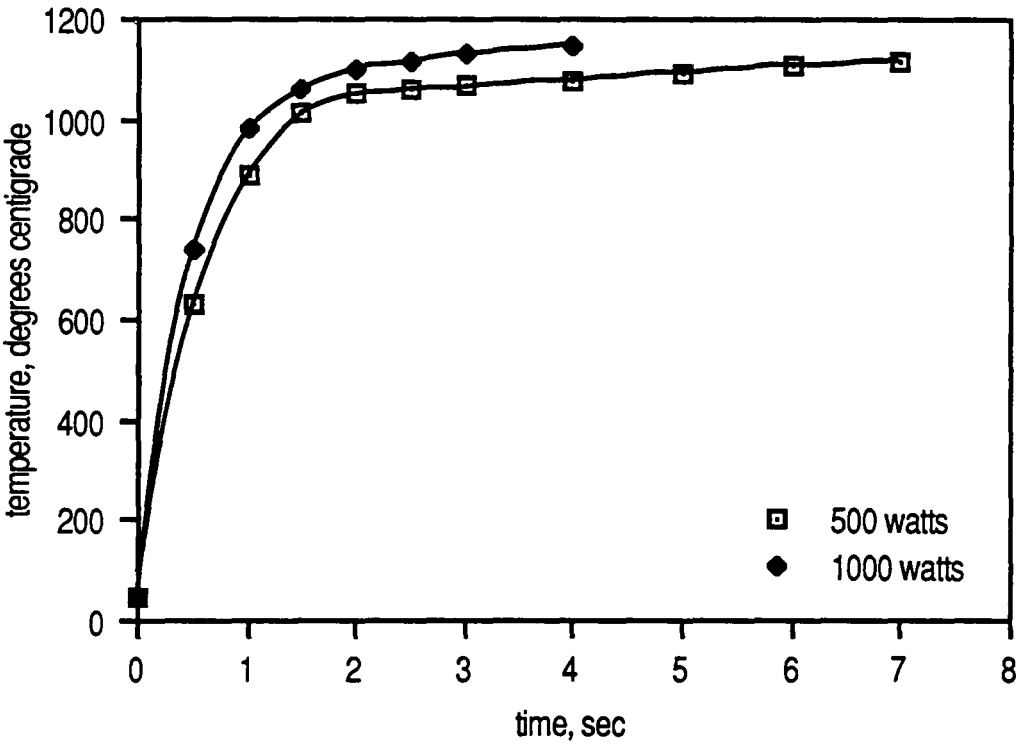

Figure 2-3: Temperature-time profile for microwave heating of iron oxide at two different power levels; reproduced from reference [9].

(Y_2O_3), barium carbonate ($BaCO_3$), and copper oxide (CuO) producing enhanced morphology and increased densification.

Another major application of microwave processing, which has received attention in the past decade and is related to our studies, is microwave processing of composites and polymeric materials. The first application of microwave processing of polymers was in the rubber industry for the heating and curing of rubber mats [33,34]. Some of the conclusions from the rubber curing studies with microwave radiation are as follows:

1) It is possible to control the microwave absorption characteristics of a given base polymer by incorporating suitable compounding ingredients, even if the base polymer itself only absorbs weakly.
2) Microwave curing can yield mechanical properties of the vulcanized product which are comparable to those obtained in a conventional curing process.
3) Measurements of dielectric constant, loss factor, and dissipation factor at microwave frequencies provide a means of predicting the suitability of a given material for vulcanization with microwave energy.
4) The optimum curing process would be to direct the extrudate into the microwave apparatus as soon as it comes out of the extruder. This not only saves energy but also ensures uniform curing throughout the material due to the more favorable dielectric properties at elevated temperatures.

The major disadvantage of microwave curing of polymers, specially rubber curing, has been the formation of hot spots, visible to the naked eye, followed by spot-like burning of the sample. The formation of hot spots is attributed to 1) non-uniformity of the electric field in the applicator and 2) thermal runaway due to the sharply rising temperature dependence of dielectric loss of the sample material.

Epoxy polymer systems based on diglycidyl ether of bisphenol A (DGEBA) and diaminodiphenyl methane (DDM) as the curing agent has also been studied extensively with microwave radiation. Le Van, et.al. [11] and others [18,24] have studied the curing of epoxies with continuous microwave radiation, and their results indicate that curing of epoxy resins was accelerated with microwave radiation as opposed to thermal curing. Gourdenne and co-workers have studied the curing of epoxy resins filled with aluminum powder [2,3], carbon black [1], and glass fiber [13,23]. Their results show that the filler concentration had a dramatic effect on dielectric and thermal properties of the epoxy resin composites. Microwave radiation has also been applied to cure poly(sulfone) modified epoxy resins [7] and the results indicate that the microwave cured two phase epoxy system had a different morphology as opposed to thermally cured epoxy.

Parallel to experimental studies mentioned above, Springer G. S. [50-54], Hawley M. C. [42,96], Wagter D. C. [49], and Haven R. E. [57] have theoretically modeled the curing reaction of epoxies with microwave radiation to predict the curing rate, heating rate, and the physico-chemical properties of the cured epoxy. Asmussen and co-workers [97] have designed a single mode cylindrical microwave cavity, which has been used in our studies, for efficient heating and diagnosis of materials for microwave heating. We should mention here that the design of microwave cavities, with uniform electric field distribution throughout, has not been addressed adequately in the literature and research is needed in this area.

Microwave radiation has also been used for radical polymerization of 2-hydroxyethylmethacrylate [15], synthesis and curing of poly(urethanes) [12,14], cross-linking of unsaturated polyester/styrene mixtures [24]. In recent years, rapid heating capability of microwave radiation has been used for thermodynamic characterization

of chemical reactions [41], sample dissolution [40], catalytic hydro-cracking [38,39], and even in laboratory scale organic synthesis [35-37].

Results from the majority of the above investigations indicate that the curing rate of polymers is accelerated by at least an order of magnitude with microwave radiation, as opposed to thermal heating. Furthermore, Jullien et. al. [14] and Gourdenne et. al. [4] have used pulsed microwave radiation to cure urethane prepolymers and epoxies, and their results shows that the rate of curing of poly(urethane) was further enhanced by pulsing the microwave as compared to continuous wave. Gourdenne and co-workers argued that the enhancement in the rate of curing by pulsing the microwave was due to a double relaxation which was a combination of dipolar relaxation at the frequency (2.45 GHz) of the electromagnetic wave, and of the segmental relaxations maintained by pulsing the microwave energy. However, they did not show explicitly any experimental proof that the heating rate of poly(urethane) was higher with pulse microwave as opposed to continuous wave, due to the double relaxation effect.

In the following chapter, the theory of microwave heating, and the kinetics of imidization of poly(amic acids) is presented.

III. Theory

3.1. Theory of Microwave Heating

The cavity employed in this research is a single mode cylindrical microwave cavity designed by department of electrical engineering at Michigan State University [42,96,97]. A schematic diagram of the side view of this cavity is displayed in Figure 3.1. In the following, we present a brief description of the applicator.

The resonant cavity is formed by the 17.8 centimeters inside diameter cylindrical brass tube (1), as displayed in Figure 3.1, and the transverse brass shorting plates (2) and (3). One of the shorts (2) is adjustable to provide a variable cavity length of 6-16 centimeters. The other shorting plate (3) is fixed in position during operation and is removable. Silver plated finger stock (4) ensures good electrical contact on the adjustable short (2) and the removable short (3). A lab jack holds the fixed plate (3) in place during cavity excitation.

When this cavity is operated at 2.45 giga-hertz (GHz), the empty cavity electromagnetic modes TE_{111}, TM_{012}, TE_{211}, TE_{011} and TM_{111} (degenerate modes), and TE_{311} can be excited independently depending on the cavity length. The cavity mode corresponding to the shortest cavity length is the TE_{111} mode. Throughout this investigation, the frequency of microwave radiation was fixed at 2.45 GHz, and all of the experiments were conducted with TE_{111} mode.

The polymer sample, which was a viscous liquid in all of the experiments, was placed inside a cylindrical Teflon bottle, mounted at the center, and raised two centimeters above the bottom surface of the cavity. The sample cell can be viewed through a copper screen window (6). Input microwave power is fed into the coaxial input port (7) and is coupled into the cavity via the adjustable coaxial probe (8).

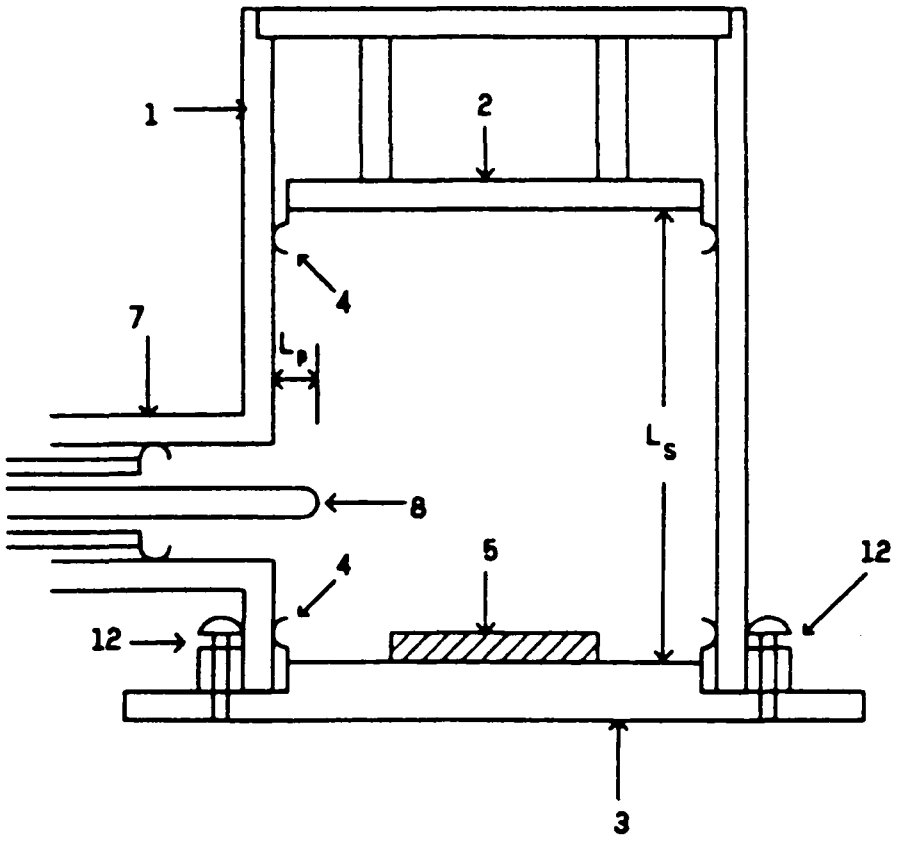

Figure 3-1: Cross-sectional view of the cylindrical cavity (the θ=0 plane passes through the coupling probe) [97]

Adjustments of short probe L_s and the coupling probe position L_p are made by normal rotation of the knobs shown on the photograph of Figure 4.1 in Chapter IV. Short and probe positions can be measured to within a tenth of a millimeter by the micrometer indicators on the coupling probe and the sliding short. A brief discussion of electric field and power distribution inside the cavity is presented next, as it pertains to the selection of sample size, sample geometry, and prediction of temperature gradients in the sample.

3.1.1. Distribution of Electric Field and Power for TE_{111} mode

The field inside the cavity has electrical as well as magnetic components. However, the magnetic field inside the cavity will not be presented here, because the polymeric sample is not magnetically susceptible. Distribution of The electric field of the power for a hollow, completely closed, circular cylindrical cavity with TE_{111} excitation mode is given by the following equation [46] :

$$P_{e,fs,n} = [J_0^2(X) + J_2^2(X) - 2J_0(X)J_2(X)\mathrm{Cos}(2\theta)\,]\,\mathrm{Sin}^2(\pi Z/L) \qquad (3\text{-}1)$$

Where $P_{e,fs,n}$ = normalized electric power distribution inside an empty cylindrical cavity tuned to TE_{111} mode.

$= P_{e,fs,n} = P_{e,fs} / P_{e,fs}(r=0,\ \theta=0\text{-->}2\pi,\ Z=L/2)$

$P_{e,fs}(r=0,\ \theta=0\text{-->}2\pi,\ Z=L/2) = 2\,P_{fs,t} / V_c$

$P_{fs,t}$ = total stored power inside cavity which is the difference between the incident and reflected powers

V_c = volume of the cavity

$P_{e,fs}$ = stored electric power density for the empty cavity

r = length along the radial direction (zero to a)

θ = azimuthal angle (zero to 360 degrees)

Z = length along the axial direction (zero to L)

a = radius of the cavity

L = height of the cavity

$J_n(X)$ = bessel function of the first kind with n^{th} order

$$= \sum \{ [(-1)^k (X/2)^{2K+n}] / [K! \Gamma(K+n+1)] \}$$

$X = X'_{11} r/a$

X'_{11} = zero of derivative of the bessel function $J'_{11} = 1.8412$

Equation 3-1 is based on the following assumptions: 1) the cylindrical cavity is empty and completely closed, 2) the inside surface of the cavity is perfectly conducting or the empty cavity quality factor (e.g., Q-factor) is infinity, and 3) the cavity is tuned to TE_{111} excitation mode. The Q-factor of the empty cavity is greater than 11,000 [96], and the second assumption is satisfied. The above equation can be solved for different values of radius, azimuthal angle, and height to find the distribution of microwave power inside the empty cavity. Table 3-1 lists the distribution of microwave power as a function of radial direction for different azimuthal angles, θ, evaluated at Z equal to L/2. Note that the azimuthal angle, θ, is defined as zero along the line joining the viewing screen and the coaxial input port, as exhibited in Figure 4-1 of Chapter IV. The data in Table 3-1 is also displayed graphically in Figure 3-2. According to Figure 3-2, for TE_{111} mode, the power density is highest at the center of cavity (e.g., r=0) and reduces to zero at the wall next to the cylindrical brass tube for azimuthal angle equal to zero. Also the power density falls off slower with radial direction as the azimuthal angle increases from zero to ninety degrees.

More importantly, Figure 3-2 indicates that the radius of sample has to be less than ten percent of the radius of cavity to ensure less than five percent variation in power density along the sample diameter. This suggests that the sample diameter

Table 3-1: Radial distribution of microwave power inside the empty cavity

radius, inches	P_r, (θ=0°)	P_r, (θ=22.5°)	P_r, (θ=45°)	P_r, (θ=67.5°)	P_r, (θ=90°)
0	1	1	1	1	1
0.0875	0.998	0.999	0.999	0.999	0.999
0.175	0.994	0.994	0.996	0.997	0.998
0.263	0.986	0.987	0.991	0.994	0.995
0.35	0.975	0.977	0.983	0.989	0.992
0.4375	0.961	0.965	0.974	0.983	0.987
0.525	0.944	0.949	0.962	0.976	0.981
0.6125	0.924	0.932	0.949	0.967	0.974
0.7	0.902	0.911	0.934	0.957	0.967
0.7875	0.877	0.889	0.917	0.946	0.958
0.875	0.85	0.864	0.899	0.934	0.948
0.9625	0.82	0.837	0.879	0.92	0.938
1.05	0.789	0.809	0.857	0.906	0.926
1.1375	0.755	0.778	0.834	0.891	0.914
1.225	0.72	0.747	0.81	0.874	0.901
1.3125	0.684	0.714	0.786	0.857	0.887
1.4	0.647	0.68	0.759	0.839	0.872
1.4875	0.608	0.645	0.732	0.82	0.856
1.575	0.569	0.609	0.705	0.801	0.84
1.6625	0.53	0.573	0.677	0.78	0.823
1.75	0.491	0.537	0.648	0.76	0.806
1.8375	0.451	0.501	0.62	0.739	0.788
1.925	0.412	0.464	0.591	0.717	0.769
2.0125	0.374	0.429	0.562	0.695	0.75
2.1	0.336	0.394	0.534	0.673	0.731
2.1875	0.3	0.36	0.505	0.651	0.711
2.2755	0.264	0.327	0.478	0.629	0.691
2.362	0.231	0.295	0.451	0.606	0.671
2.449	0.198	0.265	0.424	0.584	0.65
2.536	0.168	0.236	0.399	0.562	0.629
2.623	0.14	0.209	0.374	0.54	0.608
2.71	0.114	0.183	0.351	0.518	0.587
2.797	0.0907	0.16	0.328	0.496	0.566
2.884	0.0697	0.139	0.307	0.475	0.545
2.971	0.0513	0.12	0.287	0.454	0.523
3.058	0.0357	0.104	0.269	0.434	0.502
3.145	0.023	0.0899	0.252	0.414	0.481
3.232	0.013	0.078	0.237	0.395	0.46
3.319	0.006	0.069	0.223	0.376	0.44
3.406	0.001	0.0626	0.21	0.358	0.419
3.5	0	0.059	0.2	0.341	0.399

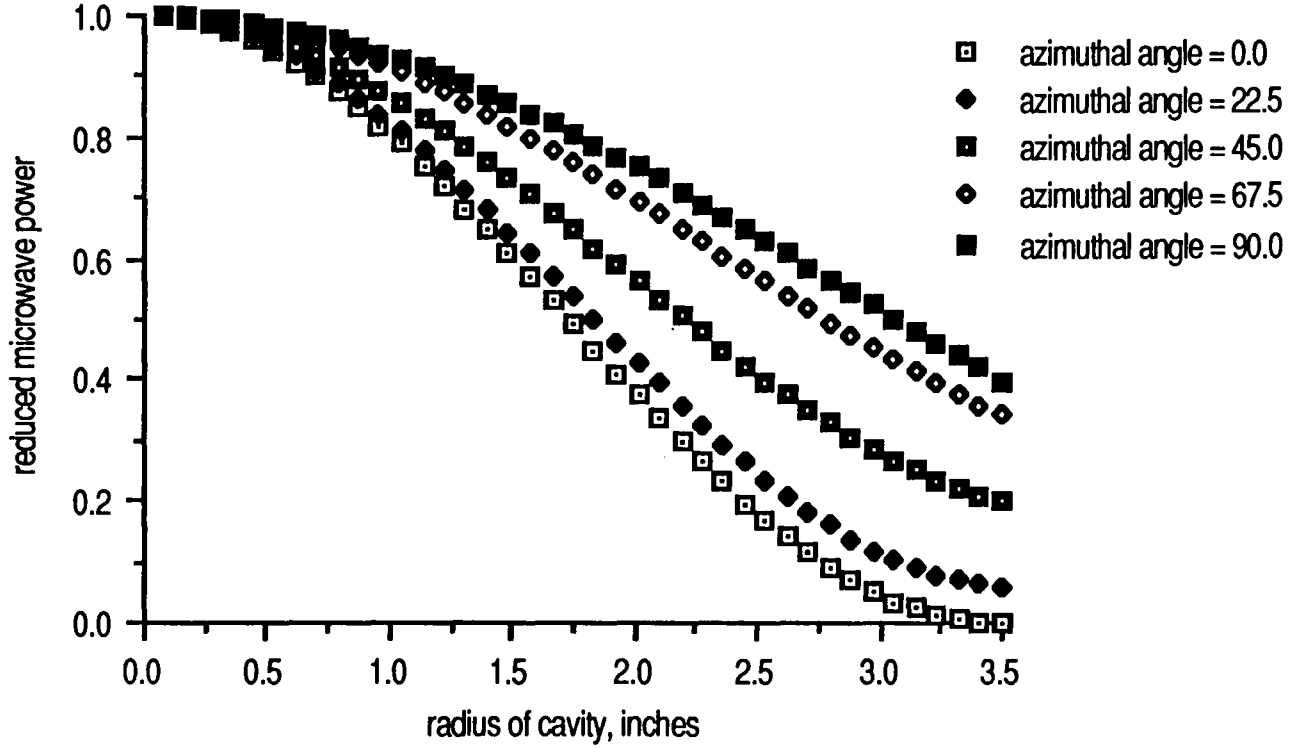

Figure 3-2: Radial distribution of microwave power inside cavity for different azimuthal angles.

should be less than two centimeters. In all of the experiments, the sample diameter was 1.5 centimeters, and therefore we do not expect significant variation in power density or heating rate along the radial direction.

Table 3-2 lists the power distribution inside the empty cavity as a function of height, Z, for a fixed azimuthal angle of zero, but with three different values of radii which are 0.01, 0.45, and 0.90 centimeter, accordingly. The data of Table 3-2 is also displayed graphically in Figure 3-3. According to Figure 3-3, the power distribution along the Z-axis does not depend significantly on radius, however there are significant variations in field intensity along the height of cavity.

The variation of power along the Z-axis depends on the sample length as well as the placement of sample inside the cavity. For example, according to Figure 3-3, there is less than five percent variation in power density for a sample with one centimeter length positioned at the center height of cavity. On the other hand, there may be as much as seventy percent variation in power density for the same sample if positioned one centimeter above the bottom surface of cavity.

Therefore, placement of sample in the axial direction plays an important role in uniform heating of the polymeric material. In chapter V, we will present experimental data that proves there is considerable variation in power density along the axial direction and more importantly, due to power distribution inside cavity, it may not be possible to define a uniform and homogeneous temperature for the sample. In fact, the designers of this cylindrical cavity recommend disk shaped or thin slab sample geometry for TE_{111} excitation mode. The cavity employed in this work had a two inches opening centered on the top surface of cavity. This opening has no effect on the power distribution for the empty cavity, because according to Figures 3-2 and 3-3 the power distribution at the top surface is zero.

Table 3-2: Axial distribution of microwave power inside the empty cavity

height, inches	P_r, r=0 in.	P_r, r=0.175 in.	P_r, r=0.35 in.
0	0	0	0
0.1625	0.00616	0.00612	0.006
0.325	0.0245	0.0243	0.0239
0.4875	0.0545	0.0542	0.0531
0.65	0.0955	0.0949	0.0931
0.8125	0.146	0.146	0.143
0.975	0.206	0.205	0.201
1.1375	0.273	0.271	0.266
1.3	0.345	0.343	0.337
1.4625	0.422	0.419	0.411
1.625	0.5	0.497	0.487
1.7875	0.578	0.575	0.564
1.95	0.655	0.65	0.638
2.1125	0.727	0.722	0.709
2.275	0.794	0.789	0.774
2.4375	0.854	0.848	0.832
2.6	0.905	0.899	0.882
2.7625	0.946	0.94	0.922
2.925	0.976	0.969	0.951
3.0875	0.994	0.988	0.969
3.25	1	0.994	0.975
3.4125	0.994	0.988	0.969
3.575	0.976	0.969	0.951
3.7375	0.946	0.94	0.922
3.9	0.905	0.899	0.882
4.0625	0.854	0.848	0.832
4.225	0.794	0.789	0.774
4.3875	0.727	0.722	0.709
4.55	0.655	0.65	0.638
4.7125	0.578	0.575	0.564
4.875	0.5	0.497	0.487
5.0375	0.422	0.419	0.411
5.2	0.345	0.343	0.337
5.3625	0.273	0.271	0.266
5.525	0.206	0.205	0.201
5.6875	0.146	0.146	0.143
5.85	0.0955	0.0949	0.0931
6.0125	0.0545	0.0542	0.0531
6.175	0.0245	0.0243	0.0239
6.3375	0.00616	0.00612	0.006
6.5	0	0	0

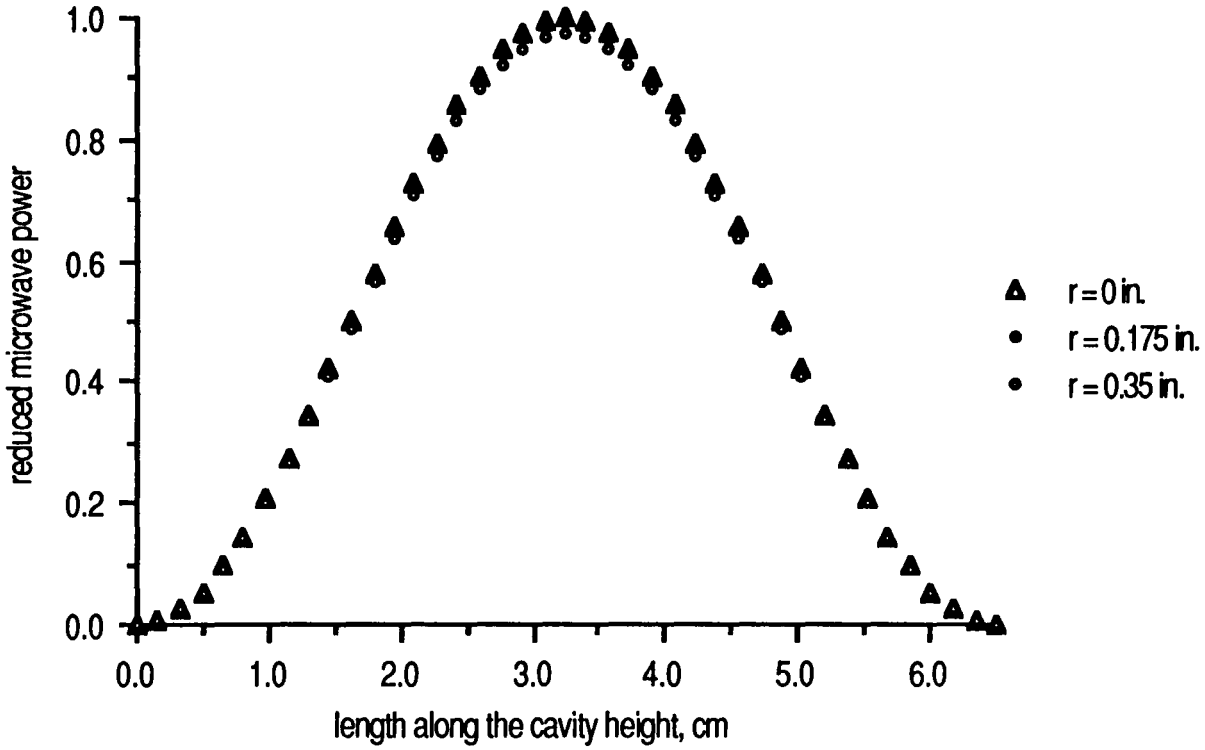

Figure 3-3: Axial distribution of microwave power inside cavity for different values of radius and azimuthal angle of zero.

The diameter of the sample cell for all of the experiments was 1.5 centimeters. The height of sample for heating rate experiments was one centimeter, and for reaction rate experiments was three centimeter, to allow the withdrawal of at least six aliquots for kinetic studies. The height of sample for experiments to study the effect of microwave power on the curing rate was 1.5 centimeters.

3.1.2. Determination of Dissipated Power for a Low Loss, Low Dielectric Constant Material

In this section, we consider the case in which the sample is a low loss, low dielectric constant material. This allows the use of perturbation theory to determine the absorbed power by the sample from a knowledge of dielectric constant, dielectric loss, and the electric field distribution for the empty cavity. This analysis is applicable to polymers below their glass transition temperature, because this class of materials exhibit low dielectric constant and dielectric loss.

Figure 3-4 displays the cavity with its material properties for the unperturbed as well as the perturbed cavity. The empty cavity electric field, relative dielectric constant, and dielectric loss are represented by E_0, $\varepsilon'_{0,r}$, and $\varepsilon''_{0,r}$, respectively. And the perturbed cavity electric field, relative dielectric constant, and dielectric loss are designated by E_s, ε'_r, and ε''_r, respectively. The assumptions inherent to perturbation theory are the following [47]: 1) there is no change in cavity mode before and after the cavity is perturbed and 2) the distribution of electric field inside the cavity does not change sharply, but it is only perturbed. Based on the above assumptions, the dissipated power inside the sample is given by the following equation [47,97] :

$$P_{d,t} = (\varepsilon_0/2)\,\omega \iiint_{Vs} [E_s.E_0^*]\, dV_s \qquad (3\text{-}2)$$

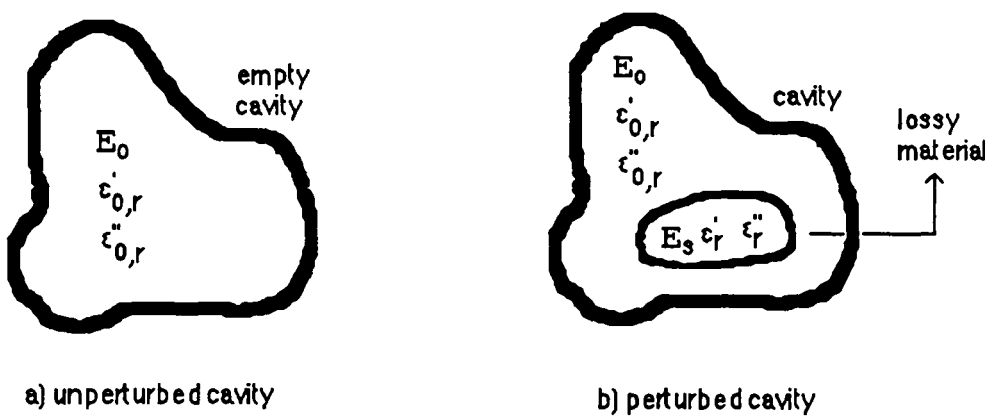

Figure 3-4: Cavity with its material properties before and after perturbation with a lossy material

Where ω = resonant frequency of the perturbed cavity

ω_0 = resonant frequency of the empty cavity

ε_0 = permittivity of free space

E_s = electric field inside the sample

E_0^* = complex conjugate of the electric field in the empty, unperturbed, cavity

V_s = volume of the sample

$P_{d,t}$ = total dissipated power inside the sample

Note that it is also assumed the permeability of the sample is the same as for free space in Equation 3-2. In other words, it is assumed the sample has no effect on the magnetic component of the field inside cavity.This is a reasonable assumption, because polymeric materials are not magnetically susceptible. To estimate the electric field in the sample, E_s, the following additional assumptions are required [96] :

1) The power absorbed and stored in the sample are much smaller than the total power stored inside the empty cavity. This assumption requires that the difference in dielectric constant and dielectric loss for the sample be small with respect to free space. According to this assumption, the difference between the unperturbed and the perturbed resonance frequency is much smaller than the unperturbed resonance frequency (e.g., $\omega_0-\omega << \omega_0$).

2) The dimensions of the sample are at least twenty times smaller than the wavelength of microwave radiation, so that the quasi-static approximation for the electric field in the sample is valid. The quasi-static approximation assumes that the electric field inside the sample is related to the electric field outside the sample in the same manner as for static fields.

Upon incorporating the above assumptions into Equation 3-2, it reduces to the following equation based on dissipated power density :

$$P_d = (\varepsilon_0/2)\,\omega_0\,F(\varepsilon'_r)\,\varepsilon''_r\,|E_0|^2 \qquad (3\text{-}3)$$

$$E_s = \varepsilon^*_r\,F(\varepsilon'_r)\,E_0$$

Where P_d = dissipated power density inside the sample

$\varepsilon^*_r = \varepsilon'_r - i\varepsilon''_r$

ε^*_r = relative complex dielectric constant of the sample

ε'_r = relative dielectric constant of the sample

ε''_r = relative dielectric loss of the sample

$F(\varepsilon'_r)$ = geometry factor to relate electric field in the sample to electric field in the empty cavity

The term $F(\varepsilon'_r)$ is a geometry factor to relate the electric field inside the sample to electric field in the empty cavity, assuming the quasi-static approximation applies [47]. The geometry factor F depends on 1) the dielectric constant of the sample, 2) the geometry of the sample, and 3) the direction of the electric field. Figure 3-5 displays four different sample geometries with their corresponding geometry factors. According to Figure 5-5, if the electric field axis is parallel to the long axis of the sample, the geometry factor is unity and the ratio of electric field inside the sample to outside is equal to the complex dielectric constant of the sample. However, if the electric field is perpendicular to the long axis of the sample, the geometry factor is less than unity by the amount depending on the dielectric constant of the sample. In general, the ratio of electric field inside the sample to outside is always equal or smaller than the complex dielectric constant of the sample.

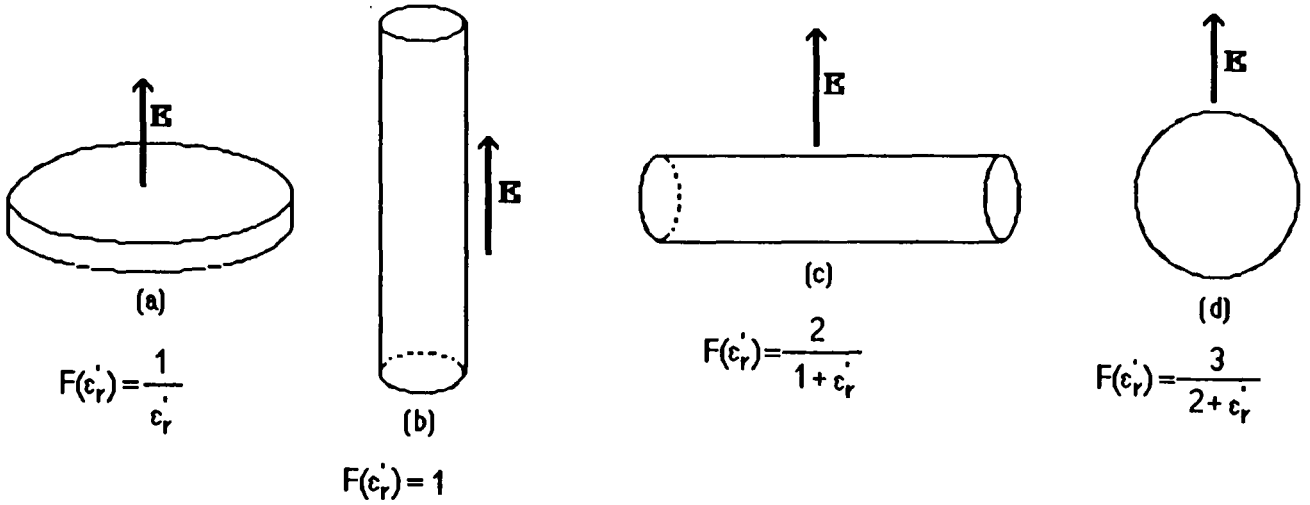

Figure 3-5: Geometry factor to relate the electric field inside the sample to the field in the empty cavity, assuming quazi-static approximation[47]

The sample in our experiments has cylindrical symmetry and the electric field is in the X-Y plane, therefore case (c) in Figure 3-5 (e.g., electric field perpendicular to the long axis of cylinder) would best represent the geometry factor for our experiments. Consequently, Equation 3-3 becomes :

$$P_d = (\varepsilon_0/2)\,\omega_0\,[\,2/(1+\varepsilon'_r)\,]\,\varepsilon''_r\,|E_0|^2 \qquad (3\text{-}4)$$

$$F(\varepsilon'_r) = 2/\,(1+\varepsilon'_r) \qquad (3\text{-}5)$$

In Equation 3-4, the term $|E_0|^2$ is the magnitude of square of the electric field inside the empty cavity, which is given by Equation 3-1. Upon substitution of Equation 3-1 for the electric field inside the empty cavity in equation 3-4, the dissipated power density would be as follows :

$$P_d = [\,4/(1+\varepsilon'_r)\,]\,(\,P_{fs,t}/V_c\,)\,\varepsilon''_r\,F_b(X)\,\mathrm{Sin}^2(\pi Z/L) \qquad (3\text{-}6)$$

$$F_b(X) = [J_0^2(X) + J_2^2(X) - 2J_0(X)J_2(X)\mathrm{Cos}(2\theta)\,]$$

Where $X = X'_{11}r/a = 1.8412\ r/a$

Since the radius of sample cell is much smaller than the radius of the cavity (e.g., radius of the cell is less than ten percent of the radius of cavity), the terms raised to a power higher than square can be neglected. Then Equation 3-6 reduces to the following :

$$P_d = [\,4/(1+\varepsilon'_r)\,]\,(P_{fs,t}/V_c)\,\varepsilon''_r\,F(r)\ \mathrm{Sin}^2(\pi Z/L) \qquad (3\text{-}7)$$

$$F(r) = [\,1 - (3/8)\,(X'_{11}r/a)^2\,]$$

$$\text{at } r = 0, \qquad 3/8\,(X'_{11}r/a)^2 = 0 \qquad (3\text{-}7a)$$

at r = 1.5 cm,	$3/8\ (X'_{11}r/a)2 = 0.01 << 1$	(3-7b)
at Z = 0,	$Sin^2(\pi Z/l) = 0$	(3-7c)
at Z = L/2,	$Sin^2(\pi Z/L) = 1$	(3-7d)

According to Equation 3-7, the dissipated power is directly proportional to the total input power in the cavity. It is directly proportional to dielectric loss for materials with low dielectric constant, however it is proportional to the ratio of dielectric loss to dielectric constant (e.g., tanδ) for materials that exhibit high dielectric constant. Also the dissipated power is a weak function of radius of the cell, according to Equation 3-7a and 3-7b, However, the dissipated power is a very strong function of height of the cell as demonstrated by Equations 3-7c and 3-7d.

Based on perturbation analysis for TE_{111} mode in a cylindrical cavity, the height of the sample has a significant effect on the dissipated power inside the sample, and therefore the sample height should be kept to a minimum. We recommend, for TE_{111} mode, disk-like geometry for the sample with radius of less than one centimeter and height at least fifty times less than the wavelength of microwave radiation to have uniform dissipated power inside the sample. We also recommend to position the sample in the center of cavity in the radial as well as axial direction to have uniform heating and maximum power dissipation.

3.1.3 Determination of dissipated power for high loss materials

If the sample has high dielectric constant and dielectric loss, the amount of energy stored and dissipated in the sample is no longer negligible, and it becomes comparable to the total stored energy inside the cavity. Under these conditions, the perturbation theory does not apply. In fact, once the cavity is loaded with a high loss material, the empty cavity modes are modified and become, in general, hybrid modes.

And depending on the material properties and placement of the sample inside the cavity, new cavity modes may be introduced. As a result, some of the assumptions in the previous section are violated for high loss materials. Consequently, there is no simple relationship between the electric field for the loaded and the empty unperturbed cavity, and Equation 3-1 is no longer applicable. The most general form for dissipated power density in a high loss material is presented by the following equation :

$$P_d = (\varepsilon_0/2)\ \omega\ \varepsilon''_r\ |E_{hybrid}\ E^*_{hybrid}|^2 = (\varepsilon_0/2)\ \omega\ \varepsilon''_r\ E_{hybrid}^2 \qquad (3\text{-}8)$$

Where ω = resonance frequency of the loaded cavity

E_{hybrid} = electric field for the loaded cavity hybrid mode

E^*_{hybrid} = complex conjugate of electric field for the loaded cavity

If the electric field is uniform throughout the volume of the sample, then Equation 3-8 can be integrated over the volume of the sample to obtain the total dissipated power presented by the following equation :

$$P_{d,t} = (\varepsilon_0/2)\ \omega\ \varepsilon''_r\ E_{hybrid}^2\ V_s \qquad (3\text{-}9)$$

Where V_s = volume of the sample

We should bear in mind that Equation 3-9 has serious limitations. In general, the dimensions of the sample should be at least twenty times smaller than the wavelength of microwave radiation so that the electric field and the material properties in the sample can be assumed uniform and homogeneous.

3.1.4. Macroscopic Energy Balance Around the Sample Cell

In this section, we make a macroscopic energy balance around the sample cell to relate the dissipated power to the rate of heating of the sample. The sample for making an energy balance is displayed in Figure 3-6. The control volume is selected as a disk with radius equal to the radius of sample and differential thickness equal to ΔZ. Note that it is assumed the temperature distributions in the radial and azimuthal directions are uniform, consistent with the theoretical distribution of power in the empty, completely closed, cavity and the theoretical dissipated power in the loaded cavity. The various contributions to the energy balance around the disk, displayed in Figure 3-6, are as follows :

rate of change in the internal energy of the disk =
rate of transfer of energy into and out of the disk by conduction +
rate of increase in energy of the disk by viscous heating +
rate of increase in energy of the disk by absorption of microwave energy +
rate of decrease in energy of the disk by free convection to atmosphere.

(3-10)

The above equation assumes that there is only temperature gradient in the axial direction. In general, the term due to viscous heating is negligible unless the rate of agitation is very fast and the sample is very viscous. The poly(amic acid) solution is not very viscous at temperatures above 140 degrees centigrade, and therefore the term due to viscous heating in Equation 3-10 can be neglected. Then the equation of energy for a newtonian fluid of constant density and heat capacity reduces to the following :

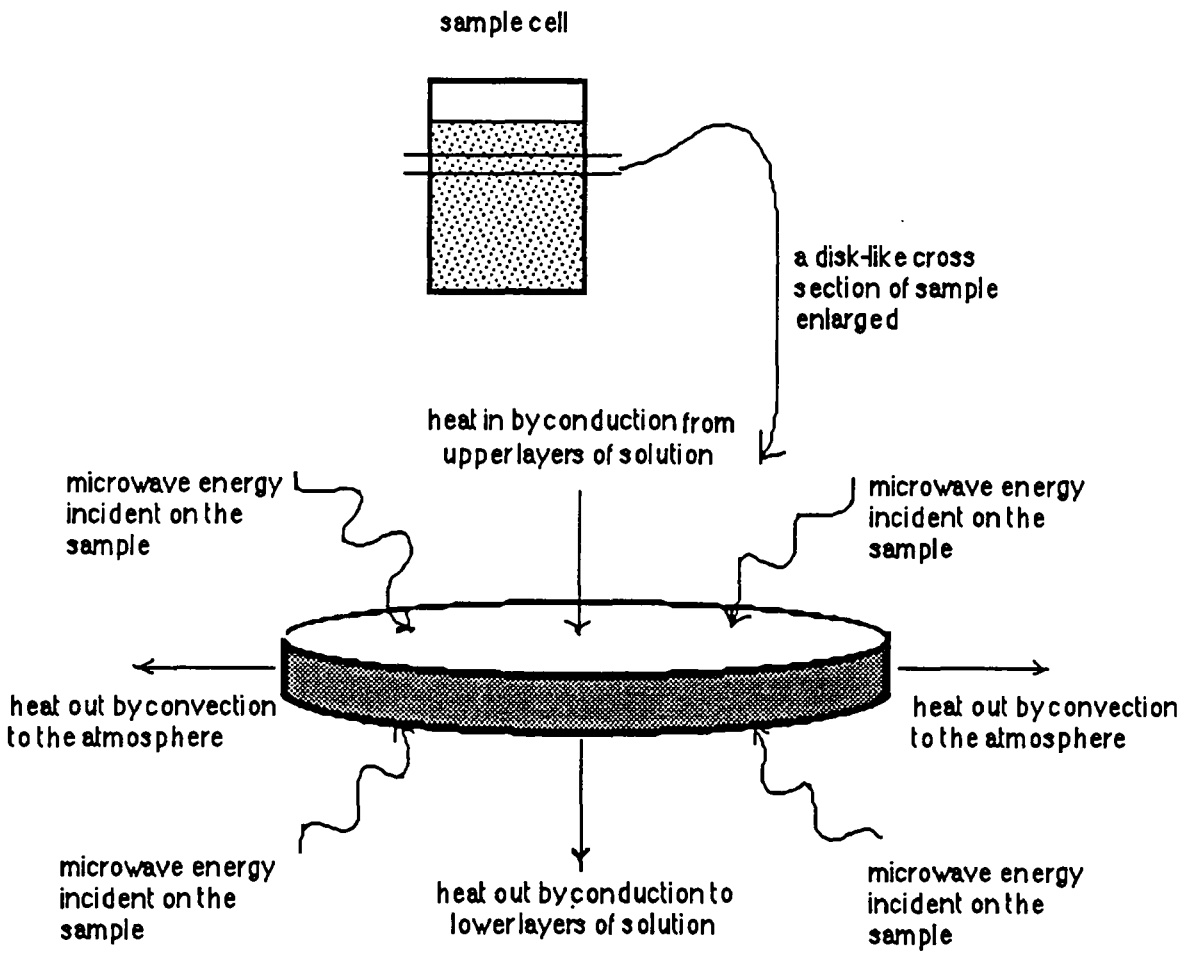

Figure 3-6: Control volume for making an energy balance around the sample.

$$\rho C_v \, dT_Z/dt = K_Z \, d^2T_Z/dZ^2 + P_d(Z) - hA_s \, [T_Z - T_0] \qquad (3\text{-}11)$$

Where ρ = density of the sample

C_v = constant volume heat capacity of the sample

T_Z = temperature of the sample as a function of axial direction

t = time

K_Z = thermal conductivity of the sample along the Z-direction

Z = axial direction or the Z-direction

Pd = dissipated power as a function of Z-direction in the sample

h = heat transfer coefficient between sample and the surrounding

A_s = surface area of the sample cell

T_0 = ambient temperature inside the cavity

The first and the third terms in Equation 3-11 are due to conduction inside the sample in the axial direction and convection to the outside, respectively. The conduction and convection terms in Equation 3-11 are evaluated for a typical fluid such as water, in Appendix 1. we have chosen liquid water for estimating the conduction and convection terms, because thermodynamic data for liquid water are available. According to the calculations in Appendix 1, the change in temperature of a section of the sample due to conduction inside and convection to outside is in the range of 1-10 degrees centigrade per minute for a typical liquid such as water. Note that for organic compounds and polymeric materials where the conductivity is smaller, the change in temperature due to conduction and convection would be even smaller than 1-10 degrees centigrade per minute.

On the other hand, Figure 3-8 displays the heating rate of poly(amic acid) solution at 140 degrees centigrade as a function of the incident microwave power, obtained from the slope of temperature-time profile displayed in Figure 3-7. The experimental results shown in Figures 3-7 and 3-8 are presented in the theory section to compare the rate of heating by absorption of microwave energy with conduction and convection heating. According to Figure 3-8, the heating rate of a section of the sample due to the application of microwave energy ranges from 100-400 degrees centigrade per minute, for incident power ranging from 10 to 50 watts, respectively. Comparison of Figure 3-8 with heating rate estimations in Appendix 1, suggests that the increase in heating rate due to absorption of microwave energy is at least an order of magnitude higher than the conduction inside the sample and convection to the outside. Conduction and convection terms in Equation 3-11 can be neglected compared to the dissipated microwave power inside the sample. Consequently, for microwave induced heating of materials, Equation 3-11 reduces to the following :

$$dT_Z/dt = (1/\rho C_v)\ P_d(Z) \qquad (3\text{-}12)$$

The preceding discussion on microwave induced heating versus conventional techniques such as conduction and convection reveals some of the characteristics of microwave heating of materials. Microwave heating can give rise to very fast heating rates only limited by the power incident on the material. Whereas, thermal oven heating rate is at least an order of magnitude smaller than microwave heating. This explains the different morphologies that are observed for block copolymers when cured via microwave radiation as opposed to thermal oven curing [7]. Also, microwave rate of heating is independent of the temperature difference

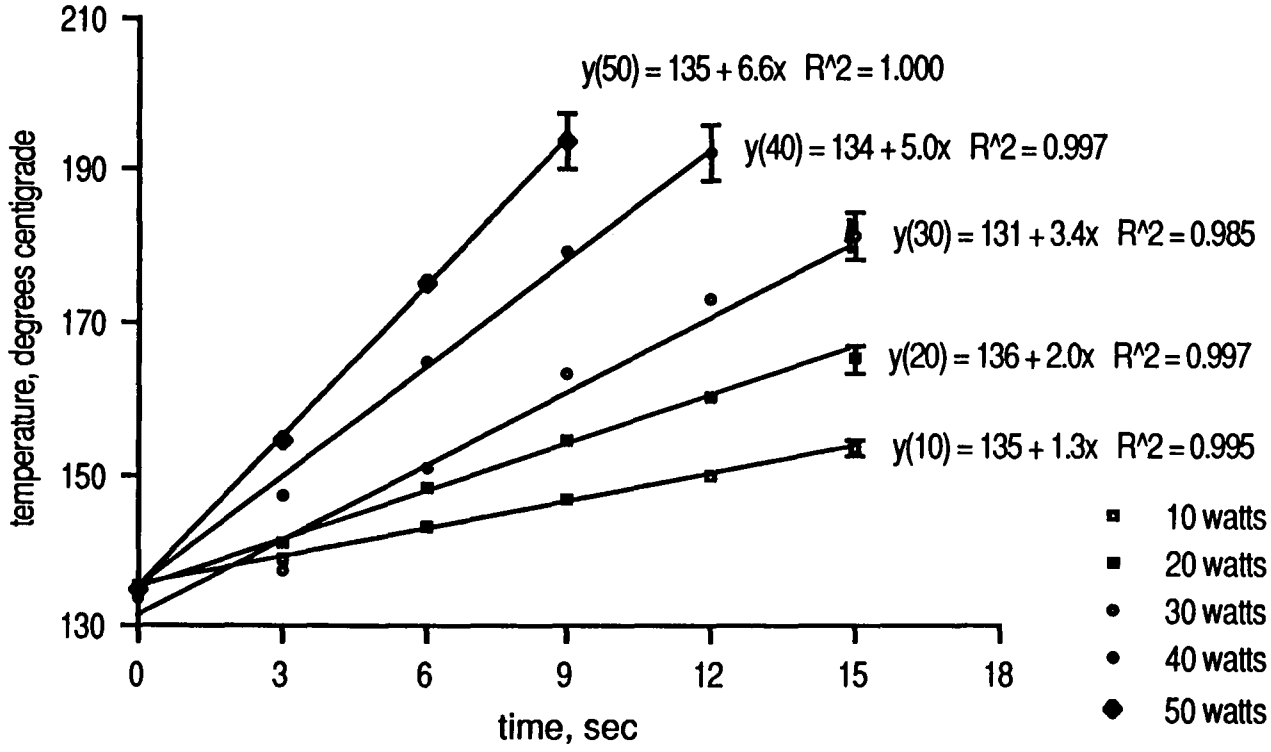

Figure3-7: Temperature-time profile for BTDA/pDDS based poly(amic acid) solution for different microwave powers at 140 C.

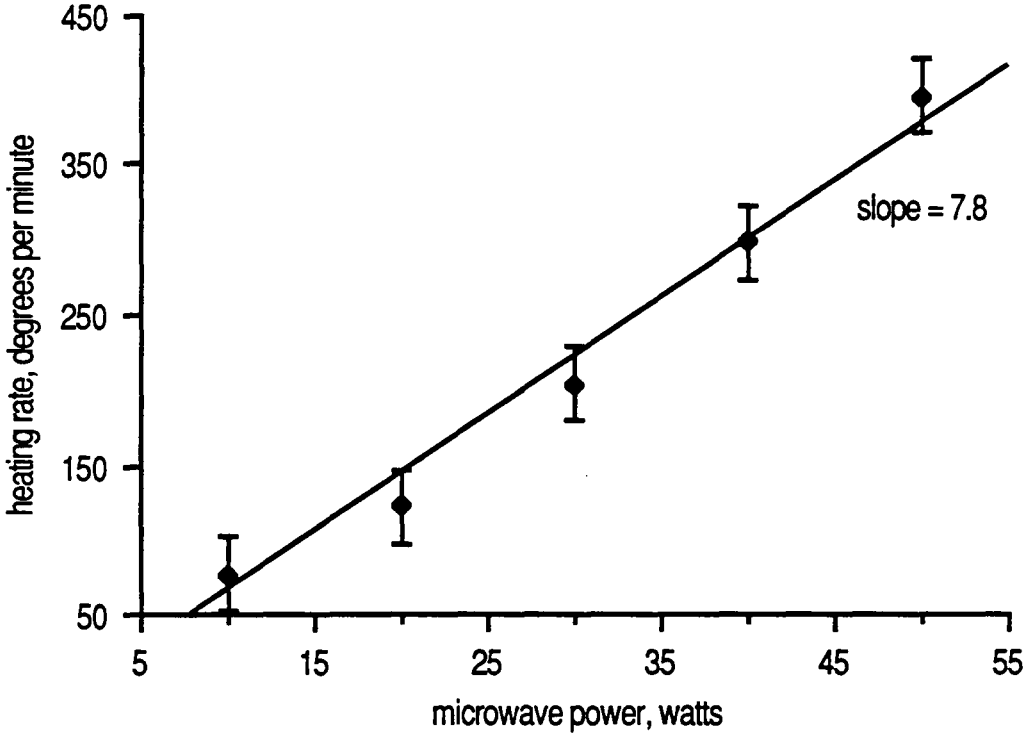

Figure 3-8: Heating rate of BTDA/pDDS based poly(amic acid) solution versus microwave power at 140 C.

sample and the source, whereas convection heating rate depends on the sample and source temperature, as displayed in Figure 3-9. According to Figure 3-9, the rate of convection heating decreases as the sample temperature approaches the source temperature. On the other hand, the rate of microwave heating is independent of the source temperature and can be controlled by the amount of power incident on the sample.

More importantly, if there is any temperature gradient in the sample due to non-uniform power distribution, these temperature gradients become very pronounced and cause the formation of "hot spots" that have been reported in the literature [31] for rubber curing with microwave radiation. The formation of "hot spots" with microwave radiation is due to 1) the slower rate of temperature redistribution by conduction and 2) the increase in dielectric loss with temperature near the glass transition temperature of the polymeric material.

From the preceding discussion, any temperature gradient in the sample can become very pronounced and significant because the redistribution of energy by conduction and convection is much slower than the rate of absorption of microwave radiation. The rate of heating of the sample can be related to the distribution of microwave power and the material properties by substituting for dissipated power from the previous section in Equation 3-12. For materials with low dielectric constant and dielectric loss Equation 3-7 applies and Equation 3-12 expands to the following :

$$dT_Z/dt = [4/(1+\varepsilon'_r)]\ (1/V_c\rho\ C_v)\ P_{fs,t}\ \varepsilon''_r\ F(r)\ \mathrm{Sin}^2(\pi Z/L)\ dV_s \qquad (3\text{-}13)$$

$$F(r) = 1-(3/8)\ (X'_{11}r/a)^2$$

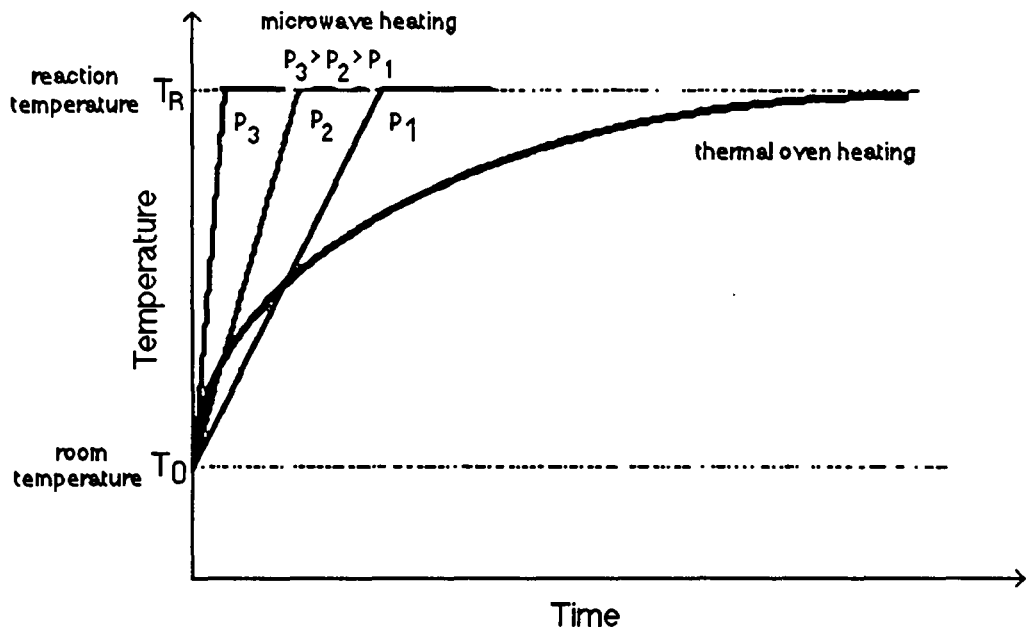

Figure 3-9: Schematic diagram of temperature-time profile for microwave and thermal oven heating.

According to Equation 3-13, for low loss materials, the rate of heating depends directly on the dielectric loss of the sample and the stored power in the cavity, and it is inversely proportional to the volume of cavity, density, and heat capacity of the sample. The rate of heating is a weak function of the radial direction, and therefore temperature gradient in the radial direction is negligible. On the other hand, the rate of heating is a very strong function of axial direction. Therefore, height of the sample should be kept to a minimum (e.g., less than 0.1 centimeter).

For materials with high dielectric loss, Equation 3-8 applies, and upon substitution Equation 3-12 becomes :

$$dT_Z/dt = (\varepsilon_0/2)\,(\omega/\rho C_v)\;\varepsilon''_r\;E_{hybrid}^2 \qquad (3\text{-}14)$$

If the electric field distribution is uniform in the sample, Equation 3-14 can be integrated over the volume of the sample to predict the sample temperature at any time.

3.2. Prediction of heating rate versus temperature near the glass transition temperature of polymers

3.2.1. Molecular motion in the solid state of polymers

The molecular motions or relaxations of polymers in the solid state have been extensively reviewed in the literature [67-69,79-80], and we only attempt to outline the basic modes of relaxation in amorphous and semi-crystalline polymers. For both semi-crystalline and amorphous polymers the spectra are broadly outlined in Figure 3-10 where tanδ (e.g., the ratio of dielectric loss to dielectric constant) versus

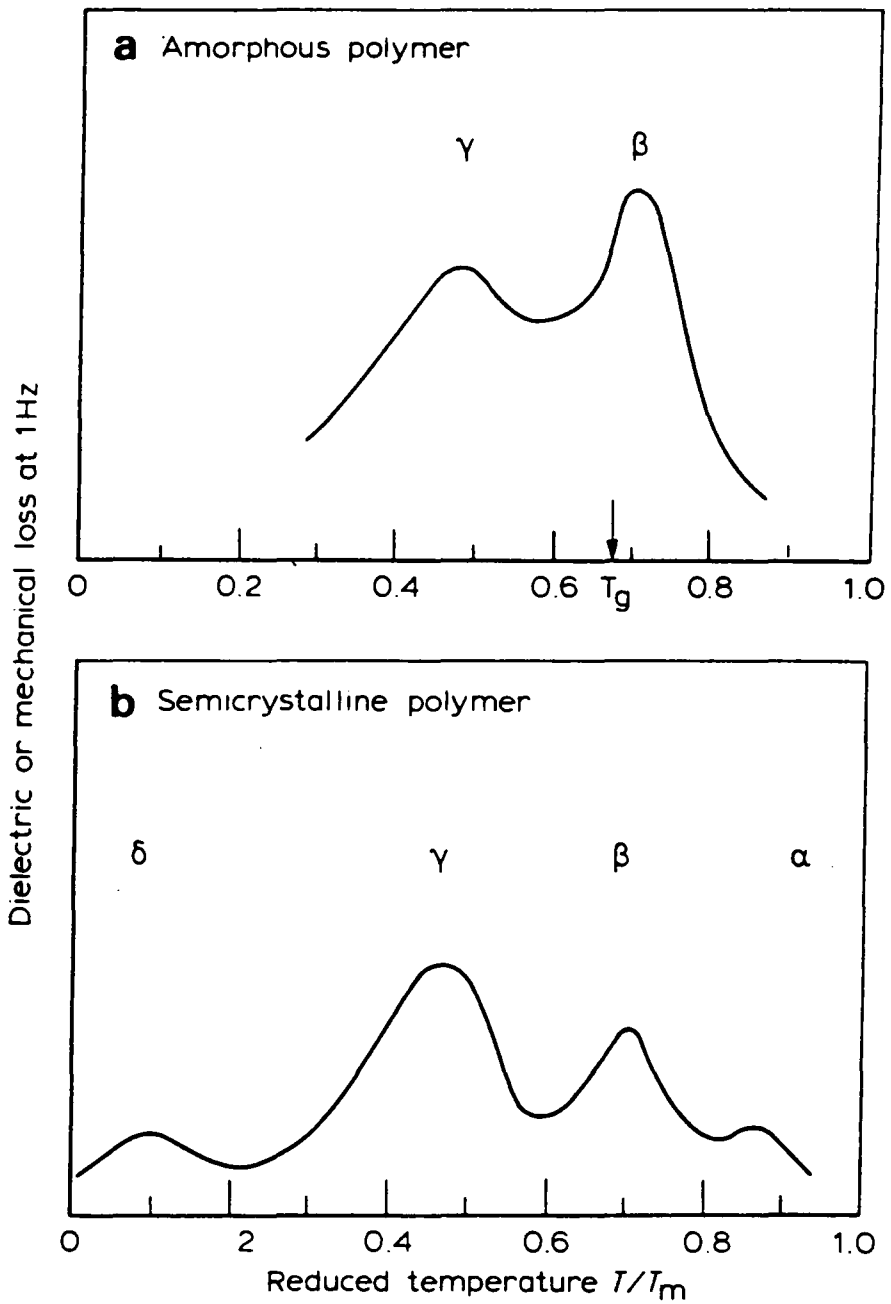

Figure 3-10: Schematic diagram of dielectric or mechanical loss at 1 Hz versus reduced temperature, T/T_m, where T_m is melting point temperature for a linear polymer molecule; T_g is the glass transition temperature [63]

temperature at constant frequency is schematically drawn. In this plot, the spectra are displayed using temperature as the independent variable, and the relationship between temperature and frequency is such that the lowest temperature loss peak will occur at the highest frequency.

For semi-crystalline polymers the spectrum has an α peak close to the melting temperature T_m, a β peak immediately above the glass transition temperature T_g, and a γ peak below the glass transition temperature due to the motion of side chains. A δ peak at lower temperatures has also been observed. For an amorphous polymer, the α peak is absent, and the β and γ peaks occur above and below the glass transition temperature.

When the temperature and frequency data for the loss peaks are plotted as the logarithm of maximum frequency (e.g., frequency of maximum dielectric loss), f_{max}, versus the inverse of the temperature, 1/T, a mapping of position of the loss peaks is seen such as that for poly(methylacrylate) displayed in Figure 3-11. Such a plot can be used to ascertain the potential for a polymer to have a loss peak at microwave frequencies for a given range of temperatures. It should be noted that, for all dispersions, the frequency of maximum absorption, f_{max}, moves to higher frequencies as the temperature increases.

3.2.2. Mechanism of dielectric absorption at microwave frequencies

The theory of dielectrics and the mechanism of dielectric absorption at microwave frequencies have been the subject of numerous articles in the literature [58-66,70-78,81]. Here we only attempt to present a brief summary of this broad subject.

The interaction of an electric field with a dielectric has its origin in the response of charge particles to the applied field. The displacement of these charge

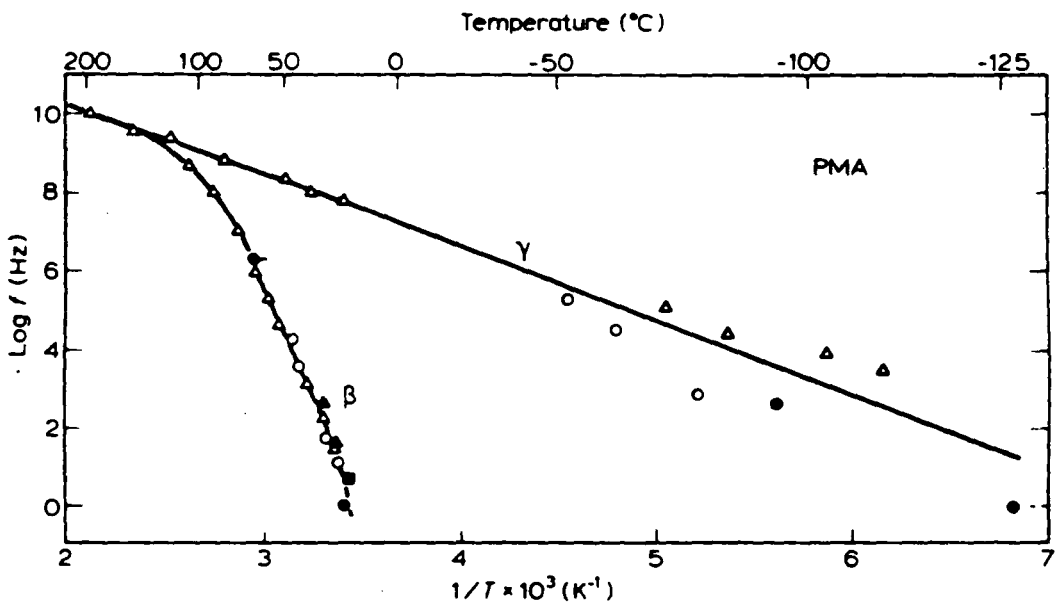

Figure 3-11: Plot of Log f_{max} versus 1/T for poly(methylacrylate); open data points are from dielectric data and closed points from mechanical data [63]

particles from their equilibrium position give rise to induced dipoles which respond to the applied field. Such induced polarization arises mainly from the displacement of electrons around the nuclei (electron polarization) or due to relative displacement of atomic nuclei because of the unequal distribution of charge in molecule formation (atomic polarization).

In addition to induced dipoles, polar dielectrics contain permanent dipoles due to asymmetric charge distribution of unlike charge partners in a molecule which tend to reorient under the influence of a changing electric field, thus giving rise to orientation polarization. Finally another source of polarization arises from charge build-up in interfaces between components in heterogeneous systems, termed interfacial, space charge, or Maxwell-Wagner polarization.

Figure 3-12 displays a schematic representation of electronic, atomic, dipole rotation (e.g., orientation polarization), and Maxwell-Wagner polarization due to an alternating electric field. Orientation polarization along with D.C. conductivity are the basis of high frequency heating of materials. However, the orientation polarization is the dominant mechanism of heating for polymeric materials in the microwave region.

The dielectric loss and dielectric constant for a glassy polymer are plotted in Figure 3-13 as a function of frequency to show the approximate frequencies at which polarization modes are operative. The resonance type losses resulting from atomic and electronic polarization are always observed in the visible and infra-red part of the spectrum, whereas the dipolar polarization is observed in the radio and microwave region of the spectrum. We should mention that the largest single source of data on dielectric properties of materials has been reports from the MIT insulation laboratory [82]. These data consist of dielectric measurements on commercially available

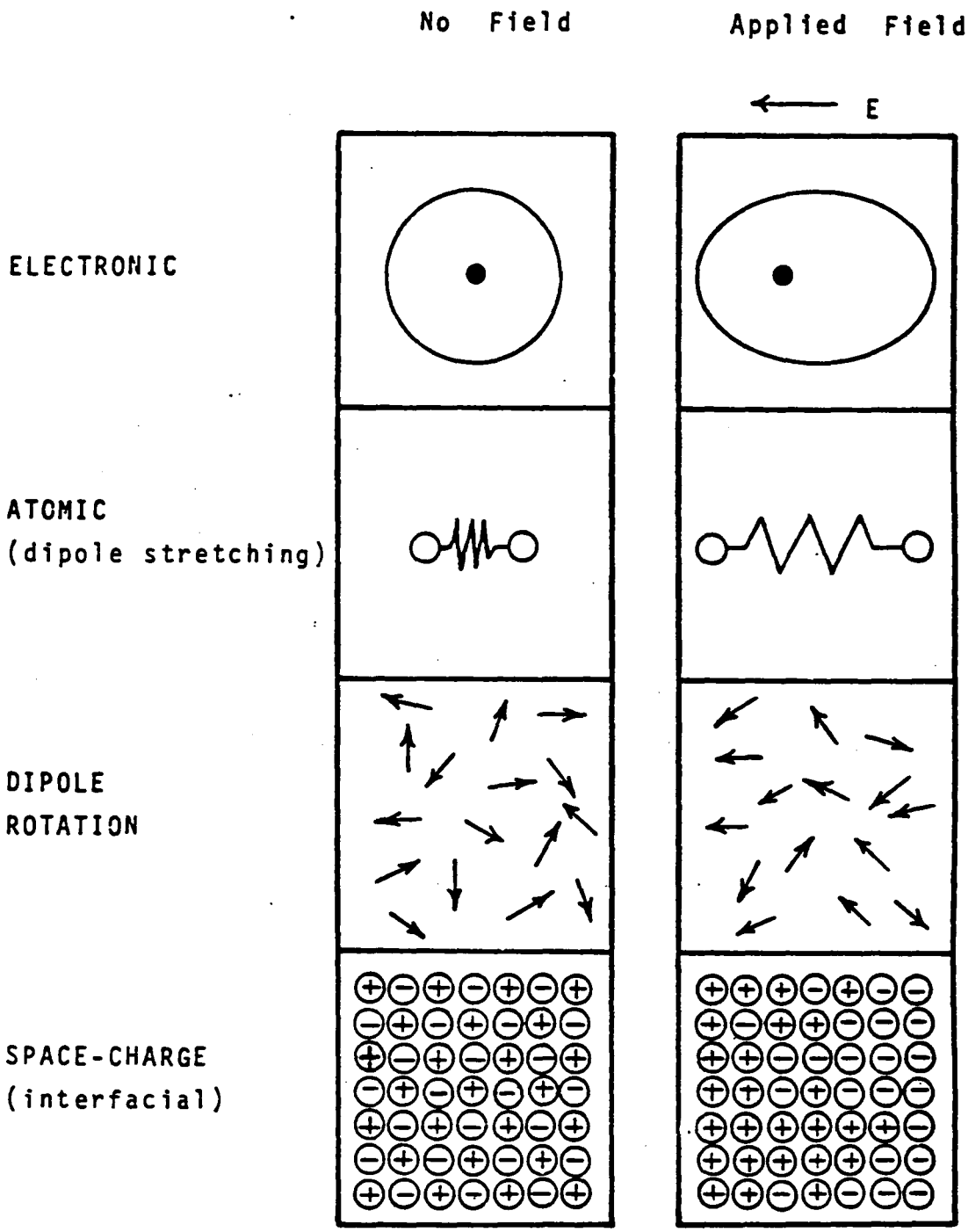

Figure 3-12: Polarization modes [106]

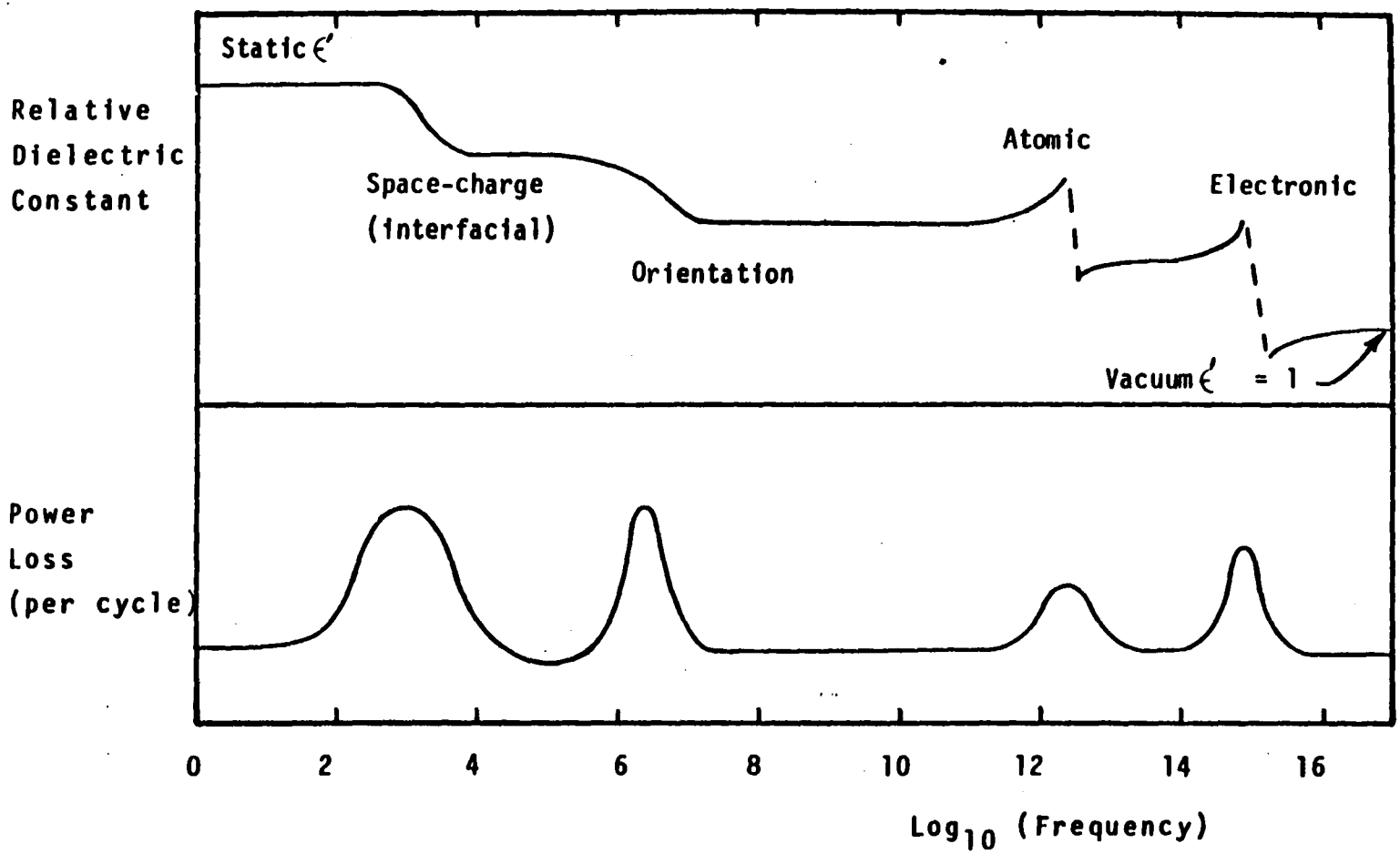

Figure 3-13: Approximate frequencies at which polarization modes are operative in glassy polymers [107]

polymer materials and composites as a function of frequency, temperature, and humidity.

3.2.3. Prediction of heating rate versus temperature near T_g

It is very well known that during the curing treatment of rubber, localized "hot spots" develop [31]. The cause for "hot spot" formation resides in thermal runaway due to the sharply rising temperature dependence of dielectric loss observed in some of the polymeric materials. It has also been observed that when a polymer passes through its glass transition temperature, there is a rapid rise in the rate of heating that causes the formation of "hot spots" [66]. It is essential to be able to predict the dependence of heating rate of polymers on temperature for precise control of temperature at any time.

Figure 3-14 displays the differences between the dielectric behavior of polar polymers at ultra-high frequencies and that at very low or at radio frequencies. At low frequencies, in addition to the β relaxation peak at T_g, which is associated with cooperative motions in the main chain, one or more secondary relaxations (e.g., γ, δ, etc.) are observed, associated with local motion in the main chain or to motions in side chains which become excited below the glass transition point. Finally in the softening region, another high loss region is noted (e.g., λ), characterized by a rapid increase of dielectric loss with increasing temperature, which is due to ionic conduction.

Passing from low to radio frequencies (e.g., up to 100 Khertz), the primary and secondary relaxation peaks are shifted toward higher temperatures, the former following an empirical WLF-type equation [98], the latter an Arrhenius-type equation. The difference in the activation energies for primary and secondary effects causes

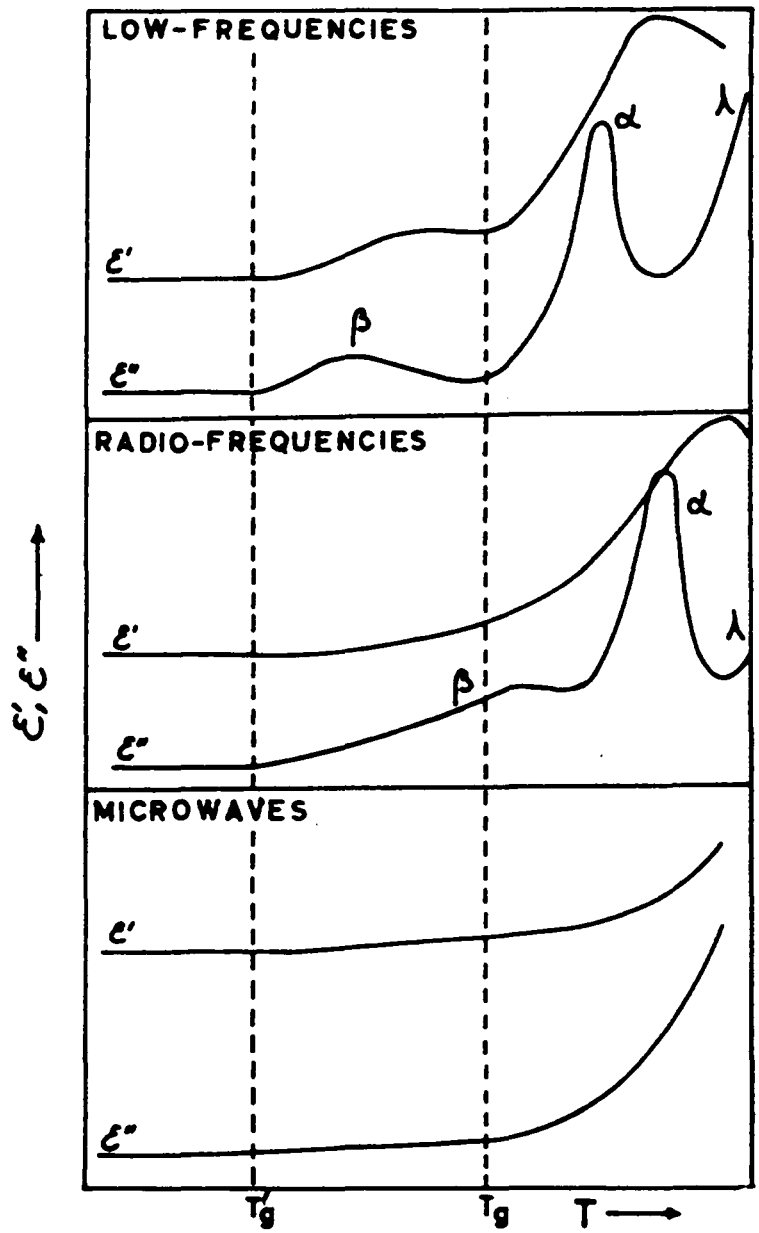

Figure 3-14: Schematic representation of the dielectric behavior (dielectric constant and loss factor) as a function of temperature for a hypothetical amorphous linear high polymer over different frequency ranges; T_g and T'_g are the temperatures for the onset of main chain and side chain motions of the polymer molecule, respectively [66]

progressive merging of the corresponding high-loss regions when frequency is increased.

Passing finally to ultra-high frequencies (e.g., microwave), all relaxation peaks, either primary or secondary, tend to merge into one peak above the glass transition temperature. The increase in dielectric loss above T_g is basically due to increased free volume of the polymer which in turn increases the mobility of dipoles. The emergence of one loss peak at microwave frequencies is what we attempt to predict theoretically in order to effectively control the temperature of polymeric materials heated with microwave radiation.

The macroscopic energy balance and two constitutive equations (e.g., an equation that relates a macroscopic variable to a molecular parameter) are required to predict the effect of temperature on the rate of heating of polymers near T_g. Figure 3-15 displays a typical heating rate data versus temperature for polymers at microwave frequency and at constant incident power. According to Figure 3-15, we define the following parameters:

$(dT/dt)_{max}$ = maximum heating rate

T_{max} = temperature corresponding to maximum heating rate

$\varepsilon''_{r,max}$ = relative dielectric loss at the temperature corresponding to maximum heating rate

The macroscopic energy balance relates heating rate to the dielectric loss of the sample. Assuming the conduction and convection heat transfer terms in the energy equation are negligible and the electric field in the sample is uniform, Equation 3-14 in the previous section applies. Rewriting Equation 3-14 once for any

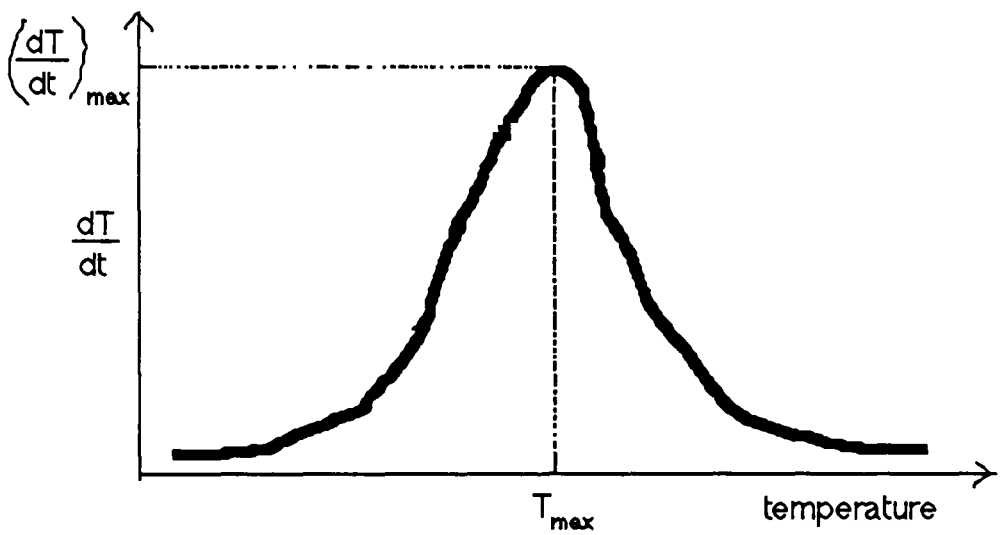

Figure 3-15: A schematic diagram of heating rate versus temperature near the glass transition temperature of polymers.

temperature, T, and again for the temperature corresponding to maximum heating rate, we have:

$$\text{at temperature T:} \quad dT/dt = (\varepsilon_0/2)\,(\omega/\rho C_v)\,\varepsilon''_r\,E_{hybrid}^2 \qquad (3\text{-}15a)$$

$$\text{at } T = T_{max}: \quad (dT/dt)_{max} = (\varepsilon_0/2)\,(\omega/\rho C_v)\,\varepsilon''_{r,max}\,E_{hybrid}^2 \qquad (3\text{-}15b)$$

Note that, in general, the electric field in the loaded cavity is a function of temperature due 1) to changes in dielectric constant and dielectric loss below and above T_g, and 2) to volume expansion of the sample. However, if the sample geometry is disk-type and the sample dimensions are much smaller than dimensions of the cavity (e.g., see section 3.1.1), then the assumption of a temperature independent electric field is satisfied. Division of Equation 3-15a by equation 3-15b results in the following equation:

$$(dT/dt) = (dT/dt)_{max}\,(\varepsilon''_r/\varepsilon''_{r,max}) \qquad (3\text{-}16)$$

One constitutive equation is required to relate the relaxation frequency or the relaxation time constant to temperature. We can apply either the Flory-Huggins [98] or the Arrhenius equation to relate relaxation frequency of dipoles to temperature. However, as displayed in Figure 3-11 for poly(methylacrylate), the frequency dependence of the dielectric loss peaks for Flory-Huggins and Arrhenius equation converge at microwave frequencies. Therefore, either one of these equations can be applied. Using the Arrhenius equation, we define the following relationships:

$$\text{for temperature T:} \quad f = 1/\tau = Ae^{-\Delta E/RT} \qquad (3\text{-}17a)$$

For $T = T_{max}$: $$f_{max} = 1/\tau_{max} = Ae^{-\Delta E/RT_{max}} \quad (3\text{-}17b)$$

Where f = relaxation frequency of dipoles at temperature T

f_{max} = relaxation frequency of dipoles at the temperature corresponding to maximum heating rate

τ = relaxation time constant of dipoles at temperature T

τ_{max} = relaxation time constant of dipoles at the temperature corresponding to maximum heating rate

A = Arrhenius equation front factor

ΔE = activation energy for relaxation of dipoles

R = gas constant = 1.987×10^{-3} Kcal/gmole/K

Assuming the activation energy for relaxation of dipoles is independent of temperature, division of Equation 3-17a by 3-17b results in the following equation:

$$f/f_{max} = e^{-\Delta E/R\,(1/T - 1/T_{max})} \quad (3\text{-}18)$$

Another constitutive equation is required to relate the dielectric loss of the sample to the relaxation frequency of dipoles. We can apply the Debye [71,72] equation that assumes there is no interaction between the dipoles or the Cole-Cole [59-62] equation which takes into account the interaction between dipoles. The Debye equation as well as Cole-Cole equation assume there is only one relaxation time constant. The Cole-Cole equation has been shown to describe the dielectric properties of polymers better than the Debye equation, however we also consider the Debye equation for comparison.

3.2.3.1. Rate of heating versus Temperature with Debye equation

According to Debye equation, the complex permittivity of a dielectric is described by the following equation:

$$\varepsilon^*_r = \varepsilon'_r - i\varepsilon''_r = \varepsilon_\infty + (\varepsilon_s - \varepsilon_\infty) / (1+i\omega\tau) \qquad (3\text{-}19)$$

Where ε^*_r = Complex permittivity of the polymer sample

ε_∞ = dielectric constant of the sample at infinite frequency

ε_s = static dielectric constant of the polymer sample

ω = frequency of the external field, Hz

$\tau = 1/f$ = relaxation time constant of dipoles

i = denotes imaginary number = $(-1)^{1/2}$

Equation 3-19 assumes that the dipoles act independently from each other and the relaxing moieties have only one relaxation time constant. Equation 3-19 can be separated into the real and the imaginary components to give the dielectric constant and the dielectric loss, respectively, as presented below:

$$\varepsilon'_r = \varepsilon_\infty + (\varepsilon_s - \varepsilon_\infty)/(1+\omega^2\tau^2) \qquad (3\text{-}20a)$$

at temperature T: $\varepsilon''_r = \omega\,\tau\,(\varepsilon_s - \varepsilon_\infty) / (1+\omega^2\tau^2)$ (3-20b)

at $T = T_{max}$: $\varepsilon''_{r,max} = \omega\,\tau_{max}\,(\varepsilon_s - \varepsilon_\infty) / (1+\omega^2\tau_{max}^2)$ (3-20c)

Division of Equation 3-20b by equation 3-20c results in the following relationship :

$$(\varepsilon''_r/\varepsilon''_{r,max}) = (\tau/\tau_{max}) / [1+(\tau/\tau_{max})^2] = (f_{max}/f) / [1+(f_{max}/f)^2] \qquad (3\text{-}21)$$

Combining Equations 3-16, 3-18, and 3-21 result in the following equation that relates the heating rate of the sample to temperature :

$$(dT/dt)_n = (dT/dt)_{max} [\, 2F_d/(1+F_d) \,] \qquad (3\text{-}22)$$

Where $F_d = e^{-\Delta E/R\,(1/\,T_{max}-1/\,T)}$

$(dT/dt)_n = (dT/dt)/(dT/dt)_{max}$ = normalized heating rate

Table 3-3 lists the normalized heating rate as a function of temperature calculated using Equation 3-22 for T_{max} equal to 350 degrees Kelvin and activation energies of 8 and 12 kilocalories per gram mole, respectively. The data in Table 3-3 is also displayed graphically in Figure 3-16. The heating rate based on Debye equation has only one adjustable parameter, namely the activation energy. As the activation energy decreases, the absorption spectrum becomes broader and unsymmetrical. The absorption spectrum of polymers is broader and more symmetrical than what the Debye equation predicts. Therefore, the Debye equation is not satisfactory for describing the absorption spectrum of polymers.

3.2.3.2. Rate of heating versus temperature with Cole-Cole equation

According to Cole-Cole equation, the complex permittivity of a dielectric is given by the following equation:

$$\varepsilon^*_r = \varepsilon'_r - i\varepsilon''_r = \varepsilon_\infty + (\varepsilon_s-\varepsilon_\infty) / [1+(i\omega\tau)^{1-\sigma}] \qquad (3\text{-}23)$$

Equation 3-23 contains two adjustable parameters which are the relaxation time constant of dipoles τ, and the parameter σ. The parameter σ is a measure of interaction between the dipoles. The interaction between the dipoles arise from 1)

Table 3-3: Heating rate versus temperature near T_g using Debye equation

temperature, °C	dT/dt, ΔE=8 Kcal per mole	dT/dt, ΔE=12 Kcal per mole
250	0.0201	0.002
260	0.0373	0.005
270	0.0661	0.012
280	0.112	0.0268
290	0.184	0.056
300	0.288	0.112
305	0.354	0.156
310	0.431	0.213
315	0.517	0.288
320	0.61	0.382
325	0.705	0.496
330	0.798	0.626
335	0.881	0.761
340	0.945	0.884
350	1	1
360	0.951	0.895
365	0.898	0.792
370	0.834	0.681
375	0.764	0.575
380	0.694	0.481
385	0.626	0.399
390	0.562	0.331
395	0.503	0.275
400	0.45	0.228
405	0.402	0.19
410	0.359	0.159
415	0.321	0.133
420	0.288	0.112
425	0.258	0.095
430	0.232	0.0806
435	0.209	0.0686
440	0.188	0.0586
445	0.17	0.05
450	0.154	0.043
460	0.127	0.032
470	0.106	0.024
480	0.0885	0.019
490	0.0747	0.0145
500	0.0634	0.0113

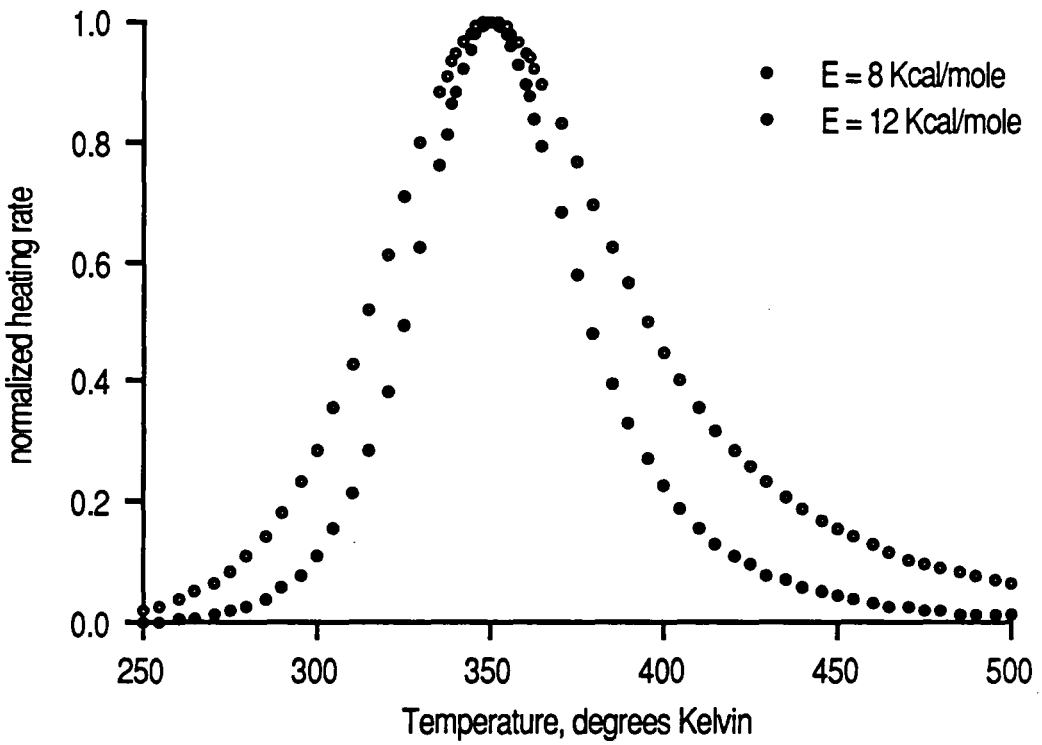

Figure 3-16: Normalized heating rate versus temperature near Tg predicted by Debye equation for two different activation energies.

dipoles interaction due to connectivity to the same macromolecular chain, 2) intramolecular interaction on the same, and 3) intermolecular interaction between two chains. Equation 3-23 can be separated into real and imaginary parts to give the dielectric constant and the dielectric loss as presented below:

$$\varepsilon'_r = \varepsilon_\infty + [(\varepsilon_s-\varepsilon_\infty)/2] \{1-\mathrm{Sinh}(X_c) / [\mathrm{Cosh}(X_c)+\mathrm{Cos}(\pi\sigma/2)] \} \qquad (3\text{-}24a)$$

$$\varepsilon''_r = [(\varepsilon_s-\varepsilon_\infty)/2] \{\mathrm{Cos}(\pi\sigma/2) / [\mathrm{Cosh}(X_c)+\mathrm{Sin}(\pi\sigma/2)] \} \qquad (3\text{-}24b)$$

Where $X_c = (1-\sigma)\,\mathrm{Ln}(\omega\tau)$

The parameter σ varies between zero and one and is a measure of interaction between the dipoles. If there is no interaction between the dipoles, the value of σ is zero. As the interaction between the dipoles increases, the value of σ increases from zero and approaches one for infinite interaction between the dipoles. Equation 3-24b also applies for dielectric loss at the temperature corresponding to maximum heating rate as presented below:

$$\text{at } T = T_{max}: \quad \varepsilon''_{r,max} = [(\varepsilon_s-\varepsilon_\infty)/2] \{\mathrm{Cos}(Y_c) / [\mathrm{Cosh}(X_{c,max})+\mathrm{Sin}(Y_c)] \} \qquad (3\text{-}24c)$$

Where $X_{c,max} = (1-\sigma)\,\mathrm{Ln}(\omega\tau_{max})$

$Y_c = \pi\sigma/2$

Division of Equation 3-24b by 3-24c results in the following relationship ::

$$\varepsilon''_r/\varepsilon''_{r,max} = \{\mathrm{Cosh}(X_{c,max})+\mathrm{Sin}(Y_c)\} / \{\mathrm{Cosh}(X_c)+\mathrm{Sin}(Y_c) \} \qquad (3\text{-}25)$$

This equation has been shown [61] to fit the relaxation spectrum of polymers at microwave frequencies if the dielectric data is in the frequency range of 10 MHz to 10 GHz. However, extrapolation of dielectric data from frequencies lower than 10 MHz to microwave frequencies is not recommended. Combining Equations 3-16, 3-18, and 3-25 result in the following equation which is the relationship between heating rate of the sample and temperature:

$$(dT/dt)_n = \{ [1+\mathrm{Sin}(Y_c)] / [\mathrm{Cosh}(F_c)+\mathrm{Sin}(Y_c)] \} \qquad (3\text{-}26)$$

Where $F_c = (1-\sigma)(-\Delta E/R)(1/T_{max}-1/T)$

$Y_c = (\pi\sigma/2)$

$(dT/dt)_n = (dT/dt) / (dT/dt)_{max}$

Table 3-4 lists the normalized heating rate as a function of temperature calculated using the Cole-Cole equation for T_{max} equal to 350 degrees Kelvin and activation energy of 12 kilocalories per gram mole. Equation 3-26 is evaluated for parameter σ equal to zero, 0.1, 0.2, and 0.3, respectively. The data in Table 3-4 is also displayed graphically in Figure 3-17. According to Figure 3-17, at constant activation energy, as the value of parameter σ increases from zero to o.3, the absorption spectrum becomes broader. The broader heating rate spectrum predicted by Cole-Cole model is a better representation of polymeric materials. Therefore, the Cole-Cole model is preferred for prediction of the relaxation spectrum and the heating rate of polymers at microwave frequencies as opposed to Debye model.

3.3. Kinetics of Imidization of Poly(amic acids)

Table 3-4 : Heating rate versus temperature near T_g using Cole-Cole equation

	ΔE=12 Kcal per mole			
temperature, °C	dT/dt, σ=0	dT/dt, σ=0.1	dT/dt, σ=0.2	dT/dt, σ=0.3
250	0.002	0.0046	0.0104	0.023
260	0.005	0.011	0.0219	0.0438
270	0.012	0.0231	0.0434	0.079
280	0.0268	0.0473	0.0814	0.136
290	0.056	0.092	0.145	0.221
300	0.112	0.169	0.245	0.341
305	0.156	0.225	0.311	0.414
310	0.213	0.294	0.389	0.495
315	0.288	0.379	0.479	0.582
320	0.382	0.478	0.577	0.671
325	0.496	0.59	0.679	0.758
330	0.626	0.708	0.779	0.838
335	0.761	0.821	0.869	0.907
340	0.884	0.916	0.94	0.958
350	1	1	1	1
360	0.895	0.924	0.946	0.962
365	0.792	0.846	0.888	0.92
370	0.681	0.756	0.818	0.868
375	0.575	0.664	0.742	0.81
380	0.481	0.576	0.667	0.748
385	0.399	0.496	0.594	0.686
390	0.331	0.426	0.526	0.625
395	0.275	0.364	0.464	0.568
400	0.228	0.312	0.408	0.514
405	0.19	0.267	0.359	0.465
410	0.159	0.229	0.316	0.419
415	0.133	0.196	0.278	0.378
420	0.112	0.169	0.245	0.341
425	0.095	0.146	0.216	0.308
430	0.0806	0.126	0.191	0.278
435	0.0686	0.109	0.169	0.251
440	0.0586	0.095	0.149	0.227
445	0.05	0.083	0.133	0.205
450	0.043	0.0726	0.118	0.186
460	0.032	0.056	0.0942	0.154
470	0.024	0.0436	0.076	0.128
480	0.019	0.0343	0.061	0.107
490	0.0145	0.0273	0.05	0.09
500	0.0113	0.0219	0.041	0.076

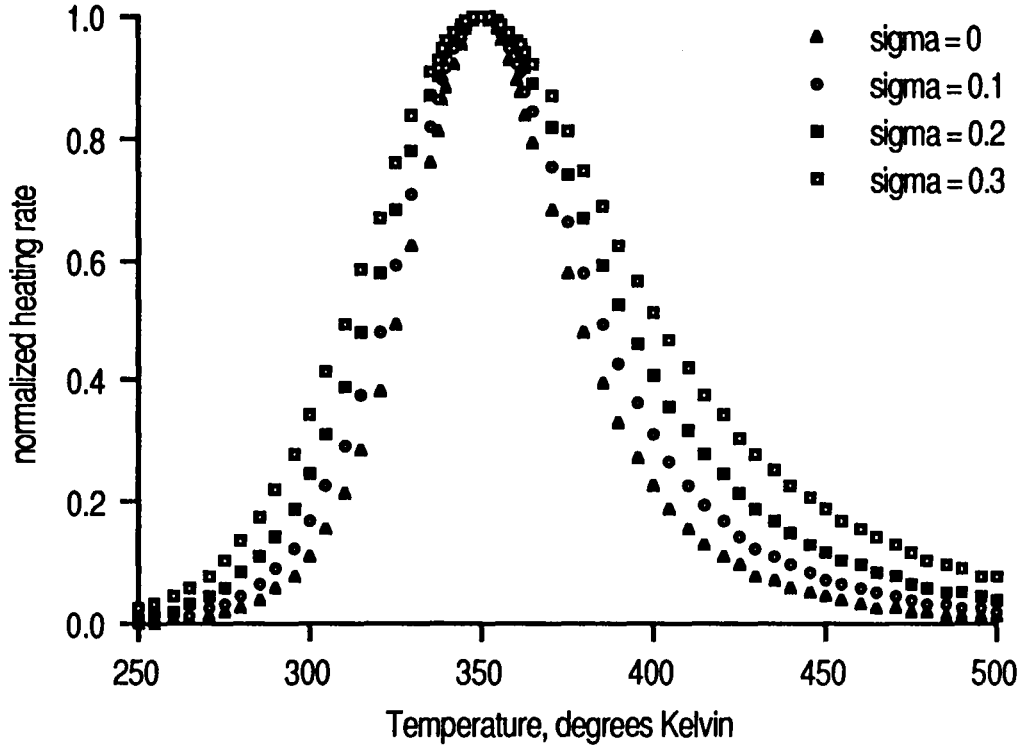

Figure 3-17: Normalized heating rate versus temperature near Tg predicted by Cole-Cole equation for E=12 Kcal/mole and different values of the interaction parameter.

Polyimides are formed by thermal cyclization of poly(amic acids) [85-87]. The poly(amic acid) precursor is formed by the reaction of two monomers, a dianhydride and a diamine. Figure 3-18 displays the first step in the synthesis of polyimides in which a diamine and a dianhydride react to form the poly(amic acid) presursor. The second step is the formation of the five membered ring to produce the polyimide.

The second step can be carried out in either bulk [88] or solution [83]. In the former method, high temperatures are required to keep the reacting polymer above its glass transition temperature. In the latter method, the imidization reaction takes place in solution and the final polyimide is soluble in a variety of polar aprotic solvents such as 1-methyl-2-pyrrolidinone (NMP). The solution imidization method is used exclusively in our studies, because the reaction takes place in a homogeneous solution.

The solution imidization is carried out in a 20 to 80 percent by volume mixture of 1-cyclohexyl-2-pyrrolidinone (CHP) and 1-methyl-2-pyrrolidinone (NMP), respectively. The co-solvent CHP is used as an azeotroping agent to remove the water from the solution as it is formed by the imidization reaction. Figure 3-19 displays the second step of polyimide formation by the solution imidization method. It is the second step of the polyimide synthesis that we have studied for comparison of thermal, continuous , and pulsed microwave radiation curing of polymers.

During the imidization step the reactions shown in Figure 3-20 can occur. The first reaction in Figure 3-20 is the intramolecular imidization of amic acid and amine groups on the same polymer chain. The second reaction is the intermolecular imidization of amic acid and amine groups on two different polymer chains. Finally, the third reaction in Figure 3-20 is the reaction of water with the imide moieties that cause the degradation of the polyimide.

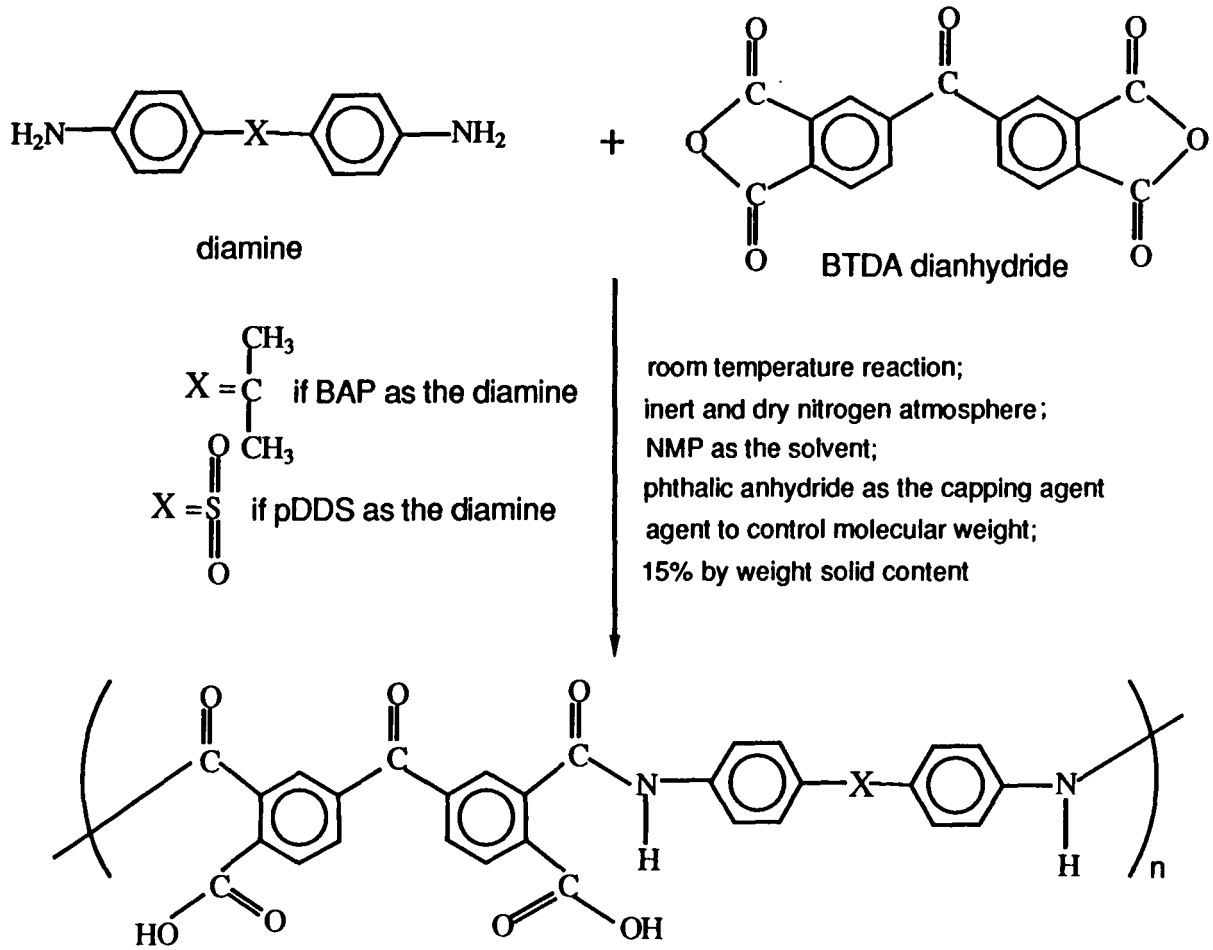

Figure 3-18: Reaction scheme for the synthesis of poly(amic acid) precursor

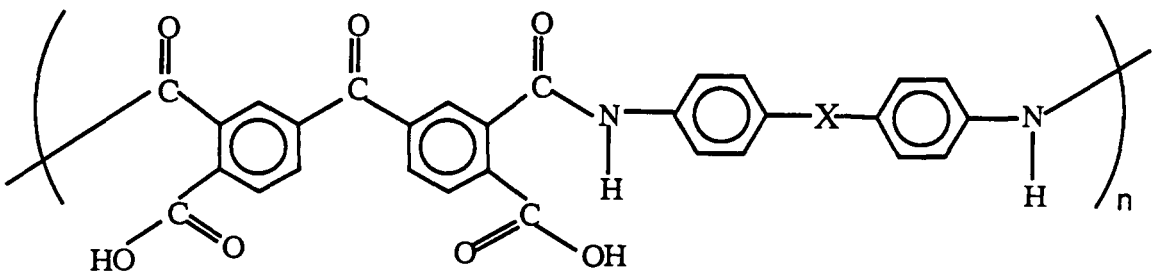

poly(amic acid)

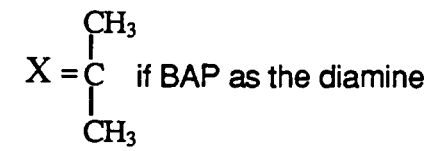

if BAP as the diamine

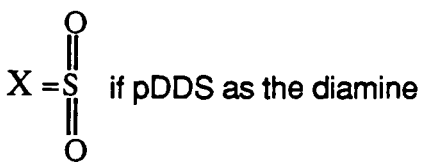

if pDDS as the diamine

temperature = 140 C;

inert and dry nitrogen atmosphere;

80/20 by volume NMP/CHP solvent mixture;

15% by weight solid content;

number average M.W. = 20,000 gr/mole

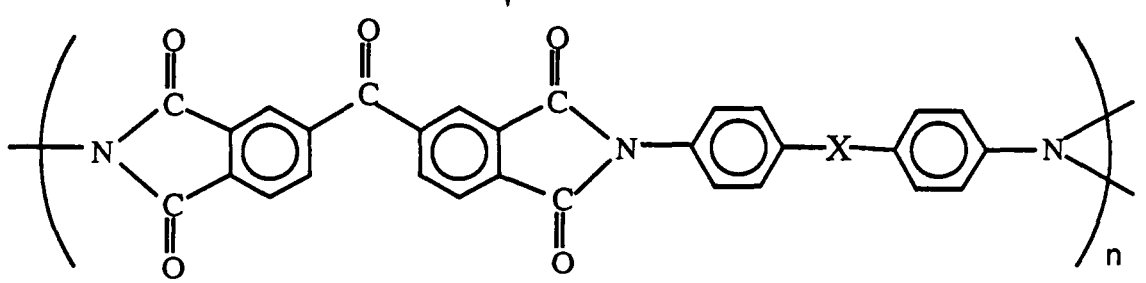

polyimide

Figure 3-19: Reaction scheme for the imidization of poly(amic acid)

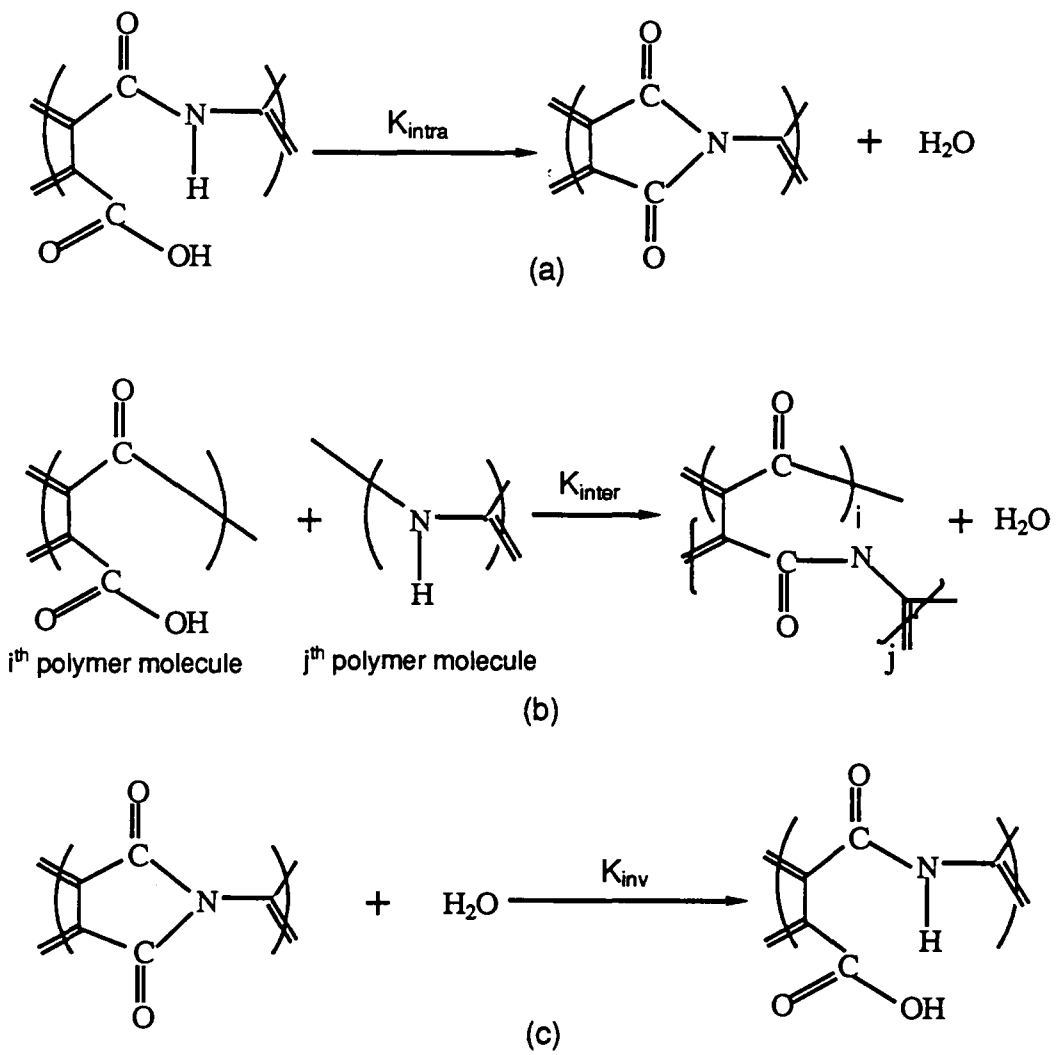

Figure 3-20: Possible reaction pathways for the imidization of poly(amic acids); (a) intramolecular, (b) intermolecular, and (c) inverse imidization.

It is also known that the solvent NMP is strongly hydrogen bonded to amic acid groups as shown in Figure 3-21 and is known to play an important role in the imidization reaction [99]. Therefore, the concentration or the fraction of the polymer in solution may influence the rate of imidization reaction. Based on reactions in Figures 3-20 and 3-21, the rate of imidization reaction can be written as follows :

$$R_i = -dC_a/dt = K_{intra}F(C_p)C_a + K_{inter}F(C_p)C_a^2 - K_{inv}F(C_p)C_IC_{H2O} \quad (3\text{-}27)$$

Where R_i = rate of the imidization reaction

C_a = concentration of the amic acid groups

t = time in seconds

K_{intra} = intramolecular imidization rate constant

$F(C_p)$ = a function depending on the concentration or fraction of the polymer in solution

K_{inter} = intermolecular imidization rate constant

K_{inv} = rate constant for the inverse reaction

C_I = concentration of the imide groups

C_{H2O} = Concentration of water in solution

The function $F(C_p)$, in Equation 3-27, compensates for the dependence of reaction rate on the concentration of polymer. This is because the solvent NMP is known to play an important role in the imidization reaction.The reaction has to be carried out under moisture free conditions as the imidization proceeds, because moisture degrades the polyimide as shown by the third reaction in Figure 3-20. The role of the co-solvent CHP is as an azeotroping agent to remove water from the

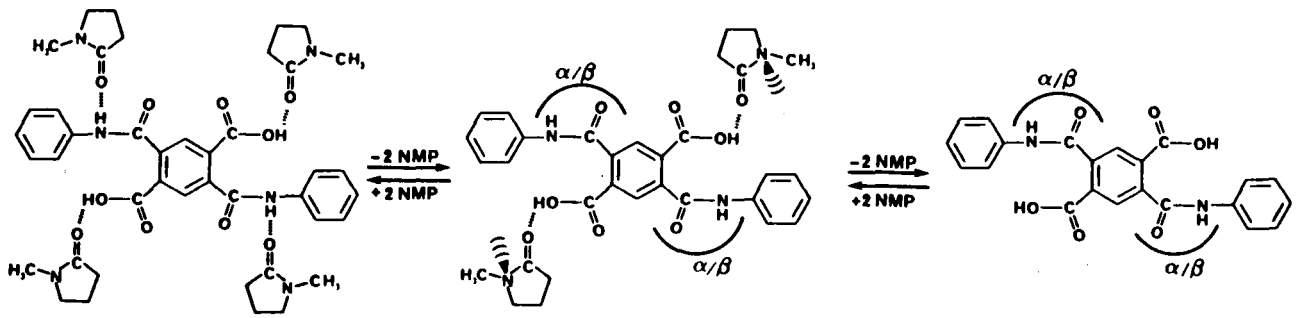

Figure 3-21: Complexation/decomplexation process: α/β indicates the possibility of two different molecular surroundings; •))) indicates the possibility of involvement into hydrogen bonding [99]

solution as it is formed by the imidization reaction. Figure 3-22 shows the concentration of water versus temperature for CHP, NMP, and a NMP/CHP (80/20) co-solvent mixture. According to Figure 3-22, the concentration of water in a NMP/CHP co-solvent mixture is less than 100 parts per million at 140 degrees centigrade reaction temperature. Therefore, the concentration of water in solution is negligible and the third term in Equation 3-27 can be eliminated.

The intermolecular imidization causes the formation of a three dimensional network and the polyimide becomes insoluble, if the rate of intermolecular imidization is significant. However, the polyimide synthesized by solution imidization has been shown to dissolve in a variety of polar aprotic solvents such as NMP [83]. Therefore, the rate of intermolecular imidization is negligible compared to intramolecular imidization, and the second term in Equation 3-27 can also be eliminated. Consequently, Equation 3-27 reduces to the following :

$$R_i = -dC_a/dt = K_{intra}\, F(C_p)\, C_a \qquad (3\text{-}28)$$

The function $F(C_p)$ relates the reaction rate to the concentration or the fraction of polymer in solution. The fraction of the poly(amic acid) in solution is kept constant at 15 percent by weight for all of the experiments. Therefore, we can define a new rate constant, K_e, such as the following:

$$K_e = K_{intra}\, F(C_p) \qquad (3\text{-}29)$$

and

$$R_i = -dC_a/dt = K_e\, C_a \qquad (3\text{-}30)$$

with initial condition : at $t = 0$ $\quad C_a = C_{a,0}$

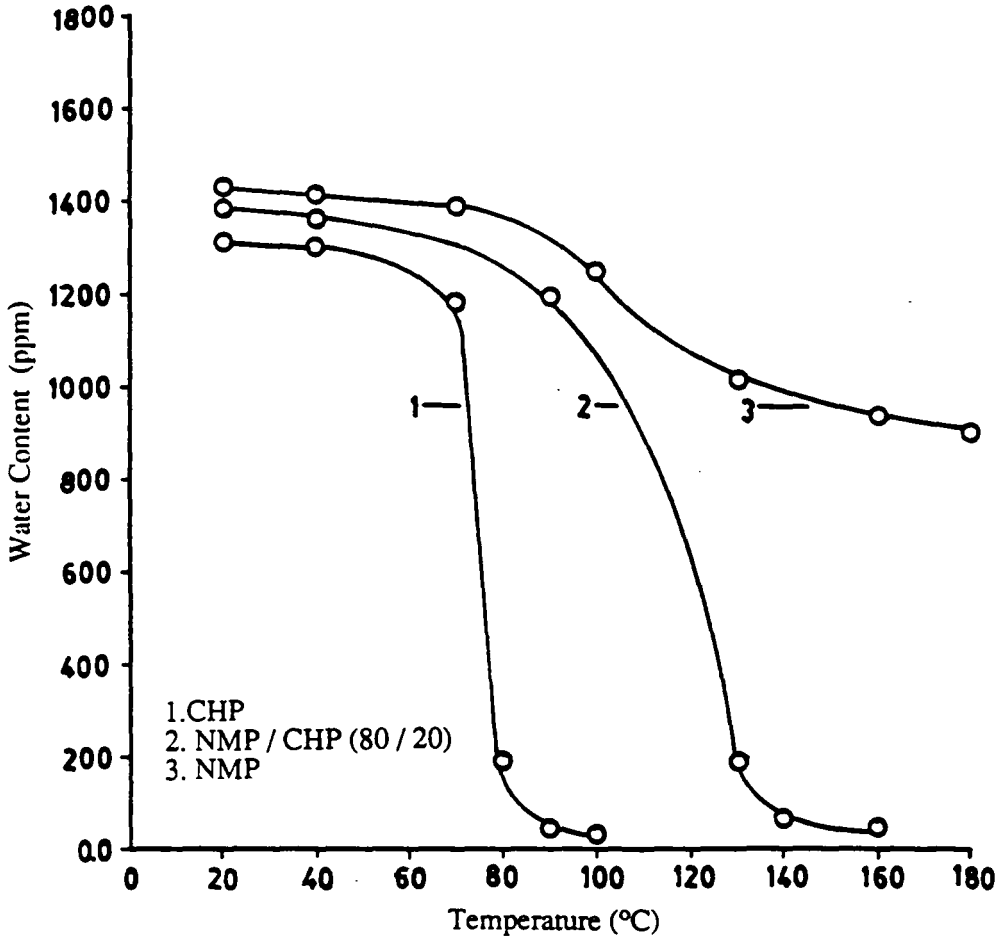

Figure 3-22: Water content versus temperature for CHP, NMP, and an NMP/CHP (80/20) co-solvent mixture; heating rate was approximately 3°C per minute [83]

Where K_e = effective rate constant for solution imidization of poly(amic acids)

The rate equation can also be written in terms of the concentration of the imide group as shown by the following equation:

$$R_i = dC_I/dt = K_e (C_{I,\infty} - C_I) \qquad (3\text{-}31)$$

with initial condition : at $t = 0$ $C_I = 0$

Where $C_I = C_{a,0} - C_a = C_{I,\infty} - C_a$

$C_{I,\infty}$ = concentration of imide groups at $t = \infty$

$C_{a,0}$ = concentration of amic acid groups at $t = 0$

Also the rate equation can be written in terms of conversion by the following equation which relates the rate of reaction to conversion at time t :

$$R_i = d\alpha_a/dt = K_e (1-\alpha_a) \qquad (3\text{-}32a)$$

$$\alpha_a = (C_{a,0} - C_a)/C_{a,0} = CI/C_{I,\infty} \qquad (3\text{-}32b)$$

with initial condition : at $t = 0$ $\alpha_a = 0$

Where α_a = conversion of poly(amic acid) at time t

Integration of Equations 3-30, 3-31, and 3-32a result in three equations that relate the concentration of amic acid, concentration of imide, and conversion to time, respectively, as presented below:

$$-Ln(C_a/C_{a,0}) = K_e t \qquad (3\text{-}33a)$$

$$-Ln[\,(C_{I,\infty}-C_I)/C_{I,\infty}\,] = K_e t \qquad (3\text{-}33b)$$

$$-Ln(1-\alpha_a) = K_e\, t \qquad (3\text{-}33c)$$

The extent of reaction is monitored with Fourier Transform Infrared Spectroscopy (FTIR). The beers-Lambert law can be used to relate conversion at time t to the absorption peak of the amic acid or the imide group. According to this law, the absorption of a chemical group is linearly proportional to its concentration as presented by the following equations :

$$A_a = \xi_a\, d\, C_a/C_p \qquad (3\text{-}34a)$$

$$A_I = \xi_I\, d\, C_I/C_p \qquad (3\text{-}34b)$$

Where A_a = absorption of the amic acid group

A_I = absorption of the imide group

ξ_a = absorption coefficient of the amic acid group

ξ_I = absorption coefficient of the imide group

d = pathlength or the thickness of the sample

C_p = concentration of polymer in solution

The absorption values in Equations 3-34a and 3-34b are normalized based on concentration of the polymer in solution to offset any changes in polymer concentration, because the samples are diluted with NMP before analysis with FTIR. Substitution of Equations 3-34a and 3-34b in Equation 3-32b relates conversion to the absorption of amic acid and imide groups:

$$\alpha_a = [\, 1 - (A_a/A_{a,0})\, (d_0/d)\, (C_p/C_{p,0})\,] \qquad (3\text{-}35a)$$

$$\alpha_a = (A_I/A_{I,\infty})\, (d_\infty/d)\, (C_p/C_{p,\infty}) \qquad (3\text{-}35b)$$

Where d_0 = film thickness for the sample at t=0

d_∞ = film thickness for the sample at t=∞

$A_{a,0}$ = absorption of the amic acid group at t=0

$A_{I,\infty}$ = absorption of the imide group at t=∞

$C_{p,0}$ = concentration of polymer for the sample at t=0

$C_{p,\infty}$ = concentration of polymer for the sample at t=∞

A reference peak is required to offset the effect of sample thickness and the polymer concentration on the measured concentration of amic acid and imide groups at different times. For the poly(amic acid) system containing para-diaminodiphenyl sulfone (pDDS), a peak at 1155 wavenumbers associated with the sulfone group was chosen as the reference peak. For the system containing 2,2'-bis(aminophenyl)propane (BAP), a peak at 1016 wavenumbers associated with the propyl group was chosen as the reference peak. Applying the Beers-Lambert law for the reference peaks, we have:

$$A_r = \xi_r d C_r \qquad (3\text{-}36a)$$

$$A_{r,0} = \xi_r d_0 C_{r,0} \qquad (3\text{-}36b)$$

$$A_{r,\infty} = \xi_r d_\infty C_{r,\infty} \qquad (3\text{-}36c)$$

Where A_r = absorption of the reference peak at time t

$A_{r,0}$ = absorption of the reference peak at t=0

$A_{r,\infty}$ = absorption of the reference peak at t=∞

ξ_r = absorption coefficient for the reference peak

C_r = concentration of a reference group in the polymer that does

not take part in the imidization reaction

$C_{r,0}$ = concentration of the reference group at t=0

$C_{r,\infty}$ = concentration of the reference group at t=∞

Substitution of Equations 3-36a, b, and c in Equations 3-35a and b result in the following equations that relate conversion to absorption of the amic acid and imide groups, respectively:

$$\alpha_a = [\, 1 - (A_a/A_{a,0})\,(A_{r,0}/A_r)\,] \qquad (3\text{-}37a)$$

$$\alpha_a = (A_I/A_{I,\infty})\,(A_{r,\infty}/A_r) \qquad (3\text{-}37b)$$

and $$-\mathrm{Ln}(1-\alpha_a) = K_e\, t \qquad (3\text{-}33c)$$

Therefore, Equations 3-37a, 3-37b, and 3-33c can be used to find the rate constant for the solution imidization of poly(amic acids). A plot of $-\mathrm{Ln}(1-\alpha_a)$ versus time should be linear and the slope is equal to the effective rate constant, K_e, for the solution imidization of poly(amic acids).

IV. Experimental

The cylindrical cavity which was described at the beginning of the theory section was used for all of the experiments with microwave radiation. A photograph of this cavity is displayed in Figure 4-1, and a more detailed description of this cavity is presented in reference [97].In all of the experiments with microwave radiation, the sample cell, which was made from Teflon [105], was inserted in the hub of the centering holder, and the centering holder was placed on the bottom surface of the cavity, as displayed in Figure 4-2. The fit between the sample holder and the sample cell was tight to prevent the cell from rotating or moving vertically inside the cavity. The outer diameter of the centering holder was identical to the inside diameter of the cavity. The sample cells used for heating and curing rate studies will be described in detail in sections 4.3 and 4.4.

4.1. System for Continuous Microwave Experiments

A schematic diagram of the system for continuous microwave experiments is displayed in Figure 4-3, and the abbreviations in this figure are defined in Table 4-1. Microwave radiation from the power generator travels through the circulator and the dual directional coupler before entering the cavity via the coaxial input port. Microwave radiation is fed into the coaxial input port (e.g., see Figure 4-1) and is coupled to the cavity via the adjustable coaxial probe. Adjustment of the short length L_s and the coupling probe position L_p are made to tune the cavity to TE_{111} mode by manual rotation of the knobs shown in Figure 4-1.

The circulator in Figure 4-3 protects the power generator from reflected radiation and the attenuator absorbs the reflected radiation coming from the cavity.

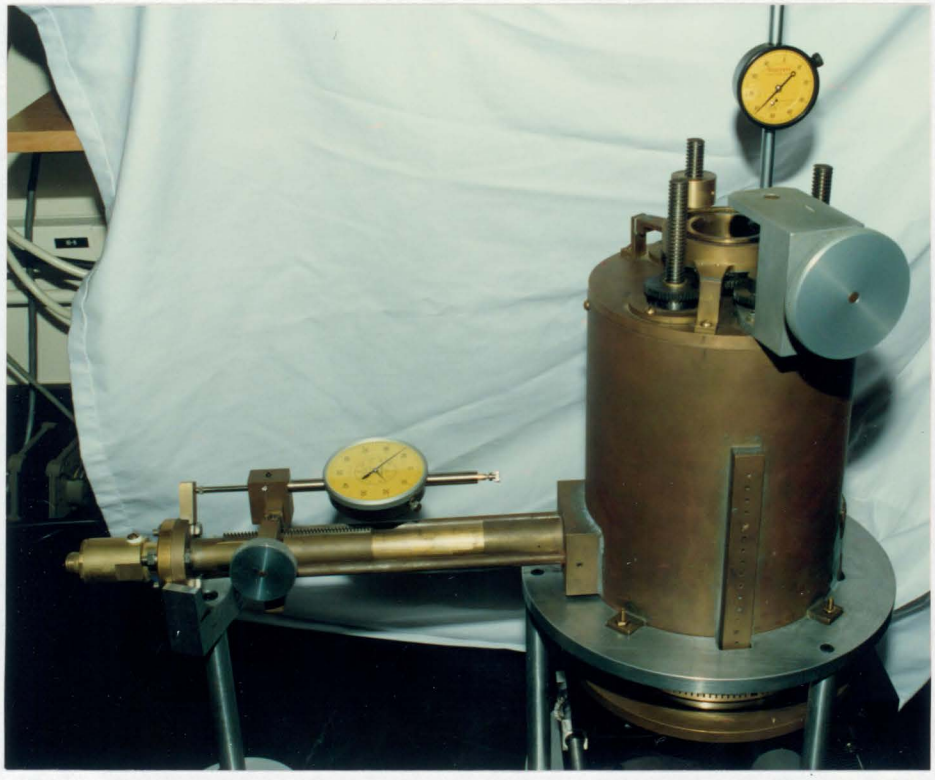

Figure 4-1: Photograph of the cylindrical cavity

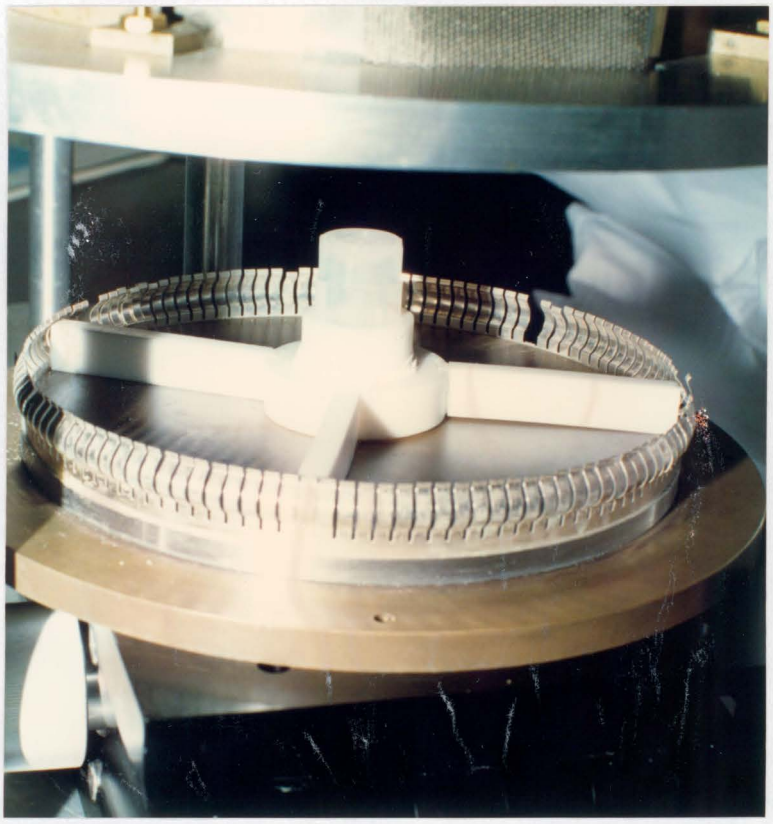

Figure 4-2: Photograph of the sample cell with the centering holder inside the cavity

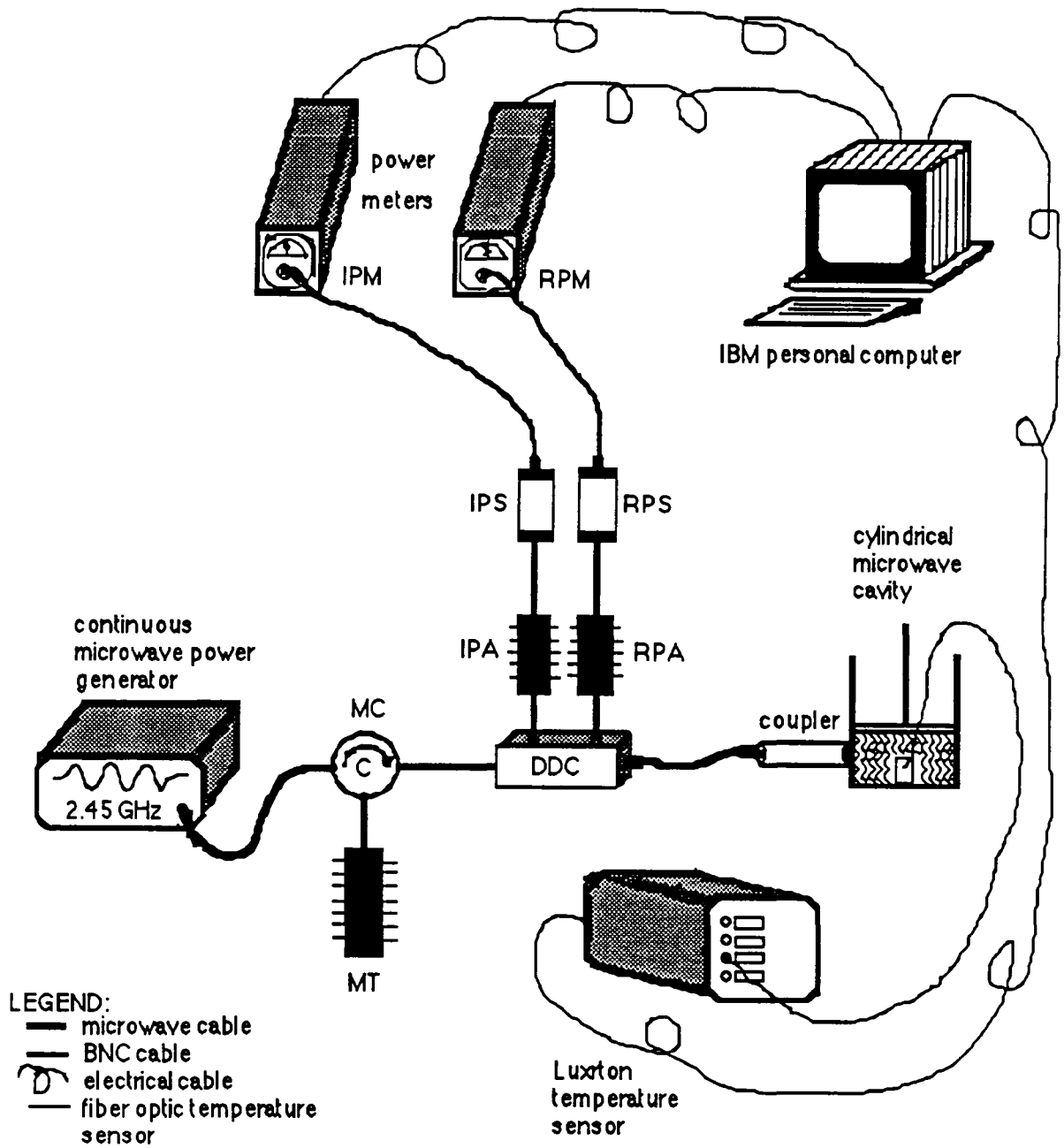

Figure 4-3: Schematic diagram of the system for continuous microwave radiation experiments

Table 4-1: Description of abbreviations for continuous microwave system

MC :	Microwave Circulator for protecting the power generator from reflected waves.
MT :	Microwave Terminator to absorb the reflected microwave power.
DDC :	Dual Directional Coupler to measure the incident and the reflected microwave power.
IPA :	Incident Power Attenuator for reducing the microwave power before entering the power sensor.
IPS :	Incident Power Sensor for measuring the incident microwave power.
IPM :	Incident Power Meter for displaying the incident microwav power.
RPA :	Reflected Power Attenuator for reducing the microwave power before entering the power sensor.
RPS :	Reflected Power Sensor for measuring the reflected microwave power.
RPM :	Reflected Power Meter for displaying the incident microwave power.

The dual directional coupler was used for sampling the incident and the reflected power. Table 4-2 shows the attenuation factor for each component and the total attenuation factor for each detector with their corresponding maximum deviation range. The deviation range for detectors includes the insertion loss for the circulator and six feet of microwave cable. The insertion loss for the cables is 0.5 decibels per three feet and for the circulator is 0.4 decibels. The incident power was monitored by incident power meter, IPM, in Figure 4-3 via the incident power sensor, IPS, with total attenuation factor of 50. And the reflected power was monitored by the reflected power meter, RPM, via the reflected power sensor, RPS, with total attenuation factor of 40.

The temperature of the sample was monitored by using a Luxtron [100] temperature sensor via a fiber optic temperature probe. The incident power, the reflected power, and temperature of the sample for continuous microwave experiments were transmitted and stored in an IBM personal computer as a function of time for later analysis of the data.

4.2. System for Pulse Microwave Experiments

A schematic diagram for the system with pulse microwave experiments is displayed in Figure 4-4, and the abbreviations in this figure are defined in Table 4-3. In continuous microwave experiments, we only needed to monitor three parameters which were the incident power, the reflected power, and temperature of the sample as a function of time. However, for pulse microwave experiments, we need to monitor three additional parameters as displayed in Figure 4-5.

Continuous microwave radiation , according to Figure 4-5, is characterized by average power of the electromagnetic wave, whereas pulsed microwave radiation is

Table 4-2: Attenuation factor for each component in continuous microwave system and the total attenuation factor for each detector.

attenuation / detector for	attenuation factor for each component			total[d] attenuation		application range[e]
	DDC[a]	IDC1[b]	IDC2[c]	in watts	in decibels	
incident power via incident power meter	20 ± 1	30 factory calibrat.	X	10^5	50 ± 2.1	linear
reflected power via reflected power meter	20 ±1	X	20 ± 1	10^4	40 ± 3.1	linear

a) see reference [103].
b) see reference [102].
c) see reference [104].
d) total error includes loss for six feet of cable and the insertion loss of the circulator.
e) see section 4.2 for definition.

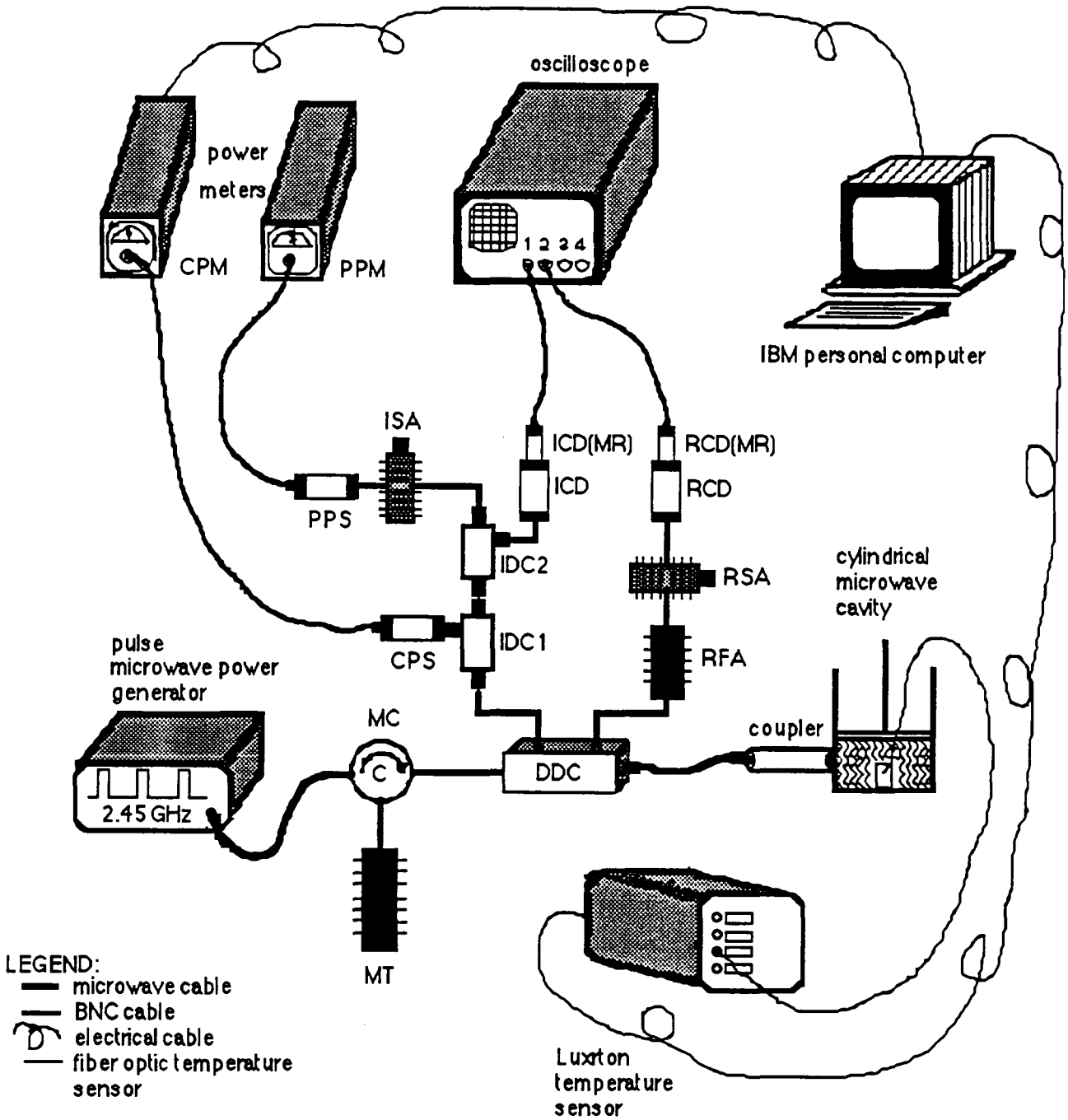

Figure 4-4: Schematic diagram of the system for pulse microwave radiation experiments

Table 4-3: Description of abbreviations for pulse microwave system

MC :	Microwave Circulator for protecting the power generator from reflected waves.
MT :	Microwave Terminator to absorb the reflected microwave power.
DDC :	Dual Directional Coupler to measure the incident and the reflected microwave average power, peak power, pulse width, and pulse repetition rate.
IDC1 :	Incident Directional Coupler #1 to divide the power for measuring the average incident microwave power.
CPS :	Continuous Power Sensor for measuring the average incident microwave power.
CPM :	Continuous power meter for displaying the average incident microwave power.
IDC2 :	Incident Directional Coupler #2 to divide the power for measuring the peak incident microwave power.
ISA :	Incident Step Attenuator for reducing the peak microwave power before entering the peak power sensor.
PPS :	Peak Power Sensor for measuring the peak incident microwave power.
PPM :	Peak Power Meter for displaying the peak incident microwave power.
ICD :	Incident Crystal Detector for measuring the incident power pulse width and pulse repetition rate in conjunction with the oscilloscope.channel #1.
ICD(MR) :	Incident Crystal Detector (Matching Resistor) for expanding the linear region of incident crystal detector.
RFA :	Reflected Fixed Attenuator for reducing the microwave power before entering the reflected power sensor.

Table 4-3: Continued

RSA :	Reflected Step Attenuator for further reduction of the microwave power before entering the reflected power sensor.
RCD :	Reflected Crystal Detector for measuring the reflected peak power in conjunction with the oscilloscope channel #2.
RCD(MR) :	Reflected Crystal Detector (Matching Resistor) for expanding the linear region of reflected crystal detector.

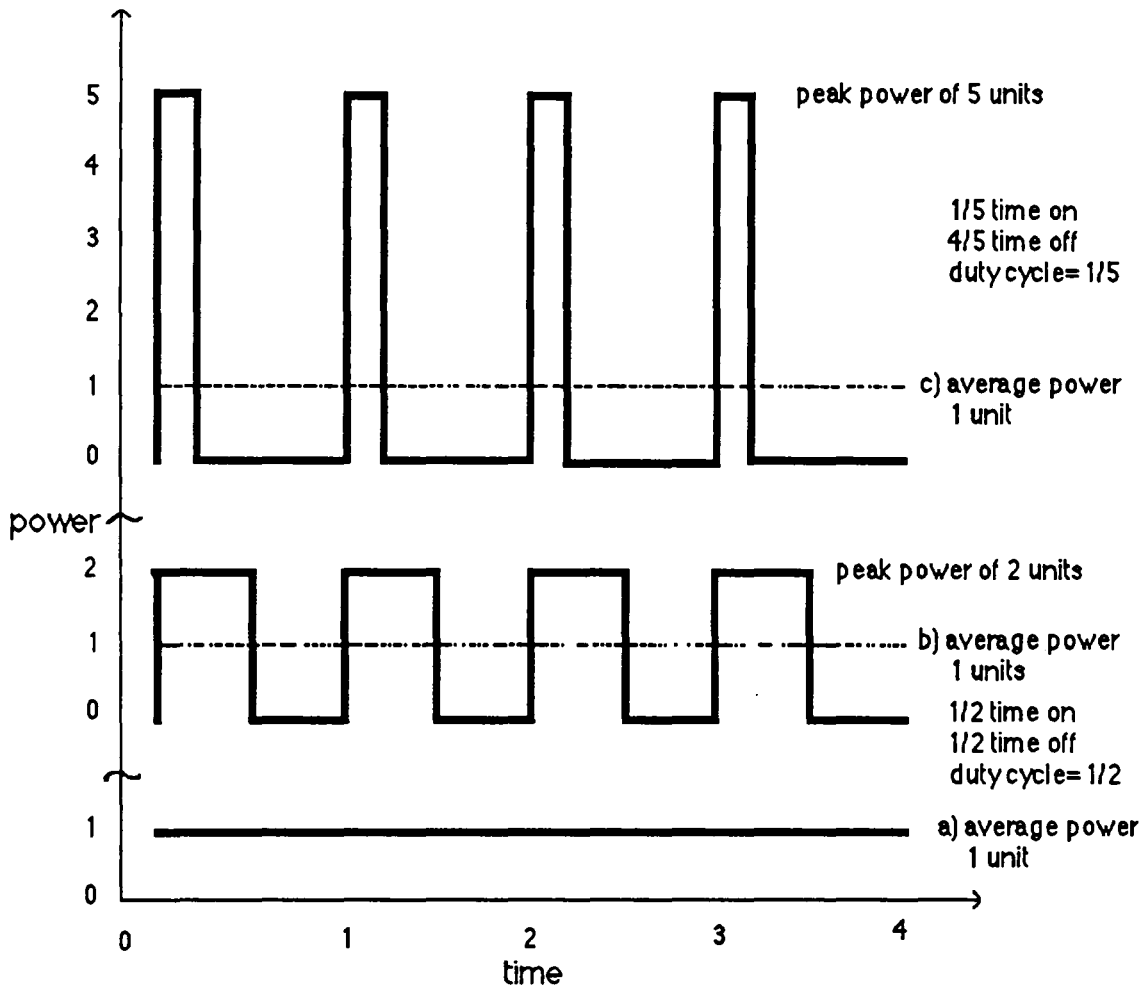

Figure 4-5: Comparison of continuous and pulse microwave radiation at the same average power [14]

characterized by three additional parameters which are pulse width, pulse repetition rate or pulse period, and pulse peak power. Note that pulse repetition rate is the inverse of pulse period. Also according to Figure 4-5, it is possible to construct infinite number of pulses all with the same average power by varying the pulse peak power, pulse period, and pulse width. The pulse width, pulse repetition rate, and pulse peak power are related to the average power by the following equation:

$$P_{avg} = 10^{-6} \tau_{pw} f_p P_p = 10^{-3} \tau_{pw} P_p / T_p \qquad (4\text{-}1)$$

Where P_{avg} = average microwave power in Watts

τ_{pw} = pulse width in microseconds

f_p = pulse repetition rate in Hertz

T_p = pulse period in milliseconds

P_p = pulse peak power in Watts

There are infinite combinations of pulse width, pulse period, and pulse peak power for the same average power, as displayed in Figure 4-5 for three different cases. Case (a) is continuous microwave with one unit of average power. Case (b) is a pulsed wave with two units of peak power but the power is on only half of the time, therefore the average power is the same as case (a) according to Equation 4-1. Case (c) is a pulsed wave with five units of peak power but the power is on one fifth of the time and it is off four fifth of the time, therefore the average power is again the same as case (a).

To measure the pulse width, pulse period, and pulse peak power in addition to the average power, through the two sampling ports of the dual directional coupler, directional couplers were utilized as power dividers. Microwave power sensors such

as crystal detectors can be divided into three range of applications as illustrated in Figure 4-6. Region I in Figure 4-6 is the linear range of the detector in which the output voltage from the detector is directly proportional to input microwave power into the detector. Region II is the operational range of the detector in which the output voltage is not directly proportional to input power. The sensitivity of the detector decreases sharply in region II but there is no damage to the detector if it is operated in this region. Operation of the detector in region III may cause permanent damage to detector and it should be avoided. To operate in the linear range, considerable attenuation of microwave power is necessary before entering the detector.

The attenuation factor for each component in pulsed microwave system and the total attenuation factor for each detector, with their corresponding maximum deviation range, are presented in Table 4-4. The average power was measured by the continuous power meter, CPM, via the continuous power sensor, CPS, with total attenuation factor of 40 which was in the linear range of detector. peak power was measured by the peak power meter, PPM, via the peak power sensor, PPS, with total attenuation factor of 50 which was in the linear range of detector. The attenuation factor for peak power sensor could be varied by the step attenuator, ISA.

Pulse width and pulse repetition rate of the incident power was measured by channel one of the oscilloscope via crystal detector, ICD, with total attenuation factor of 50 in the operating range of detector. Note that the voltage from channel one of the oscilloscope was not directly proportional to the incident peak power because the crystal detector, ICD, was in the operating range. However, the peak incident power was measured separately via the peak power sensor. Pulse width, pulse repetition rate, and peak for the reflected power were measured by channel two of the

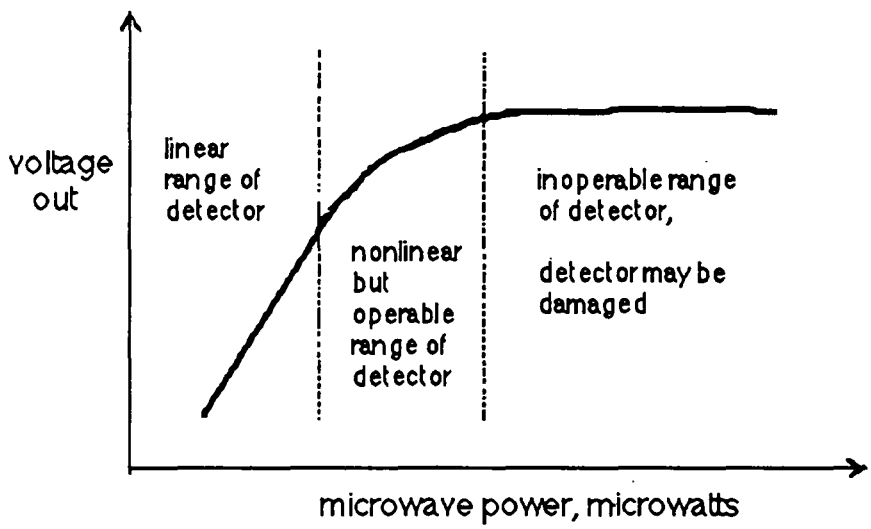

Figure 4-6: Output voltage from the microwave power detector versus input power to the detector

Table 4-4 : Attenuation factor for each component in pulse microwave system and the total attenuation factor for each detector

attenuation / detector for	attenuation factor for components in pulse microwave system						total[d] attenuation		application range
	DDC[a]	IDC1[a]	IDC2[a]	ISA[b]	RFA[c]	RSA[b]	in watts	in decibles	
continuous power via continuous power meter	20 ±1	20 ±1					10^4	40 ±4.4	linear
peak power via peak power meter	20 ±1	0±0.2	0±0.2	30 ±0.5			10^5	50 ±4.3	linear
pulse width and repetition rate via oscilloscope	20 ±1	0±0.2	30 ±1				10^5	50 ±4.6	oparable
reflected power via oscilloscope	20 ±1				20 ±1	20 ±0.5	10^6	60 ±4.9	linear

a) see reference [103].
b) see reference [102].
c) see reference [104].
d) total error includes loss for six feet of cable and the insertion loss of the circulator.

oscilloscope via the crystal detector, RCD, with total attenuation factor of 60 in the linear range of detector.

Figure 4-7 displays the input power to crystal detector, RCD, for reflected power versus the output voltage from the detector measured by channel two of the oscilloscope. The input microwave power to the detector was measured with the continuous power meter by operating the pulse microwave system in continuous mode, via the continuous power generator. In this mode of operation, the peak incident power to the detector was the same as the average power because the microwave power is continuous. The output voltage measured by the oscilloscope was directly proportional to the input power for the reflected power detector, RCD, as displayed in Figure 4-7. Therefore, we were in the linear range of this detector and the peak reflected power could be measured from the voltage of the oscilloscope in conjunction with Figure 4-7.

It was observed that the peak power measured independently by the peak power meter was always less than the peak power calculated by equation 4-1. This can be explained by spurious losses in the directional couplers IDC1 and IDC2 in Figure 4-4. Therefore, the power measured by peak power meter was named the lossy peak power because of the losses in the components preceding the peak power detector. To measure the true peak power, the step attenuator, ISA, was disconnected from the directional coupler, IDC2, and was directly connected to the dual directional coupler, DDC (limits of directivity ±1 decibels), to bypass the two directional couplers IDC1 and IDC2. Figure 4-8 displays a plot of lossy peak power (e.g., peak power measured with the two directional couplers in line) versus the true peak power (e.g., peak power measured without the two directional couplers) on a decibel scale (e.g., Log-Log scale). The losses in the system were linear in

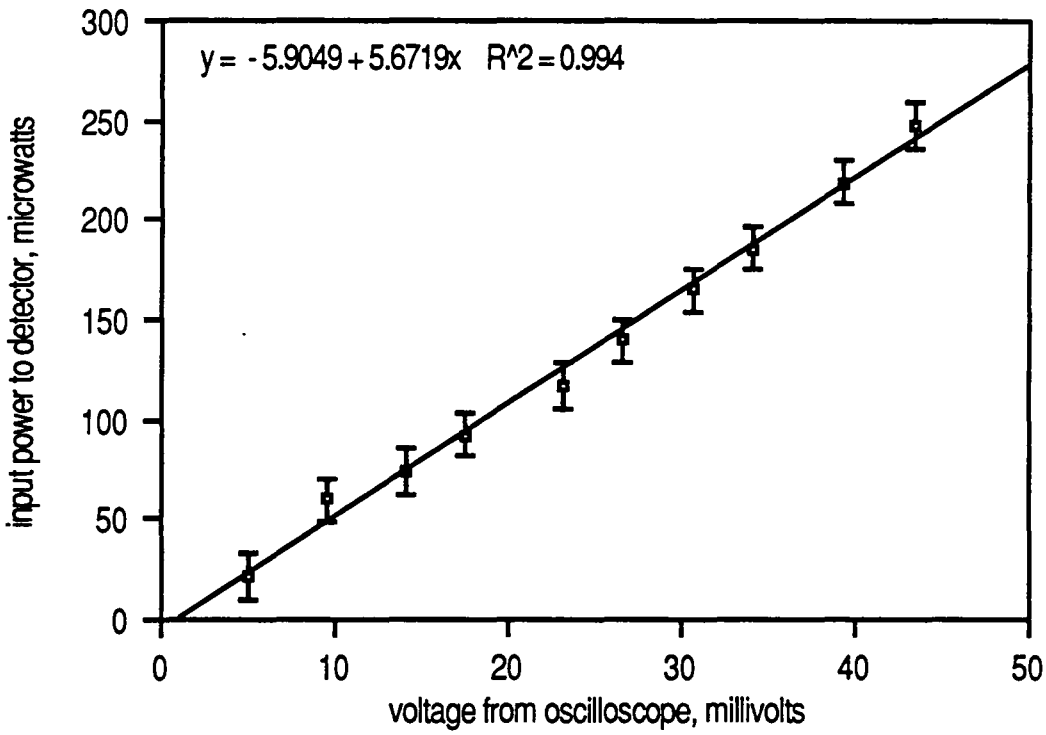

Figure 4-7: Calibration curve for the reflected power to detector versus voltage out of detector and measured by oscilloscope

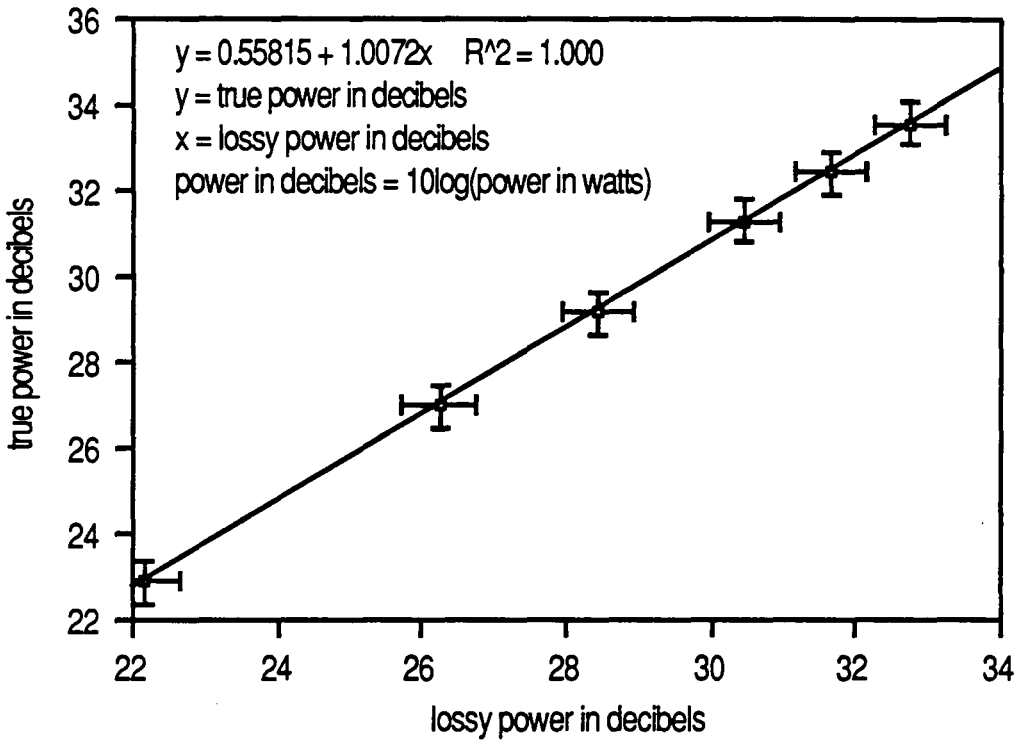

Figure 4-8: Calibration curve for true peak microwave power versus lossy or measured microwave power in decible scale

logarithmic scale as displayed in Figure 4-8. After adjustments were made to the lossy peak power using Figure 4-8, the peak power measured corresponded very well (e.g., within five percent) to the peak power calculated by Equation 4-1.

Attenuation factors for the peak power sensor, PPS, and the reflected crystal detector, RCD, could be varied by the step attenuators, ISA, and RSA, respectively. The step attenuators could be varied from zero to seventy decibels of attenuation. The choice of attenuation factor depended on the range of peak power from the pulse power generator. Table 4-5 presents the suggested attenuation factors for attenuators ISA and RSA as a function of the peak power range of the source. The suggested attenuation factors for attenuators ISA and RSA in the range of one to ten kilowatts of peak power are 30 and 20, respectively.

Two major shortcomings of the pulse power generator were 1) the range of duty cycle of the source was two low and 2) the peak power was not independent of duty cycle. The duty cycle of the pulse source is defined as the ratio of pulse width to pulse period. The range of pulse period and peak power of the power source was satisfactory, however the pulse width was very small ranging from 0.1 to 100 microseconds. The small value of the pulse width in turn limited the average power attainable by the source which was up to 12 watts under the experimental conditions shown in Figure 4-4.

The dependence of peak power on duty cycle is displayed in Figure 4-9 reproduced from the manufacturer's specifications [101]. The peak anode current in Figure 4-9 is measured by the power source and is directly proportional to the peak power from the source. According to Figure 4-9, the peak power is independent of the duty cycle up to a duty cycle of 0.003 (e.g., a pulse width of 6 microseconds), and then the peak power drops dramatically for higher duty cycles or higher pulse width.

Table 4-5: Recommended attenuation factors for incident and reflected step attenuators versus peak pulse power

peak power from pulse power generator	attenuation factor for ISA	attenuation factor for RSA	total attenuation for PPS	total attenuation for RCD
1 - 10 watts	0	0	20	40
10 - 100 watts	10	0	30	40
100 - 1000 watts	20	10	40	50
1000 - 10000 watts	30	20	50	60

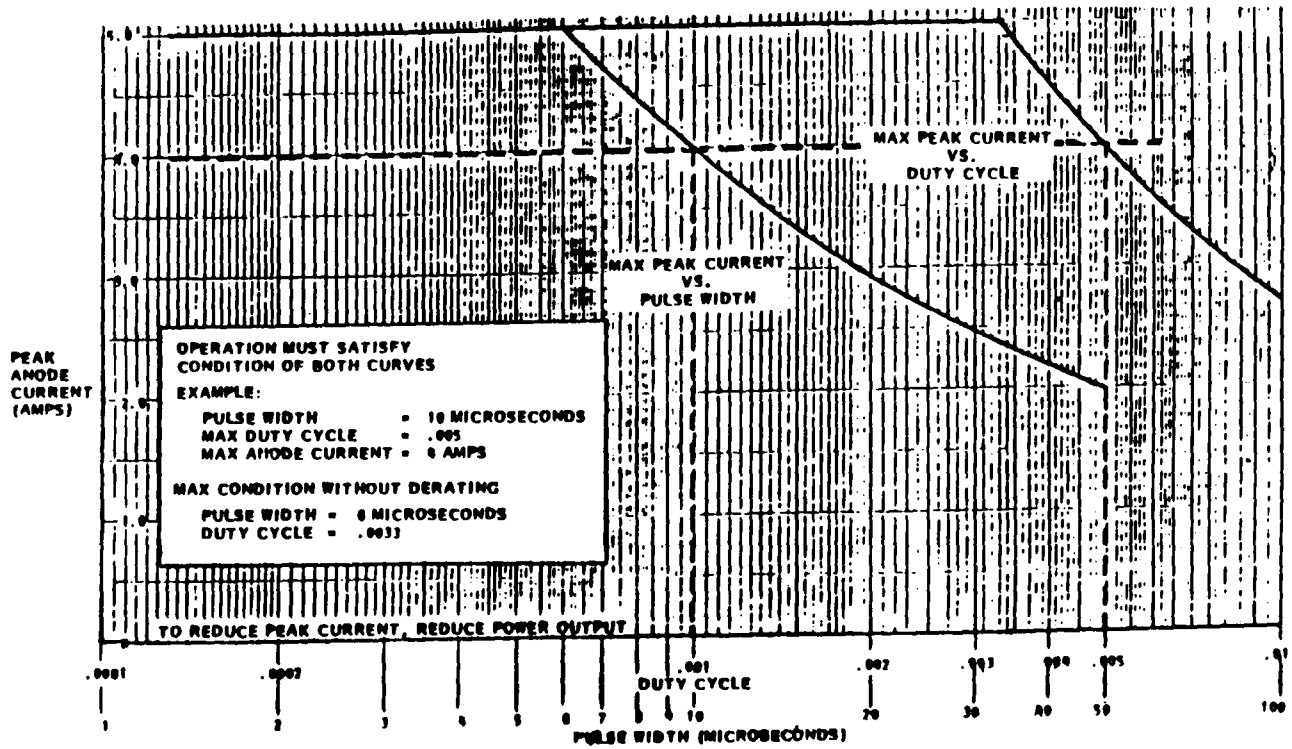

Figure 4-9: Dependence of peak power on duty cycle for the pulse power generator [101]

Therefore, the choice of pulse width, pulse period, and pulse peak power was not independent of each other which was one of the major limitations of the pulse power generator.

The experiments for studying the heating rate of poly(ethylene glycol) and poly(propylene glycol) were carried out at constant low average power of five watts to ensure the pulse period, pulse width, and pulse peak are independent of each other. Also for heating rate experiments, it was very important to have a constant average power of five watts for both continuous and pulse experiments. Therefore, the microwave system which is displayed in Figure 4-4 was employed for continuous as well as pulse microwave experiments, with only the power source interchangeable between the continuous and pulse experiments.

4.3. Experimental Conditions for Heating Rate Studies

Heating rate studies were done with poly(ethylene glycol) with average molecular weight ranging from 200 to 10,000 grams per mole and poly(propylene glycol) with average molecular weight ranging from 425 to 4000 grams per mole. The experiments were conducted with continuous as well as pulsed microwave radiation. The samples were dried in a vacuum oven at 30 degrees centigrade for 48 hours prior to the experiment. For each heating rate experiment, one gram of the polymer in liquid form was weighted and placed in the sample cell displayed schematically in Figure 4-10. For poly(ethylene glycol) experiments, the initial temperature of the sample was 70 degrees centigrade and for poly(propylene glycol) it was 35 degrees to ensure all samples were above their corresponding melting point. This was to ensure no phase transition occurred during the heating rate experiment. The cap was

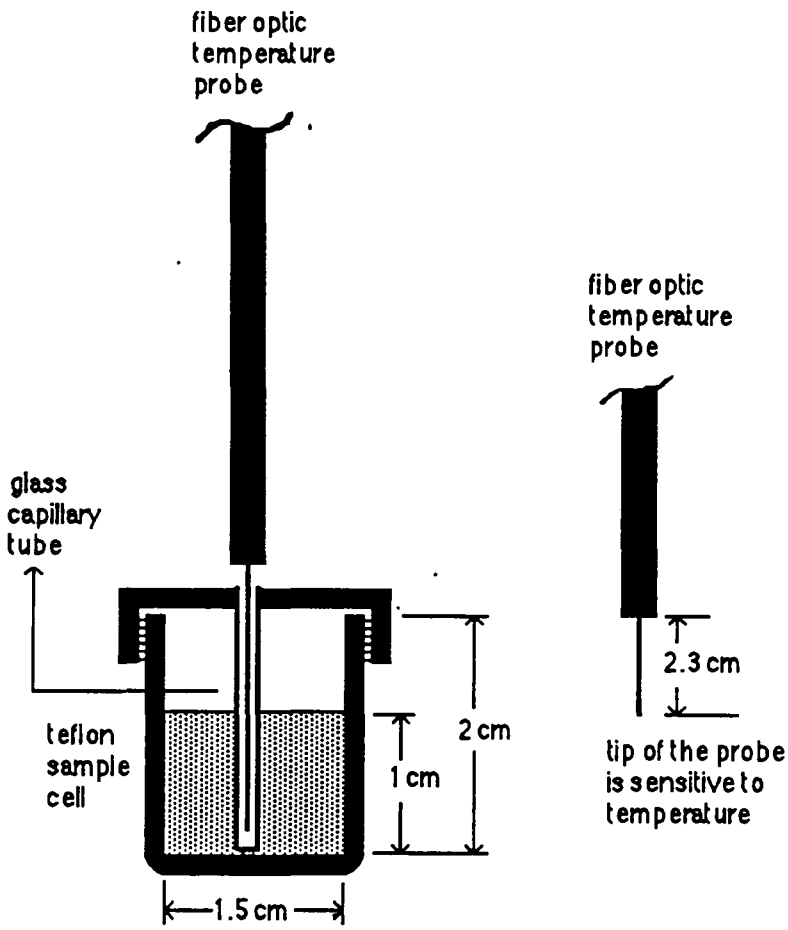

Figure 4-10: Schematic diagram of the sample cell for studing the heating rate of polymers with microwave radiation

screwed tightly on the sample cell to prevent any moisture entering the cell. Additional experimental conditions for heating rate studies are as follow:

1) The sample cell was raised two centimeters above the lower surface of the cylindrical cavity for more uniform and maximum heating rate.

2) Height of solution in the sample cell was between 0.9 to 1.0 centimeter depending on the density of the sample.

3) The temperature probe was not in direct contact with solution. A glass capillary tube was inserted inside the opening on top of the sample lid. Then the probe was inserted into the glass capillary tube and the glass tube was in contact with solution.

4) The average microwave power for continuous as well as pulse experiments was fixed at five watts with less than one percent reflected power.

5) For pulse experiments, peak microwave power was set at 1000 watts. The pulse width was 10 microseconds and pulse repetition rate was 500 Hertz for poly(ethylene glycol) as well as poly(propylene glycol) experiments.

4.4. Experimental Conditions for Imidization of Poly(amic acid)

4.4.1. With Microwave Radiation

4.4.1.1. Without Cooling And Agitation

Poly(amic acids) based on 3,3',4,4'-Benzophenonetetracarboxylic dianhydride (BTDA) as the dianhydride and 2,2'-bis(aminophenyl) propane (BAP) were used for studying the rate of curing of poly(amic acids) with thermal energy, continuous , and pulse microwave radiation. The poly(amic acid) based on BTDA as the dianhydride and para-diaminodiphenyl sulfone (pDDS) as the diamine was also

study the rate of curing with thermal energy and continuous microwave radiation.

The sample cell was preheated and dried at 120 degrees centigrade before the experiment in an oven for 48 hours. Dry nitrogen was continuously running through the sample cell to prevent moisture from the atmosphere entering the cell. For each experiment, four milliliters of the poly(amic acid) solution was poured in the sample cell, which is displayed schematically in Figure 4-11, and the lid was tightly screwed on the sample cell. The lid was fitted with a 1/16 inch opening for withdrawing aliquots from the solution for kinetic studies. A relatively large sample cell was employed for these experiments so that at least six aliquots of the solution could be withdrawn for kinetic studies.

Kinetics of imidization was followed by taking 0.2 milliliter aliquots from the solution at different time intervals, diluted with one milliliter of freshly distilled NMP, and stored at -10 degrees centigrade in two milliliter microvials. The microvials were preheated and dried previously under nitrogen. The microvials had closures with a hole on top for use with septum. The samples were analyzed with Fourier Transform Infrared Spectroscopy (FTIR) as will be described in section 4.7. Additional experimental conditions are as follows:

1) The height of solution in the sample cell was three centimeters.

2) Temperature probe was not in direct contact with solution, as shown in Figure 4-11. A capillary tube was inserted into the opening on top of the sample lid. Then the probe was inserted inside the glass capillary tube, and the glass tube was in contact with solution.

3) The temperature probe consisted of a jacketed section with diameter greater than the capillary tube diameter and a bare section with diameter less than the capillary tube diameter. Consequently, only the bare section of the probe, which

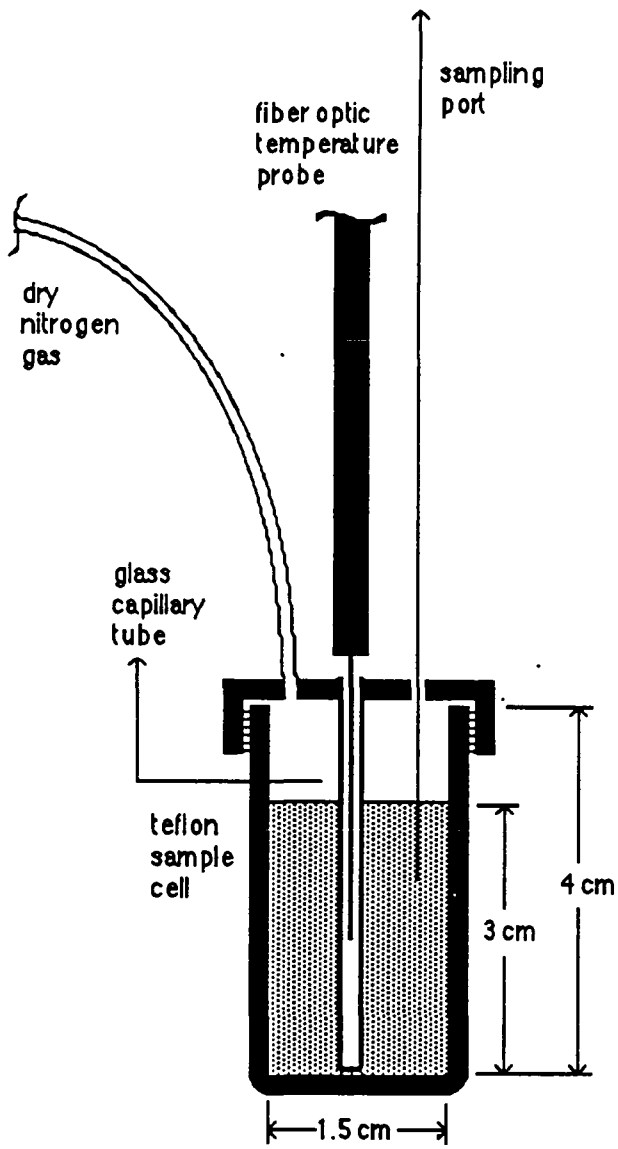

Figure 4-11: Schematic diagram of the apparatus for BTDA/BAP system; continuous and pulsed microwave radiation.

was 0.9 centimeter long, could penetrate inside the capillary tube. The length of the bare section of probe and the length of the sample cell were such that the tip of the probe containing the sensing element was right at the center height of the sample cell.

4) The solution in the sample cell was heated with a heat gun, through the screen window on the side of cavity, to the desired reaction temperature (e.g., 140 degrees centigrade) before the sample was irradiated with microwave energy. There was no significant change in the cavity quality factor, by monitoring the change in resonant height of cavity, as the cavity was heated.

5) The average microwave power level was 8-12 watts. The power level was adjusted continuously by tuning and detuning the cavity to control the temperature at 140 degrees centigrade.

6) For pulse experiments, peak microwave power was between 2000 to 2500 watts, and the peak power was adjusted continuously to control the temperature of the sample. For each experiment, pulse width and pulse repetition rate were fixed and the two were related by Equation 4-1. The effect of pulse repetition rate on the rate of imidization was studied by varying the pulse repetition rate from 50 to 30,000 Hertz. The pulse width was varied from 0.1 to 65 microseconds, respectively.

4.4.1.2. With Cooling and Agitation

Poly(amic acid) based on 3,3',4,4'-benzophenonetetracarboxylic dianhydride (BTDA) as the dianhydride and para-diaminodiphenyl sulfone (pDDS) as the diamine was used for studying the imidization of poly(amic acids) with simultaneous cooling and agitation. The sample was irradiated with microwave energy and cooled at the same time to increase the microwave power applied to the sample. Also the solution

was agitated to reduce temperature gradients in the cell due to the significant distribution of microwave power in the axial direction.

For each experiment, 1.5 milliliters of the poly(amic acid) solution was poured in the sample cell which is displayed schematically in Figure 4-12. A relatively smaller sample cell was used for experiments with cooling and agitation to reduce temperature gradients in the sample. Kinetics of imidization was followed by withdrawing only one aliquot (0.2 milliliter) from the solution after 1200 seconds. The volume of the solution was too small for taking more aliquots from the solution for a more complete kinetic study. Additional experimental conditions are as follows :

1) Height of solution in the sample cell was 1.5 centimeters.

2) Temperature probe was in direct contact with the solution, as displayed in Figure 4-12. A glass capillary tube was inserted inside an opening at the center of the sample lid. Then the probe was inserted into the glass capillary tube with the end of the glass tube cut, such that the probe was in direct contact with solution.

3) The solution was agitated by the vibration (e.g., up and down) of the cooling coil, via a motor connected to the inlet and outlet tubes of the cooling coil, as displayed in Figure 4-12. The amplitude of vibration was 0.5 centimeter.

4) The solution was cooled by a cooling coil of annular geometry with outside diameter of 11 millimeters, inner diameter of 9 millimeters, and height of 7 millimeters, as displayed in Figure 4-13. The cooling coil was made from quartz glass and its outer surface was sand blasted to improve the efficiency of agitation.

5) The cooling fluid was a nonpolar 50/50 mixture by volume of octane and heptane to ensure microwave radiation is not absorbed by the cooling fluid. Preliminary heating rate experiments with heptane and octane indicated that this mixture was transparent to microwave radiation.

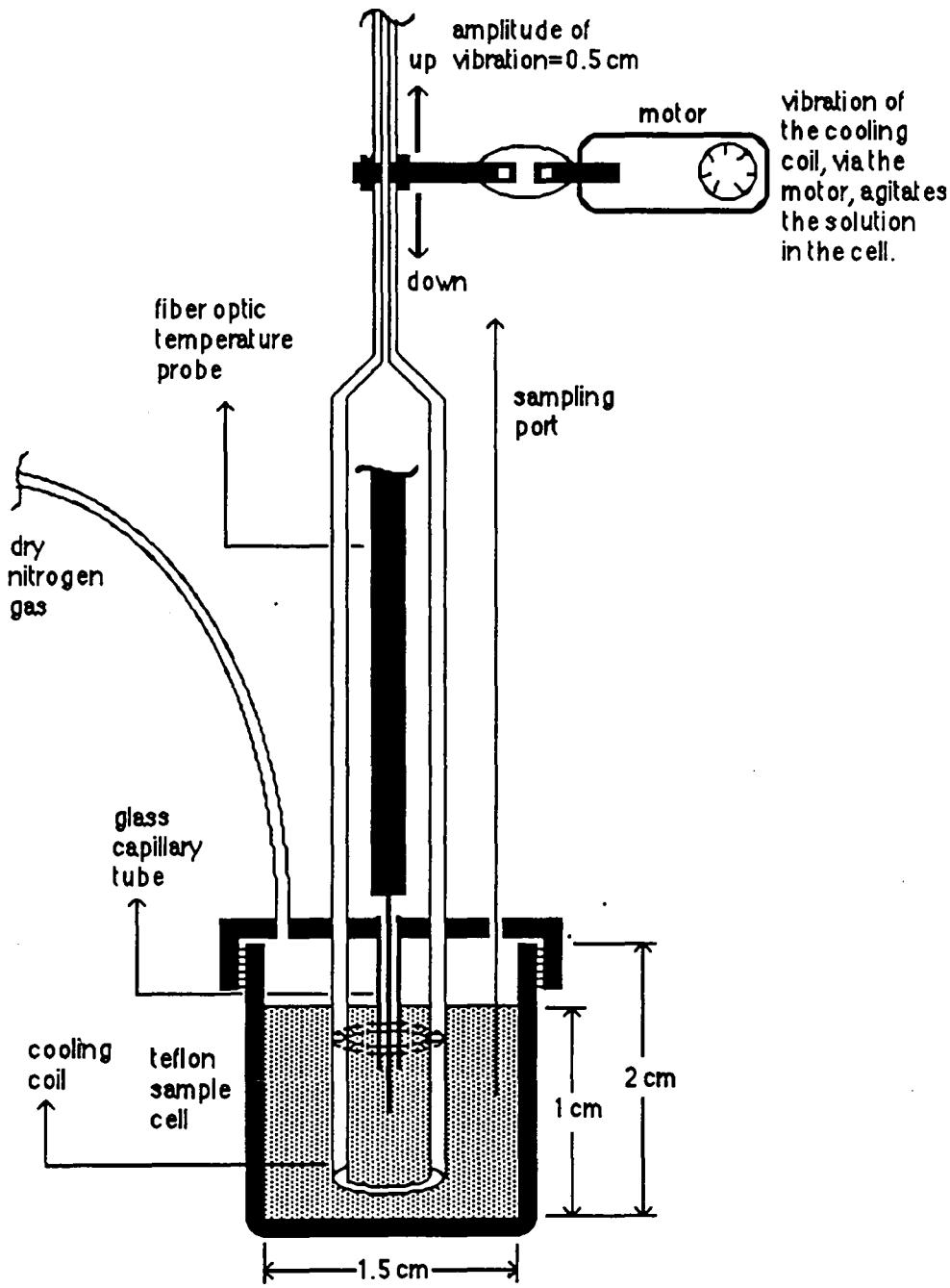

Figure 4-12: Schematic diagram of the apparatus for BTDA/pDDS system; continuous microwave radiation, cooling, and agitation.

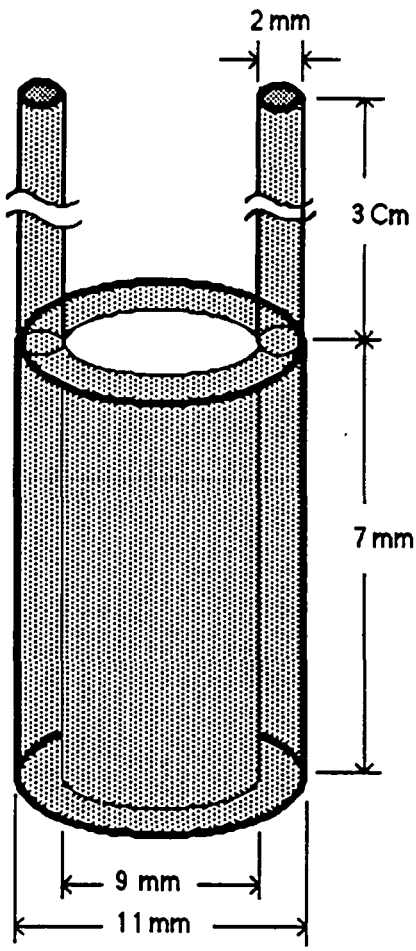

Figure 4-13: Schematic diagram of the cooling coil

6) The cooling system, as displayed in Figure 4-14, consisted of a cooling fluid reservoir with volume of one liter, a magnetic pump for circulating the cooling fluid, a heat exchanger for cooling the fluid back to room temperature, and the glass cooling coil.

7) Continuous microwave radiation was used and the power level could be varied from 10 to 60 watts depending on the rate of cooling. The cooling rate could be varied by adjusting the inlet temperature to the cooling coil or the flow rate of the coolant.

4.4.2. Thermal Imidization of Poly(amic acid) Precursor

4.4.2.1. Bulk Thermal Imidization

The poly(amic acid) precursor was cyclized to the polyimide using the cure schedule described here [83]. The bulk imidization method was primarily used to measure the ratio of FTIR peak height for amic acid and imide groups to the reference peak for kinetic studies.

First, the preformed poly(amic acid) in its original reaction solution was removed from the freezer and allowed to come to room temperature. A drop of the solution was then placed onto a clean dry KBr salt plate and drawn into a smooth flat film. The salt plate was then placed in a level vacuum oven set at 70 degrees centigrade and the vacuum was gradually raised to full vacuum via a mechanical pump. The polymer was kept under full vacuum for an additional hour to remove most of the reaction solvent. The salt plate was then placed in a forced air convection oven set at 100 degrees centigrade for one hour. The temperature was then raised to 200 degrees for another hour and then finally raised to 300 degrees for one hour. After

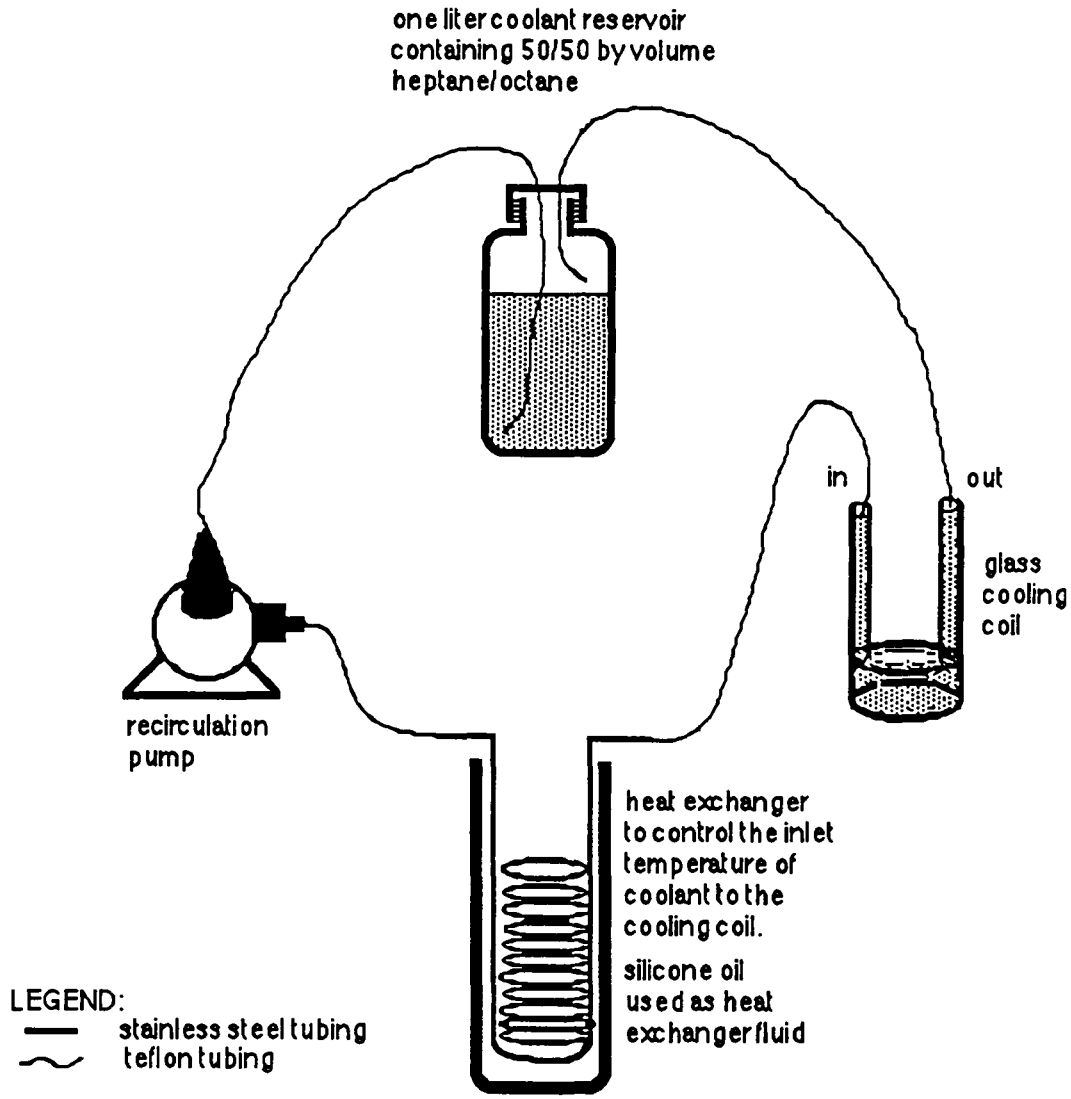

Figure 4-14: Schematic diagram of the cooling system

slow cooling, the film was analyzed by Fourier Transform Infrared Spectroscopy (FTIR).

4.4.2.2. Thermal Solution Imidization

This method was used exclusively for all of the polyimide kinetic studies because the poly(amic acid) stayed in solution throughout the entire course of the reaction [83]. Since the solution stayed homogeneous during the course of the reaction, a kinetic model was developed and the rate of imidization of poly(amic acid) was studied. The kinetics of thermal solution imidization was studied at a total solid content of 15 percent using an NMP/CHP co-solvent ratio of approximately 80/20 by volume. The kinetics of thermal solution imidization was studied by the following procedure:

A multineck 100 milliliters round bottom flask was fitted with a mechanical stirrer, nitrogen inlet, thermometer, Dean Stark trap, condenser, drying tube, and a sample port sealed with a rubber septum. Figure 4-15 displays the various components in their final assembled form. Next, the reaction flask was placed inside a temperature bath equipped with temperature controller and a magnetic stirring plate. Then the flask and the temperature bath were heated to the desired temperature for kinetic studies. Fifteen grams of the poly(amic acid) solution which was synthesized as outlined in section 4.5 plus three milliliters of freshly distilled CHP were added to the flask. The mixture was allowed to equilibrate with the constant temperature bath (e.g., a few minutes). Finally, kinetics of imidization was followed by withdrawing aliquots (0.2 milliliter) from the solution at different time intervals.

4.5. Synthesis of End-Capped Poly(amic acid) Precursor

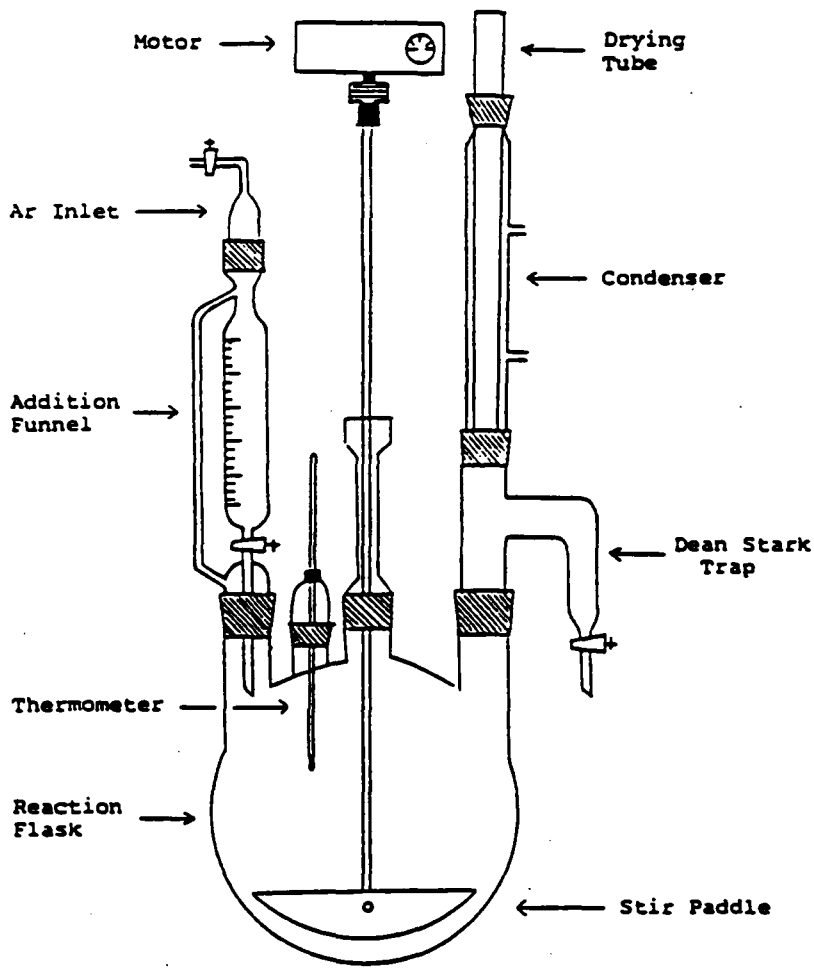

Figure 4-15: Apparatus employed for solution imidization [83]

The imide containing polymers were synthesized through the classical two step method initially involving the generation of soluble amic acid precursors through the reaction of aromatic amines with aromatic dianhydrides and end-capped with phthalic anhydride to control the molecular weight [83]. The amic acid intermediates were then cyclodehydrated with thermal energy as well as microwave radiation to form the imide moieties.

The amic acid containing materials were synthesized in an apparatus similar to the one displayed in Figure 4-16. This standard apparatus consisted of a three neck round bottom flask, overhead stirrer, inert gas inlet, thermometer, addition funnel, and a drying tube. The assembled apparatus was flamed under inert gas purge immediately before every reaction to remove residual moisture. A Typical procedure for synthesizing an amic acid containing intermediate based on BTDA as the dianhydride, 4,4'-diaminodiphenyl sulfone as the diamine, and phthalic dianhydride as the capping agent is as follows:

The standard reaction apparatus shown in Figure 4-16 was employed using a 250 milliliters three neck flask. After flaming the apparatus, 19.1000 grams (0.07692 moles) 4,4'-DDS was added to the flask and dissolved by the addition of 48 milliliters of NMP. A solution of BTDA (21.5623 grams, 0.06692 moles) and phthalic anhydride (3.1900 grams, 0.02154 moles) in 100 milliliters of the same reaction solvent was placed in the addition funnel. The anhydride solution was then added to the stirring diamine solution over a ten minutes period. A slight reaction exotherm of three degrees centigrade was detected during this addition period. The reactants were stirred at room temperature for eight hours to allow the poly(amic acid) to form. The resulting poly(amic acid) was bottled and stored at -10 degrees until needed.

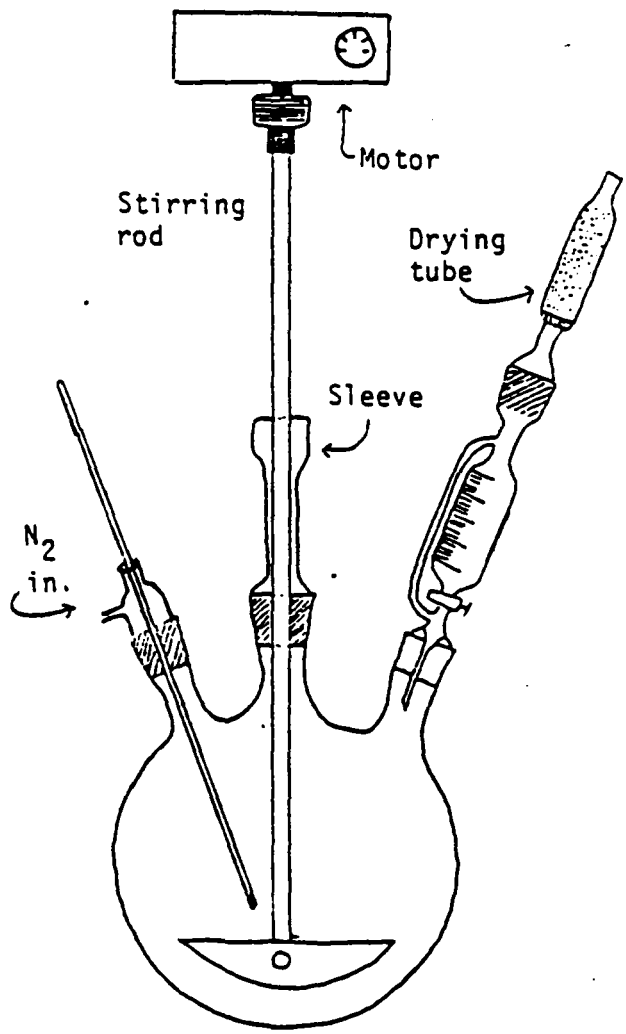

Figure 4-16: Apparatus used for the synthesis of poly(amic acids) [83]

4.6. Chemicals

In order to synthesize imide containing materials of high molecular weight, it was necessary to obtain extremely pure starting materials and to maintain anhydrous conditions throughout the synthetic process [83]. Therefore, reagents and monomers were carefully purified by various techniques and polymerization solvents were distilled from drying agents using the apparatus displayed in Figure 4-17. This apparatus allowed for vacuum distillation of high boiling point solvents. In all distillations, the constant boiling middle fraction was collected and stored in a round bottom flask sealed with a rubber septum. After distillation, the dried solvents were generally handled using syringe techniques to minimize atmospheric exposure.

1) 1-methyl-2-pyrrolidinone (NMP: Fisher) was dried by stirring over phosphorous pentoxide powder for at least 12 hours. The dried solvent was then distilled under reduced pressure generated by a mechanical vacuum pump to avoid significant degradation.

2) 1-cyclohexyl-2-pyrrolidinone (CHP: Aldrich) was dried by stirring over phosphorous pentoxide powder for at least 12 hours. The dried solvent was then distilled under reduced pressure generated by a mechanical vacuum pump to avoid degradation.

3) 4,4'-diaminodiphenyl sulfone (pDDS: FIC corporation) was obtained as a white finely ground powder (m.p. = 163-165 C). It was purified by recrystallization from deoxygenated solvents. Therefore, 500 milliliters of methanol was poured into an erlenmeyer flask and purged with nitrogen for at least five hours. Approximately 50 grams of pDDS was then added to the flask and complete solution was obtained upon boiling the methanol. Then, hot deoxygenated water was added slowly to the pDDS solution until the precipitation point was reached. White crystals formed upon

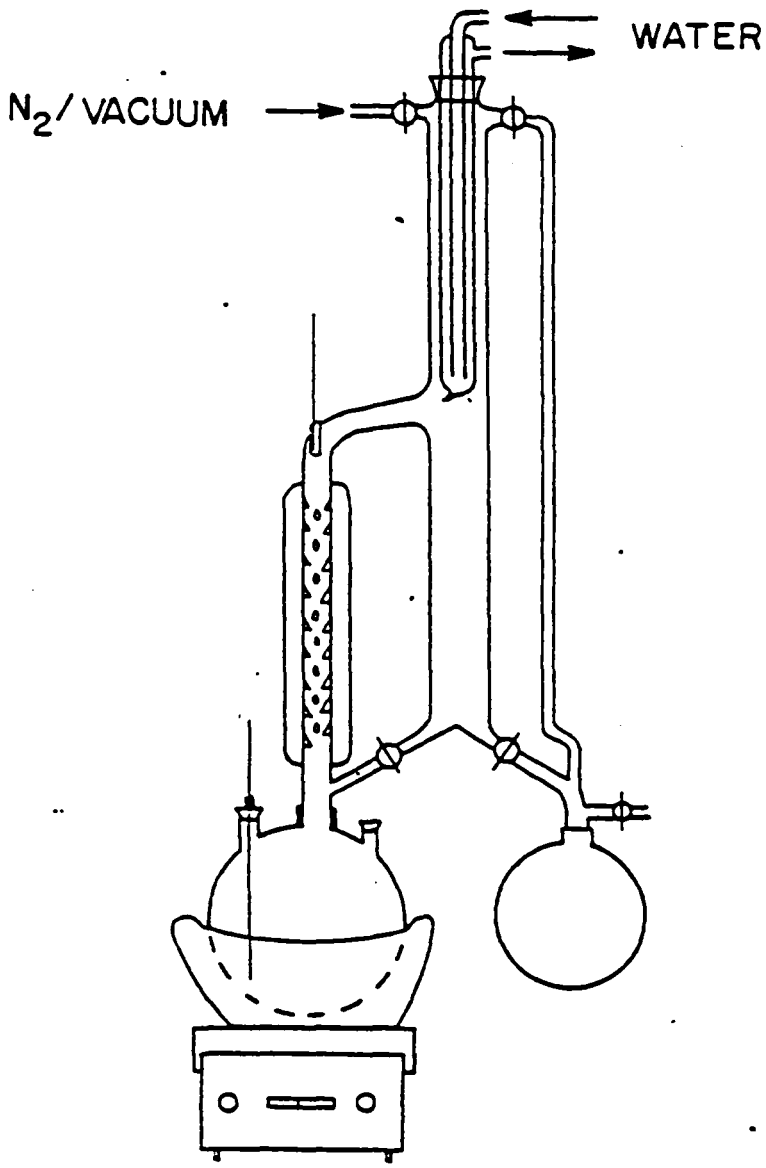

Figure 4-17: Apparatus used for the distillation of solvents [83]

cooling the solution to room temperature. The crystals were isolated by vacuum filtration, washed with deoxygenated methanol, crushed, and dried in a vacuum oven for 12 hours at 70 degrees centigrade. The material was then bottled and stored in a desiccator until needed (m.p.= 172-173 C).

4) 2,2'-bis(aminophenyl) propane (BAP: Air Products and Chemicals Inc.) was obtained as a fine white powder of monomer grade purity and was used as received without further purification (m.p.= 124-126 C).

5) 3,3',4,4'-benzophenonetetracarboxylic dianhydride (BTDA: Chriskev Company) was obtained as a fine white powder of essentially monomer grade purity. This compound was sufficiently pure to be used directly if it was first placed in a forced air convection oven at 150 degrees centigrade for 12 hours immediately prior to use (m.p.= 224-226 C). This thermal treatment served to reform the anhydride moieties from any remaining diacid functionalities (the main impurity of dianhydrides).

6) Phthalic anhydride (Aldrich) was received as a certified grade material of nominal purity. The raw material could be sublimed to yield highly pure phthalic anhydride. The crude product was placed in the bottom of a vacuum sublimator and the cold finger was filled with a mixture of dry ice and acetone. Upon warming the raw material under vacuum conditions, phthalic anhydride readily sublimed onto the cold finger. This material was isolated, vacuum dried, and stored in a sealed bottle under a blanket of nitrogen until needed (m.p.= 132-134 C).

7) Ethylene glycol (Aldrich) was received as an anhydrous liquid with purity greater than 99 percent. It was used without further purification for heating rate studies with continuous as well as pulsed microwave radiation.

8) Poly(ethylene glycol) (Aldrich): Poly(ethylene glycols) with average molecular weights of 200, 300, 400, 600, 1000, 1500, 2000, 3400, 8000, and 10,000

grams per mole were received as a certified grade material of nominal purity. The polydispersity of each polymer was generally less than 1.15. Poly(ethylene glycols) with average molecular weights of 200, 300, and 400 were liquid at room temperature, that with a molecular weight of 600 was a moist solid, those with molecular weights of 1000 and 1500 were waxy solids, that with a molecular weight of 2000 was chip-like, that with a molecular weight of 3400 was a powder, that with a molecular weight of 8000 was a crystalline powder, and that with a molecular weight of 10,000 was a flaky solid. The poly(ethylene glycols) were dried in a vacuum oven at 30 degrees centigrade for at least 48 hours prior to heating rate experiments with continuous as well as pulse microwave radiation.

9) Propylene glycol (Aldrich) was received as an anhydrous liquid with purity greater than 99 percent. It was used without further purification for heating rate studies with continuous and pulse microwave radiation.

10) Poly(Propylene glycol) (Aldrich): Poly(propylene glycols) with average molecular weight of 425, 725, 1000, 2000, 3000, and 4000 grams per mole were received as a certified grade material of nominal purity. All of the poly(propylene glycols) were in liquid form at room temperature. The poly(propylene glycols) were dried in a vacuum oven at 30 degrees centigrade for at least 48 hours prior to heating rate experiments with continuous and pulse microwave radiation.

4.7. Fourier Transform Infrared Spectroscopy (FTIR)

Kinetic studies monitoring the progress of the amic acid transformation were undertaken using a Nicolet MX-1 [108] spectrophotometer. Samples were removed during the course of the imidization reaction and analyzed as free standing thin films

on KBr salt plates. The thin film on KBr salt plates were kept under vacuum for 45 minutes at 60 degrees centigrade to partially remove the solvent.

FTIR bands in the absorption spectra occurring at 1782 and 1371 wavenumbers were used to monitor the appearance of the imide structure. The absorbance at 1410 wavenumbers for BTDA/BAP as well as BTDA/pDDS systems was used to monitor the disappearance of amic acid moieties. And the absorbances at 1155 wavenumbers for BTDA/pDDS and at 1016 for BTDA/BAP systems were used as reference peaks to normalize the amic acid and the imide peaks. The reference peak at 1016 wavenumbers for BTDA/BAP system is due to the propyl group of BAP, and the one at 1155 for BTDA/pDDS system is due to the sulfone group of pDDS. Therefore, they are both directly proportional to the concentration of polymer in solution. Fingerprint regions were expanded to enhance the identification of the spectra. The error due to absorbance measurements was 1X10^-3 per absorption unit (e.g., a.u.).

4.8. Measurement Errors and Error Analysis

The analysis of measurement errors are presented in Appendix 2. For heating rate studies with poly(ethylene glycol) and poly(propylene glycol), temperature measurement was accurate to ±0.05°C, time to ±2X10^-5 seconds (e.g., measured by computer), the incident power to ±0.2 watt, and the reflected power to ±0.06 watt. For heating rate studies with NMP, the incident and reflected power measurements were accurate to ±1 watt and 2.5 watts, respectively. For poly(ethylene glycol) and poly(propylene glycol) experiments, the incident power was the controlled variable and was fixed at five watts. For heating rate studies with NMP, the incident power varied from 10 to 50 watts. The measurement error for the reflected power was

significantly higher with NMP experiments, as compared to poly(ethylene glycol), because at higher incident microwave power it is more difficult to tune the cavity. The sensitivity of the power meters could be varied from 100 watts to 1 watt depending on the level of the incident power. For heating rate studies, the uncertainty in the measurement of power was the dominant source of error. For heating rate studies with poly(ethylene glycol) and poly(propylene glycol), the measurement error was six percent, and for NMP heating rate studies in which power was a controlled variable, the measurement error was ±24°C.

For curing rate studies, absorbance measurement was accurate to ±1X10^-3 per absorbance unit and time to ±10 seconds. There was a large uncertainty in time measurement, because it took on average twenty seconds to withdraw a sample for kinetic studies. The error due to time and absorbance measurements was less than two percent each. For curing studies, temperature was the controlled variable and was fixed at 140°C. For thermal solution imidization, temperature was controlled to within ±1°C and for microwave imidization, it ranged from ±2°C to ±5°C. For curing rate studies, temperature was the major source of measurement error. Total measurement error ranged from 12% to 43% for ±1°C and ±5°C temperature control, respectively.

V. Results and Discussion

5.1. Comparison of Heating Rate and Reaction Rate of Polymers with Thermal Energy, Continuous, and Pulsed Microwave Radiation

Jullien and co-workers [14] have reported that the curing rate of poly(urethanes), at constant average power, can be accelerated using pulsed microwave as compared to continuous microwave radiation. The polymeric material they studied was an ethyl acetate solution (75% solid content) of the stoichiometric mixture of two prepolymers: a triisocyanate as the hard phase, and a polyester-polyalchohol as the soft phase. The average microwave power was stabilized at 30 watts for continuous as well as pulse experiments. The pulse peak power was varied from 30 to 2500 watts and the pulse period from 20 to 200 milliseconds, independently by varying the pulse width.

Figure 5-1 is a typical diagram of the sample temperature-time profile reported by Jullien and co-workers. The first and second phases, S1 and S2 respectively, are associated with the sample heating and evaporation of the solvent. The slight hump which appears near 120-140 degrees centigrade was attributed to the initiation of exothermic curing of the poly(urethane) prepolymer. Jullien and co-workers have employed the parameter T_{max}, as marked in Figure 5-1, to characterize the effect of pulsing the microwave radiation on the curing rate.

According to the results of Jullien and co-workers, displayed in Figures 5-2a and 5-2b, the maximum temperature attained by the sample (e.g., T_{max}) increased by the application of pulsing at constant average power. Figures 5-2a and 5-2b, which are reproduced from reference [14], display the maximum temperature attained by the sample versus pulse peak power and pulse period, respectively. Figure 5-2a suggests that the curing rate is accelerated as the pulse peak power is increased

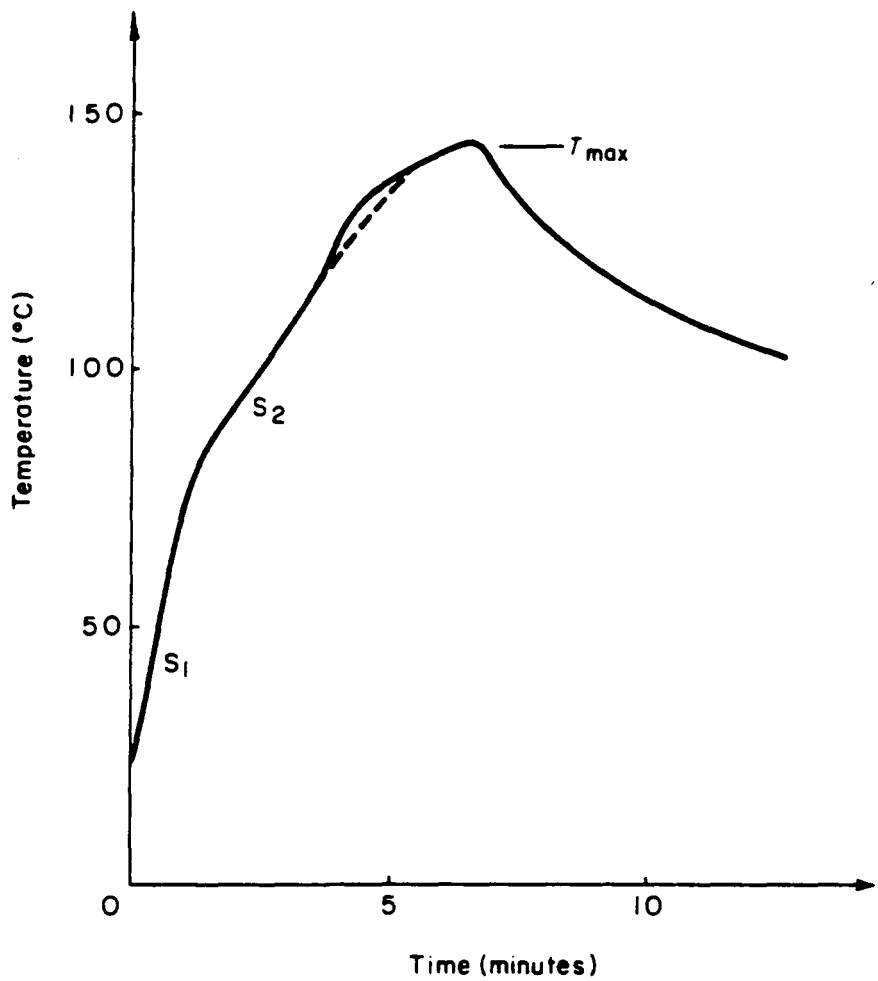

Figure 5-1: Typical diagram of the time dependence of temperature in pulsed microwave cured poly(urethane) samples [14]

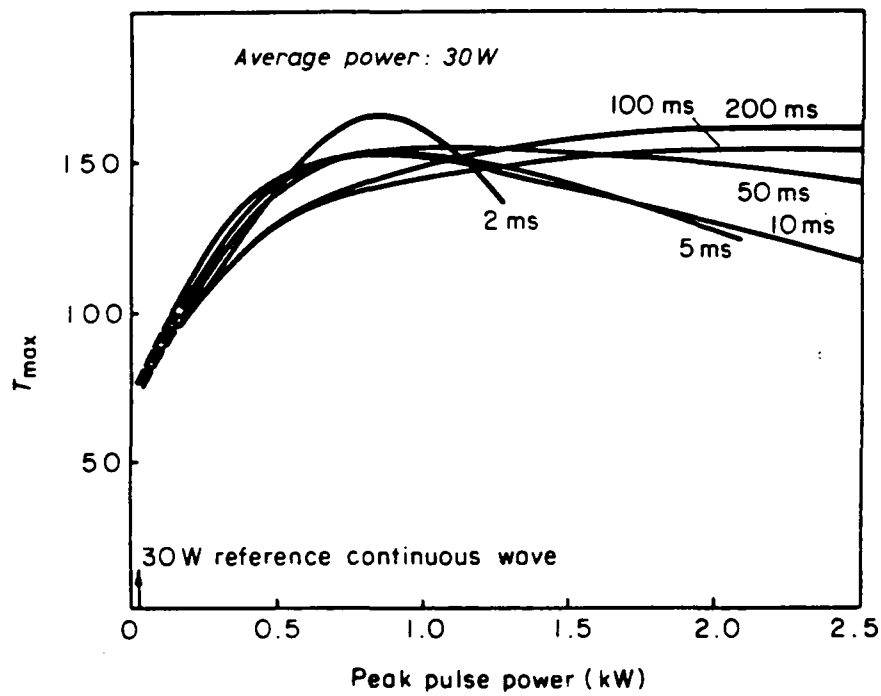

Figure 5-2a: Peak pulse power dependence of the maximum temperature T_{max}; second parameter: pulse period [14]

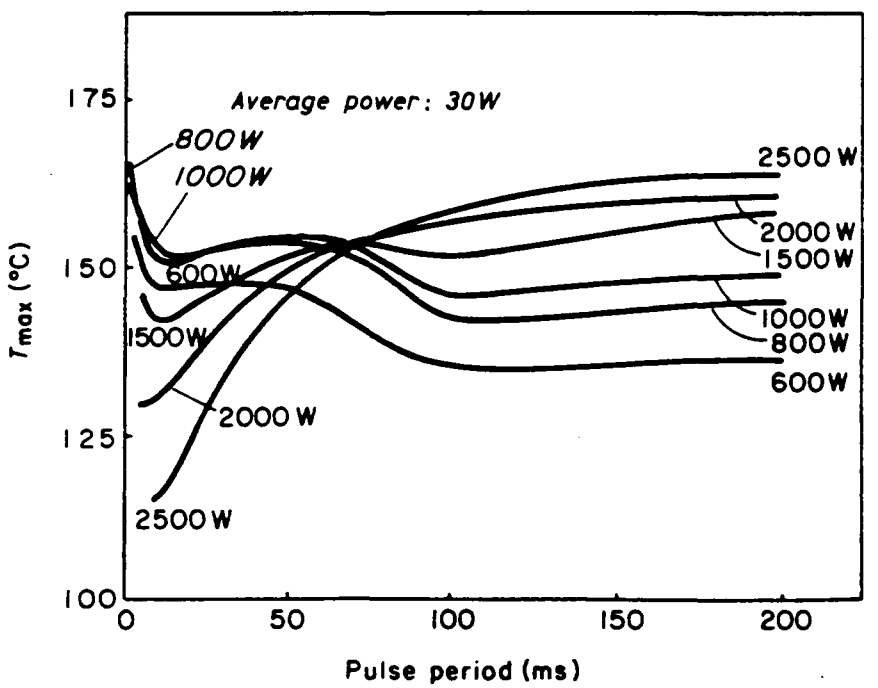

Figure 5-2b: Pulse period dependence of the maximum temperature T_{max}; second parameter: peak pulse power [14]

from 30 to 1000 watts. Also Figure 5-2b suggests that the curing rate is enhanced as the pulse period is increased from 20 to 200 milliseconds. Note that the range of pulse repetition rate, which is the reciprocal of pulse period, ranged from 5 to 50 Hertz in their study.

The enhancement in curing rate by the application of pulsing at constant average microwave power may be attributed to the following: 1) an increase in the heating rate of sample by pulsing the microwave power or 2) an increase in the reaction rate by pulsing as compared to continuous microwave power, at constant temperature. The latter interpretation implies that microwave radiation has a special effect on the reaction rate or it is intrinsically different from thermal energy. This interpretation was derived from the experimental results of Lewis et. al. [8] in which they reported 20-35 times enhancement in the curing rate of poly(amic acid) precursors with microwave radiation, at constant temperature.

The heating rate of polymeric materials with pulse as well as continuous microwave radiation and the curing rate of polymeric reactions with thermal energy, continuous, and pulse microwave radiation are studied in this work to better understand the interaction between pulsing and polymeric materials.

5.1.1. Comparison of the Heating Rate of Polymers for Continuous and Pulse Microwave Radiation

The heating rate of poly(ethylene glycol) and poly(propylene glycol) were studied as a function of molecular weight (e.g., number average) ranging from 200 to 10,000 and from 425 to 4000 grams per mole, respectively. These polymers were chosen for heating rate studies for the following reasons: 1) availability with high purity, 2) low polydispersity of the samples, and 3) simplicity of their chemical

structure for interpretation of the data. Table 5-1 lists the polydispersity index of poly(ethylene glycols) for molecular weights ranging from 200 to 8000 grams per mole. In general, the polydispersity index of poly(ethylene glycols) and poly(propylene glycols) were less than 1.5 which indicated that the samples had a narrow molecular weight distribution.

The average microwave power for continuous as well as pulse experiments was five watts with no reflected power (i.e., the reflected power measured was less than one percent of incident power for all heating rate experiments). For pulse experiments, the peak power was fixed at 1000 watts, pulse width at 10 microseconds, pulse repetition rate at 500 Hertz, and pulse period at two milliseconds.

Typical temperature-time profiles for poly(ethylene glycol) of molecular weight 2000 grams per mole with continuous microwave radiation and poly(propylene glycol) of molecular weight 3000 grams per mole with pulse microwave radiation are displayed in Figures 5-3 and 5-4, respectively. Table 5-2 and 5-3 present the numerical values for the corresponding temperature-time profiles in Figures 5-3 and 5-4. The initial temperature for heating rate experiments were 35 degrees centigrade for poly(propylene glycol) and 70 degrees centigrade for poly(ethylene glycol) samples to ensure all of the samples were above their melting temperature. The heating rate for each polymer sample was determined from the slope of temperature-time profile averaged over five trials (for a few molecular weights only four trials were used such as the one shown in Table 5-2), and the slope was calculated by the method of least squares analysis. The slope of temperature-time profiles had correlation coefficients close to unity, as shown in Figures 5-3 and 5-4, demonstrating that the profiles were linear in the time interval studied.

Table 5-1: Polydispersity of poly(ethylene glycol) for different molecular weights

number average molecular weight of poly(ethylene glycol), gr/mole	polydispersity index†
200	1.04
400	1.06
1000	1.06
3000	1.08
8000	1.14

† polydispersity index is defined as the weight average molecular weight divided by number average molecular weight of the polymer; (source of data: Aldrich Chemicals)

Table 5-2: Temperature-time data for poly(ethylene glycol) [M.W. 2000 gr/mole] with continuous microwave.

time, sec	trial 1	trial 2	trial 3	trial 4
0	70.4	70.2	70.4	70.3
1	71	70.7	70.7	70.7
2	72	71.4	71.4	71.3
3	72.8	72.2	72.3	72.3
4	73.8	73.1	73.2	73.1
5	74.8	74.3	74.2	74.2
6	75.8	75.2	75.4	75.2
7	76.8	76.3	76.5	76.2
8	78	77.5	77.7	77.3
9	78.9	78.5	78.6	78.4
10	80	79.7	79.6	79.3
11	81	80.6	80.9	80.4
12	82	81.7	81.9	81.5
13	82.9	82.7	83.1	82.5
14	84.1	83.7	84	83.5
15	84.8	84.8	85	84.5
16	85.7	85.8	85.9	85.5
17	86.6	86.7	86.8	86.4
18	87.6	87.5	87.8	87.3
19	88.4	88.4	88.5	88.2
20	89	89.4	89.4	89

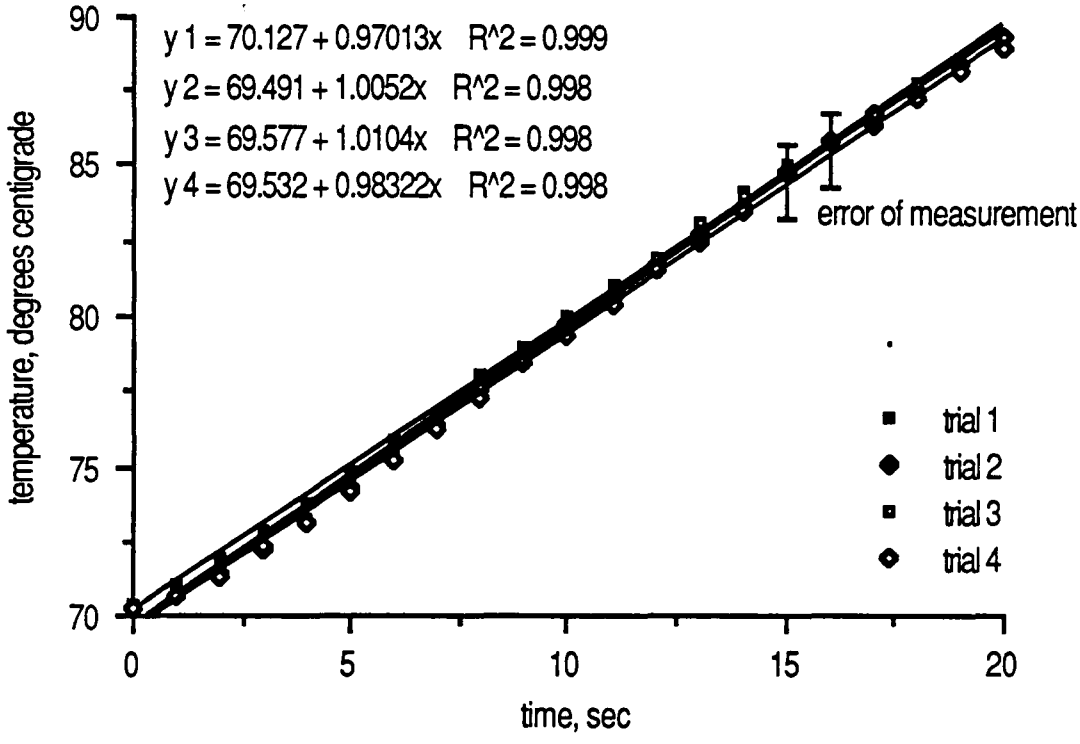

Figure 5-3: Temperature-time profile for poly(ethylene glycol) with molecular weight of 2000 grams/mole and continuous microwave radiation

Table 5-3: Temperature-time data for poly(propylene glycol) [M.W. 3000 gr/mole] with pulsed microwave.

time, sec	trial 1	trial 2	trial 3	trial 4	trial 5
0	35.5	34.6	35	34.8	34.7
2	37.6	36.5			
3	38.8	37.5	35.8	38.2	36.6
4	39.9	38.6			
6	42.3	40.7	40.4	41.7	39.8
8	44.7	43.1			
9	45.8	44.6	44.1	44.3	42.2
10	47.1	45.5			
12	49.2	47.9	47.6	49	47.2
14	51.4	50.3			
15	52.5	51.5	51.4	51.6	52
16	53.8	52.6			
18	55.5	55	55.2	55.1	55.6
20	57.6	57.1			
21	58.6	58.1	58.5	57.4	57.9
22	59.6	59.1			
24	61.2	61.1	61.6	61.3	60.8
26	62.9	63.1			
27	63.6	63.9	63.6	63.1	62.8
28	64.3	64.9			
30	65.6	66.5	66.1	65.8	64.5

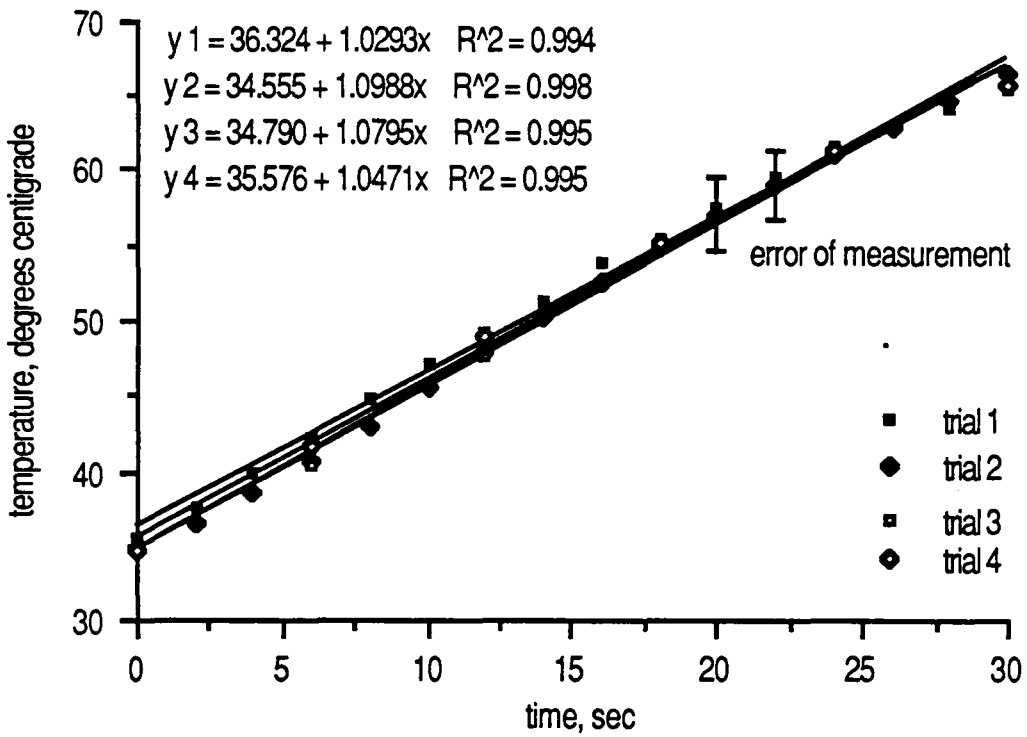

Figure 5-4: Temperature-time profile for poly(propylene glycol) with molecular weight of 3000 grams/mole and pulsed microwave radiation

Table 5-4 lists the numerical values for the heating rate of poly(ethylene glycol) as a function of molecular weight for continuous as well as pulse microwave radiation along with their corresponding measurement error bars. The measurement errors, which were calculated from equations in Appendix 2, were six percent of the heating rate values. The data for poly(ethylene glycol) with continuous microwave radiation is also displayed graphically in Figure 5-5 as a function of natural logarithm of the number of repeat units. The number of repeat units for poly(ethylene glycol) and poly(propylene glycol) are defined by the following equation:

$$n_e = (MW_e - 18) / 44 \quad (5\text{-}1)$$

$$n_p = (MW_p - 18) / 58 \quad (5\text{-}2)$$

Where n_e = number of repeat units for poly(ethylene glycol) with molecular weight MW_e

n_p = number of repeat units for poly(propylene glycol) with molecular weight MW_p

MW_e = molecular weight of the poly(ethylene glycol)

MW_p = molecular weight of the poly(propylene glycol)

The numbers 18, 44, and 58 in Equations 5-1 and 5-2 are molecular weights of the end group, ethylene oxide repeat unit, and propylene oxide repeat unit, respectively. The highest and the lowest slopes from the temperature-time profiles are also shown in Figure 5-5, along with the measurement error bars. Also the sample with natural logarithm of repeat unit equal to zero (e.g., number of repeat units equal to one) was the ethylene glycol monomer. According to Figure 5-5, the heating rate of poly(ethylene glycol) is higher than ethylene glycol monomer, in the liquid state [95]. Since the heating rate is proportional to dielectric loss of the polymer, as

Table 5-4: Heating rate of poly(ethylene glycol) versus molecular weight for continuous and pulse microwave radiation at 70 C

molecular weight of poly(ethylene glycol), gr/mole	No. of repeat units		heating rate, degrees per seconds	
	n	Ln(n)	continuous	pulse
62	1	0	0.691 ± 0.04 †	0.582 ± 0.03
200	4	1.39	1.02 ± 0.06	0.817 ± 0.05
300	6	1.79	0.976 ± 0.06	0.840 ± 0.05
400	9	2.20	1.08 ± 0.06	0.831 ± 0.05
600	13	2.57	0.930 ± 0.06	0.878 ± 0.05
1000	22	3.10	0.962 ± 0.06	0.933 ± 0.06
1500	34	3.53	1.00 ± 0.06	0.941 ± 0.06
2000	45	3.81	0.993 ± 0.06	0.941 ± 0.06
3400	77	4.34	1.11 ± 0.07	1.01 ± 0.06
8000	181	5.20	1.19 ± 0.07	1.04 ± 0.06
10,000	227	5.43	1.07 ± 0.06	1.05 ± 0.06

† error of measurement

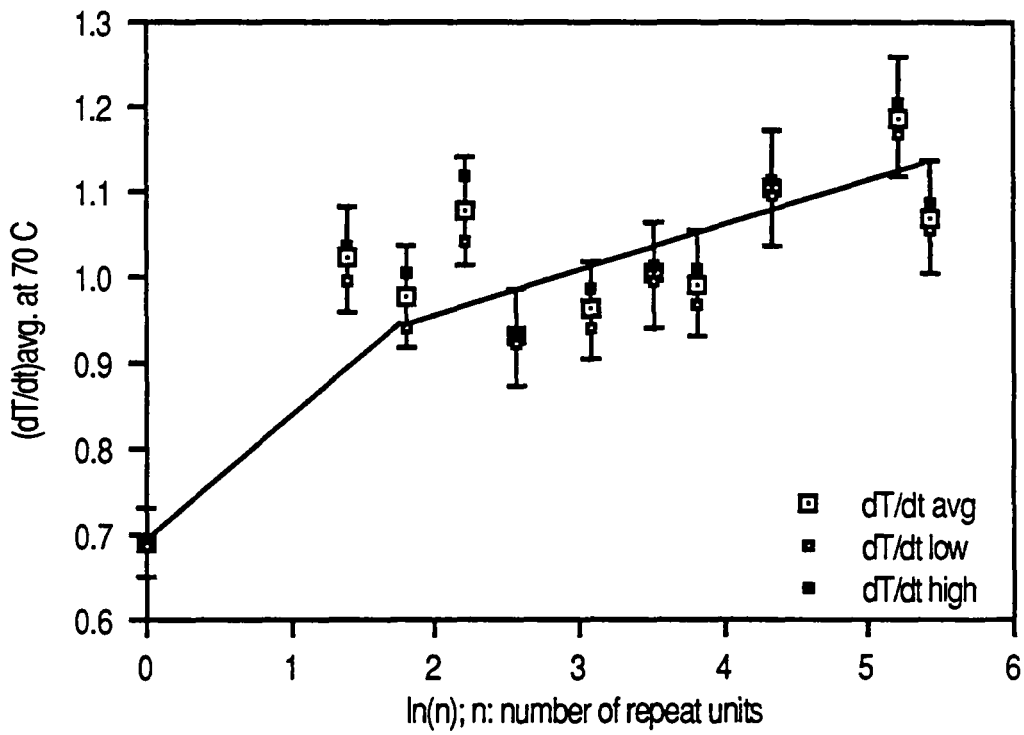

Figure 5-5: heating rate of poly(ethylene glycol) versus molecular weight for continuous microwave radiation at 70°C

demonstrated in the theory section, this means that the dielectric loss of poly(ethylene glycol) is higher than the ethylene glycol monomer.

Figure 5-6 compares the heating rate for poly(ethylene glycol) as a function of molecular weight for continuous as well as pulse microwave radiation. According to Figure 5-6, the heating rate of poly(ethylene glycol) with pulsed microwave energy was slightly lower than continuous microwave radiation for repeat units ranging from one to 15 and it was almost identical for repeat units greater than 15. Therefore, for poly(ethylene glycol) no significant improvement in heating rate was observed by pulsing the microwave radiation.

The numerical values for heating rate of poly(propylene glycols), along with their measurement errors, with continuous as well as pulsed microwave radiation are listed in Table 5-5 as a function of molecular weight. The data for poly(propylene glycol) with continuous microwave radiation is also displayed graphically in Figure 5-7. According to Figure 5-7, the heating rate of poly(propylene glycol) increases initially up to the repeat units equal to five and then decreases for repeat units greater than five. This transition, located at repeat units close to five, may be a structural transition which has been reported by James E. Mark [90-93]. This structural transition is caused by chains having a preference for gauche conformation over the trans around certain skeletal bonds in the range of repeat units from one to ten. Heating rate studies with a wide range of molecular weights, from the monomer to 1000 grams per mole, for poly(ethylene glycol) and poly(propylene) glycol along with dielectric studies are needed to confirm that the peak in Figure 5-7 is a structural transition.

Figure 5-8 compares the heating rate of poly(propylene glycol) versus number of repeat units for continuous as well as pulse microwave radiation. Contrary to poly(ethylene glycol), the heating rate of poly(propylene glycol) with pulsed

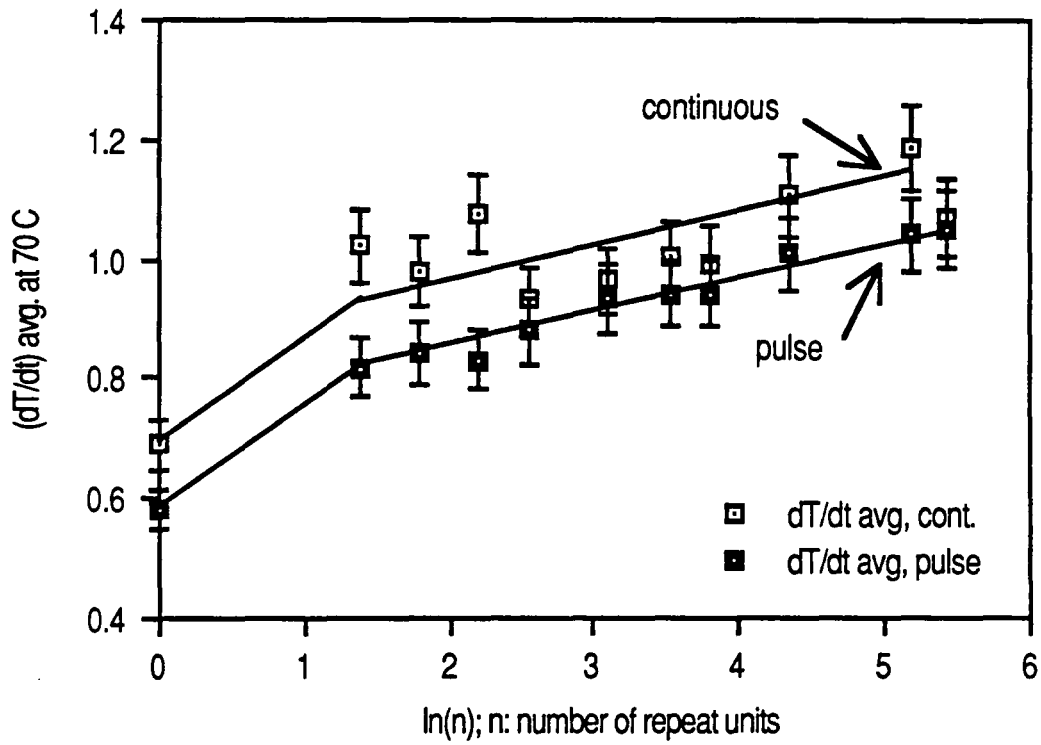

Figure 5-6: heating rate of poly(ethylene glycol) versus molecular weight for continuous and pulsed microwave radiation at 70°C

Table 5-5: Heating rate of poly(propylene glycol) versus molecular weight for continuous and pulse microwave radiation at 35°C

molecular weight of poly(propylene glycol), gr/mole	No. of repeat units, n	heating rate, degrees per seconds	
		continuous	pulse
76	1	0.764±0.05 †	0.830±0.05
425	7	0.818±0.05	0.991±0.06
725	12	0.791±0.05	0.826±0.05
1000	17	0.783±0.05	0.991±0.06
2000	34	0.717±0.04	1.03±0.06
3000	51	0.545±0.03	1.06±0.06
4000	67	0.725±0.04	1.13±0.07

† error of measurement

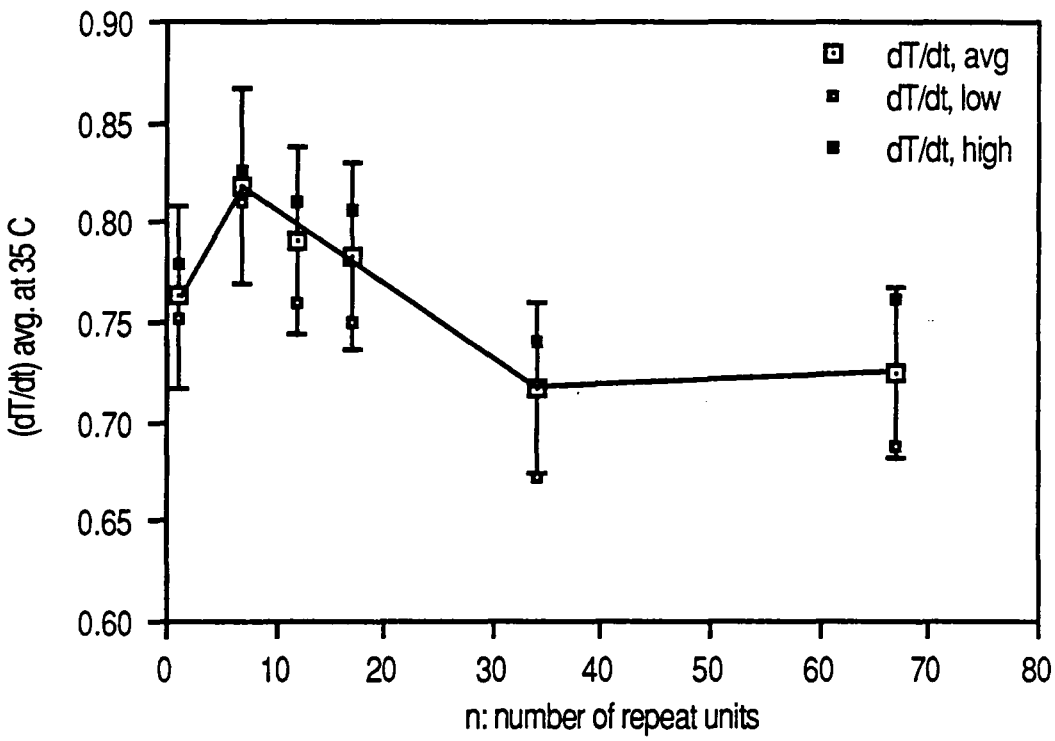

Figure 5-7: Heating rate of poly(propylene glycol) versus molecular weight for continuous microwave radiation at 35°C

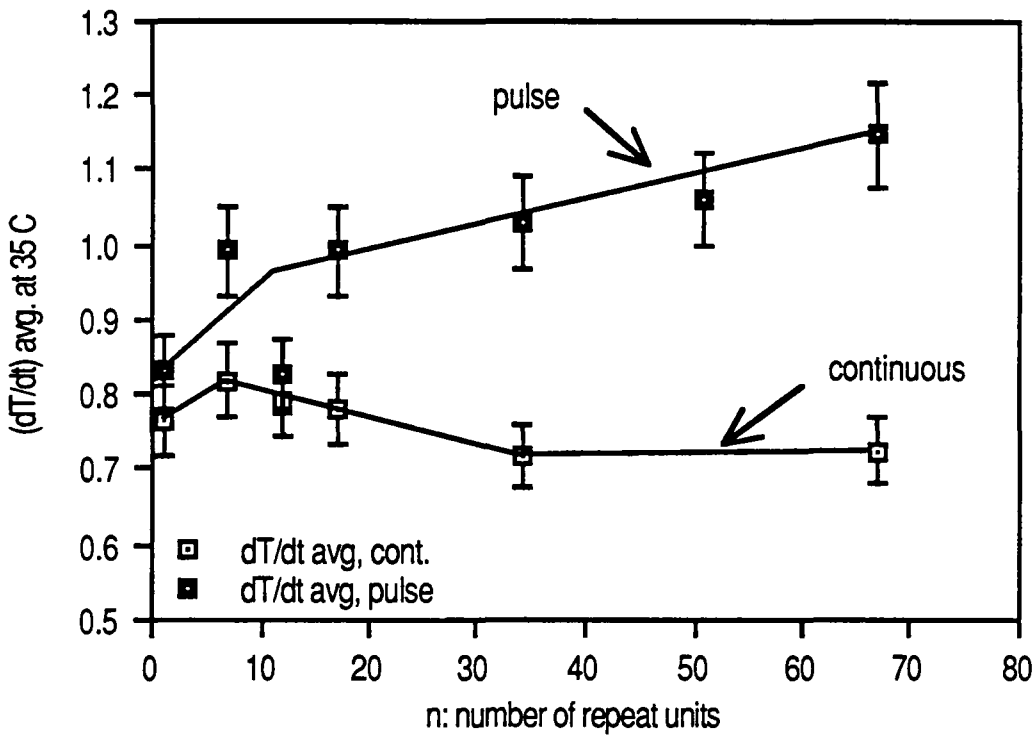

Figure 5-8: Heating rate of poly(propylene glycol) versus molecular weight for continuous and pulsed microwave radiation at 35°C

microwave was higher than continuous microwave for all molecular weights studied. Although the results are contradictory, this anomaly can be explained by comparing the low frequency dielectric spectrum of poly(ethylene glycol) and poly(propylene glycol).

Figure 5-9 compares the dielectric loss of poly(ethylene) and poly(propylene) in the solid state at room temperature, reproduced from reference [63]. According to Figure 5-9, polymers derived from propylene have a loss peak in the low frequency region of the dielectric spectrum ranging from 100 to 10,000 Hertz. On the other hand, polymers derived from ethylene do not posses such a loss peak in the low frequency region. Figures 5-10a and 5-10b display the dielectric loss spectrum for poly(propylene oxide) with number average molecular weight of 1800±300 and 3700±600 grams per mole, respectively, in the liquid state [94]. Figure 5-10c displays the arc plot (e.g., plot of dielectric loss versus dielectric constant) for poly(propylene oxide) with number average molecular weight of 1800±300 grams per mole, in the liquid state [94]. Consistent with Figure 5-9, poly(propylene oxide) has a low frequency loss peak in the frequency range of 100 to 10,000 Hertz at -30 degrees centigrade. Since the polymers in Figures 5-10a to 5-10c are in the liquid state, the loss peak can not be attributed to anomalous transitions or dispersions in the semicrystalline state, and therefore it is a characteristic of propylene oxide derived polymers. We should bear in mind that the data in Figures 5-10a, 10b, and 10c was taken at -30 degrees centigrade. On the other hand, in our experiments the temperature was +35 degrees centigrade. The low frequency absorption peak, displayed in Figure 5-10a, 10b, and 10c, may shift to higher frequencies, by as much as 10,000 Hz depending on molecular weight [94], as the temperature is raised to +35 degrees centigrade.

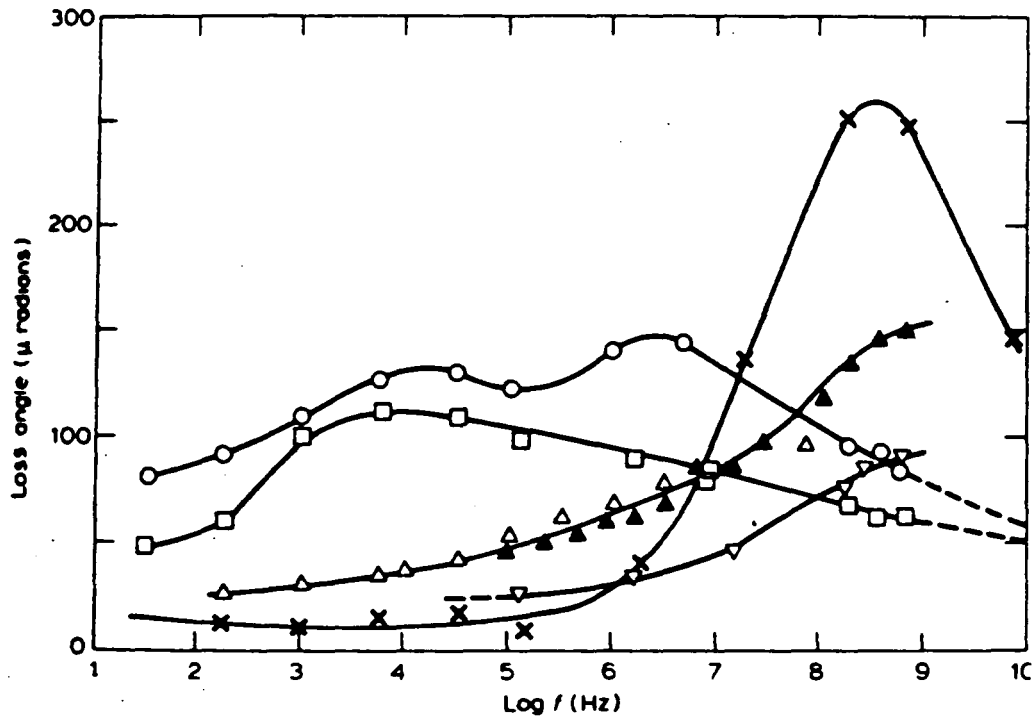

Figure 5-9: Loss angle versus Log frequency for several polymers at room temperature: poly(propylene); Δ Δ poly(ethylene) ρ=0.923 g/cc; ∇ poly(ethylene) ρ=0.934 g/cc; x poly(tetraflouroethylene); and o poly(ethylene)/poly(propylene) copolymer [63]

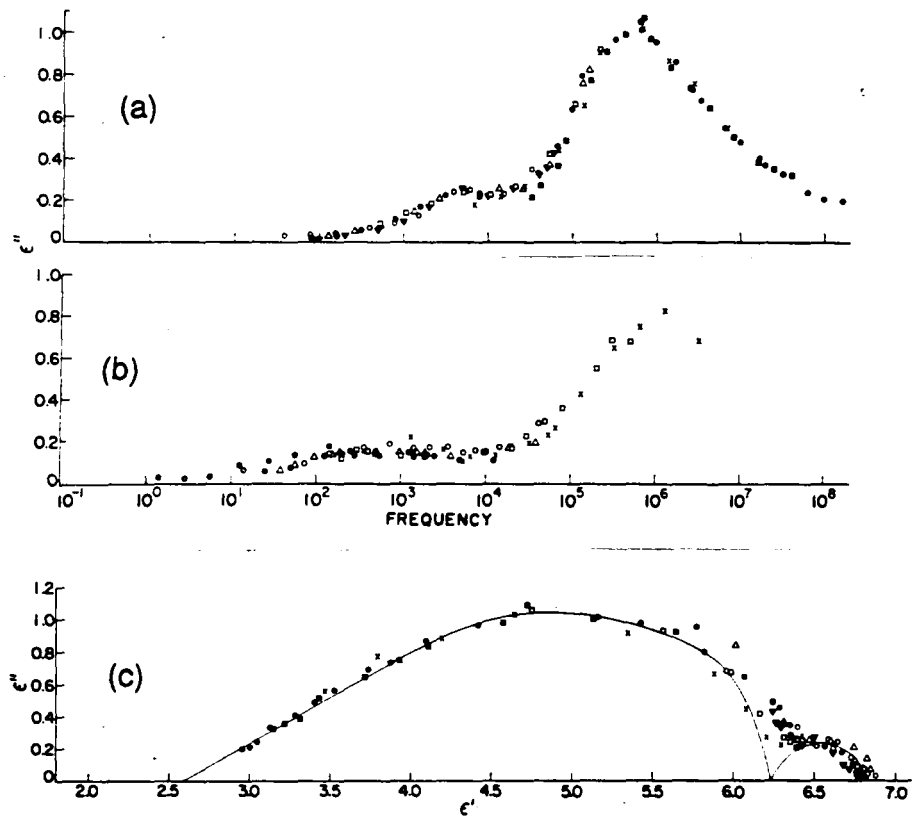

Figure 5-10: plots of relative dielectric loss (ε") versus frequency for liquid poly(propylene oxide) at -30°C; (a) M.W.=1800±300 g/mole; (b) M.W.=3700±600 g/mole; (c) arc plot of relative dielectric loss versus dielectric constant for the M.W.=1800±300 g/mole [94]

The methyl side group in poly(propylene oxide) is not perpendicular to the main chain, and therefore the dipole moment of the chain has two components [94]. One component of the dipole moment is parallel to the main chain axis and the other component is perpendicular to the main chain. The component of the dipole moment parallel or along the main chain axis gives rise to the low frequency dielectric absorption in propylene derived polymers such as poly(propylene glycol). This low frequency absorption is also a function of molecular weight because the dipole moment is along the main chain axis. The additional microwave energy dissipated in the sample by pulsing at a repetition rate in the vicinity of the low frequency dielectric absorption peak of poly(propylene glycol) may partially explain the higher heating rate of poly(propylene glycol) with pulse microwave as opposed to continuous microwave radiation.

The effectiveness of pulsing the microwave radiation for heating polymeric materials may be partially attributed to the low frequency dielectric absorption spectrum of the material. If the polymeric material has a low frequency absorption near the repetition frequency of the pulsed microwave, then pulsing would be effective, as illustrated in Figure 5-8 for poly(propylene glycol). On the other hand, if the material does not have a low frequency absorption peak, pulsing would not be effective, as illustrated in Figure 5-6 for poly(ethylene glycol).

5.1.2. Comparison of Curing Rate of Polymers with Thermal Energy, Continuous, and Pulsed Microwave Radiation.

The purpose of this set of experiments was to establish whether pulsing the microwave energy has any special effect on the curing rate at constant temperature, as was reported previously by Lewis et. al. [8] for continuous microwave radiation.

Lewis et. al. have reported that the imidization rate of poly(amic acids) was enhanced 20-35 times at constant temperature by the application of continuous microwave radiation. They proposed that the absorption of microwave radiation by the polymer sample produced "localized hot spots" that were 1-2 Angstroms in diameter.

The reaction that we have studied was the curing of poly(amic acids) in solution. The poly(amic acid) was based on 3,3',4,4'-benzophenonetetracarboxylic dianhydride (BTDA) as the dianhydride and 2,2'-bis(aminophenyl) propane (BAP) as the diamine. The reaction for imidization of poly(amic acids) in solution is depicted in Figure 5-11. For all of the experiments in this section, the poly(amic acid) was imidized at 140 degrees centigrade, under inert and dry nitrogen atmosphere, with 15 percent poly(amic acid) content by weight, and in 80/20 NMP/CHP solvent mixture. The extent of reaction was followed as a function of time by taking 0.2 milliliter aliquots from the reaction mixture and analyzing with Fourier Transform Infrared Spectroscopy (FTIR). Figure 5-12 displays the FTIR spectrum of BTDA/BAP based poly(amic acid) reaction mixture before imidization and after it was completely cured by bulk thermal imidization method in an oven. The peaks of interest in the FTIR spectra of BTDA/BAP based poly(amic acid) are marked in Figure 5-12 and are also listed in Table 5-7. The imide peak at 1363±1.9, the amic acid peak at 1408±1.6, and the reference peak at 1016±0.1 wavenumbers were used exclusively in this study to follow the extent of imidization. This was because the baseline was very well defined for the the latter peaks. The peaks listed in Table 5-7 shifted by maximum of ±3 wavenumbers, but they remained as singlet peaks during the course of imidization reaction.

Typical temperature-time profiles for imidization of poly(amic acid) with continuous and pulse microwave radiation are displayed in Figure 5-13a and 5-13b,

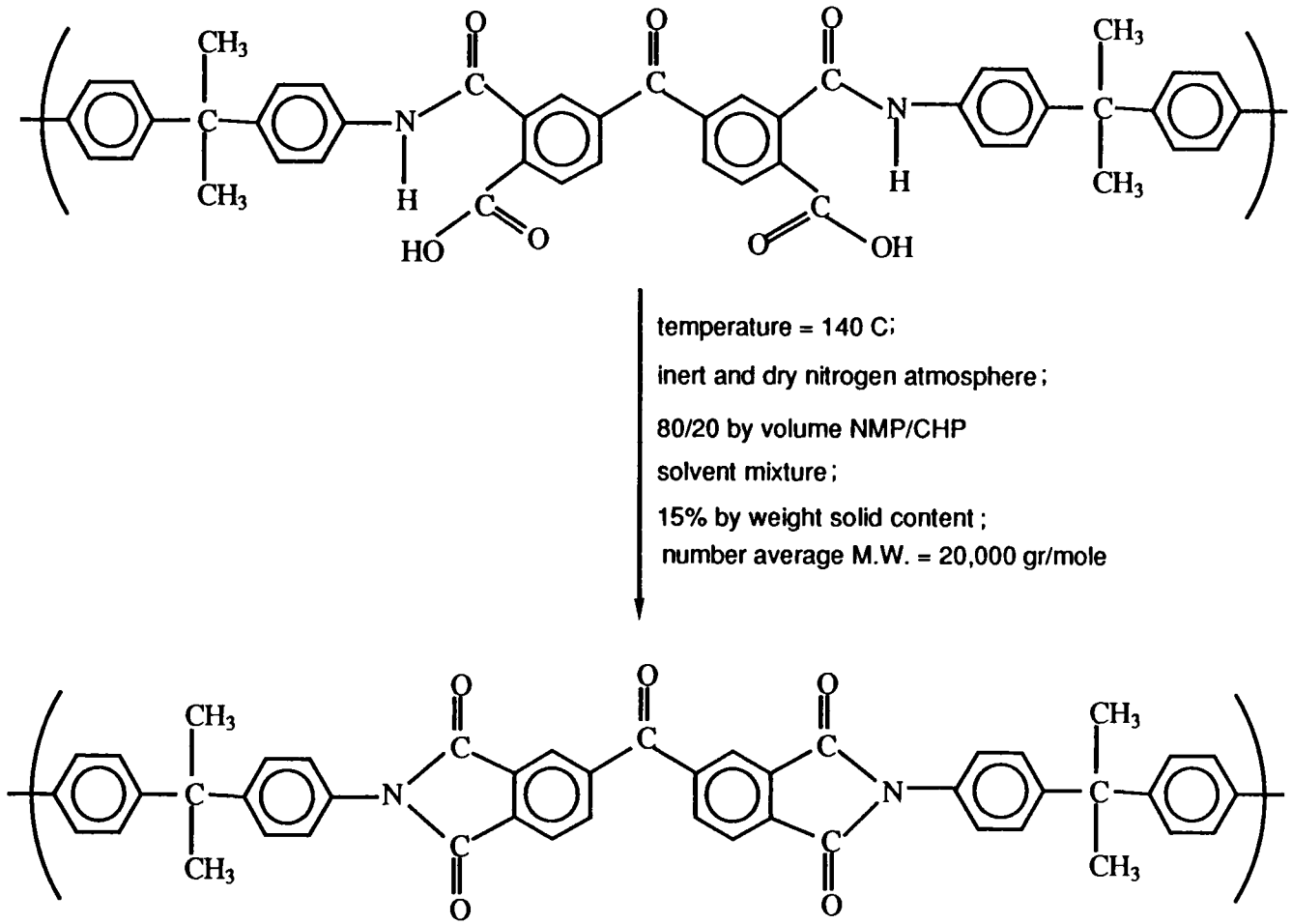

Figure 5-11: Reaction scheme for imidization of BTDA/BAP poly(amic acid)

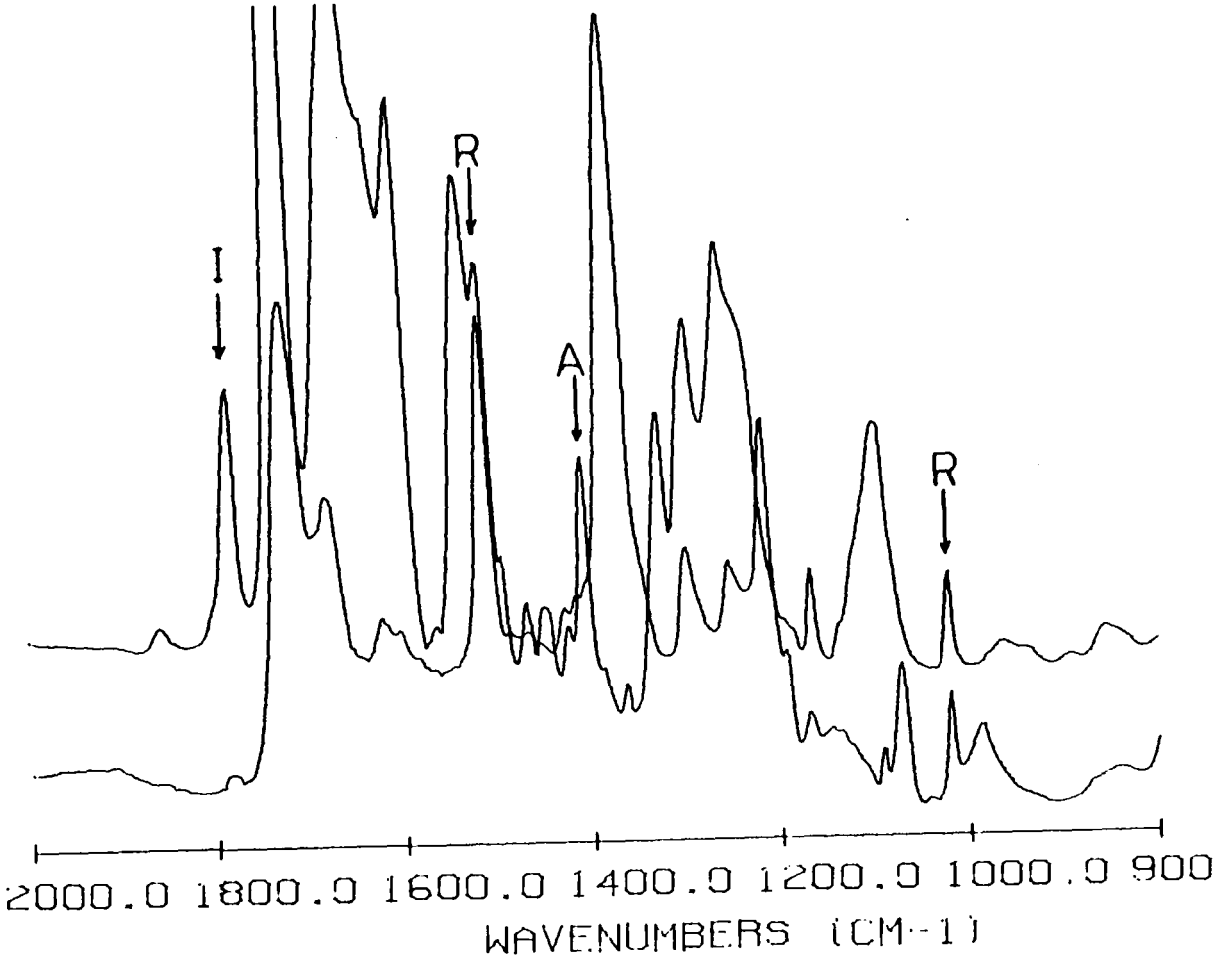

Figure 5-12: FTIR spectra of BTDA/BAP poly(amic acid) reaction mixture before imidization and after it is completely imidized thermally in an oven

Table 5-7: Useful peaks in the FTIR spectra of BTDA/BAP based poly(amic acid) for studying the kinetics of imidization

FTIR peak, wavenumbers	band assignment
1780.7-1783.3	imide peak
1512.4-1513.3	reference peak due to vibrations of the benzene ring
1406.3-1409.6	amic acid peak
1361.5-1365.3	imide peak, more intense than the peak at 1778
1016.6-1016.7	reference peak due to vibrations of the propyl group

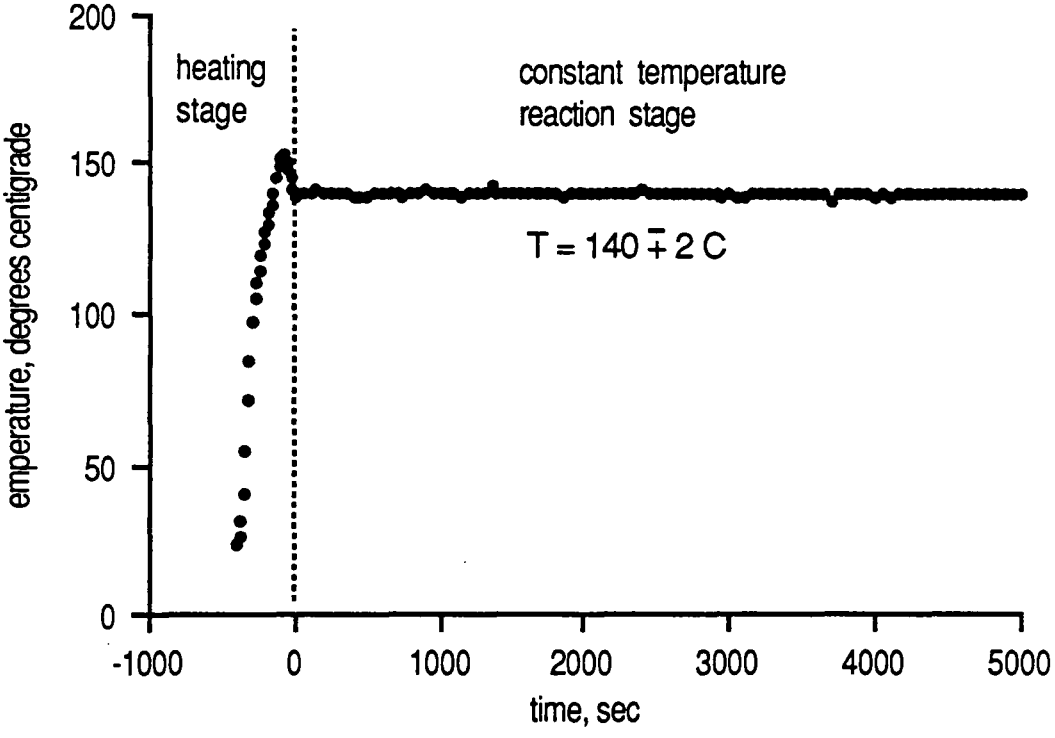

Figure 5-13a: Temperature-time profile for continuous microwave imidization of BTDA/BAP based poly(amic acid) at 140°C

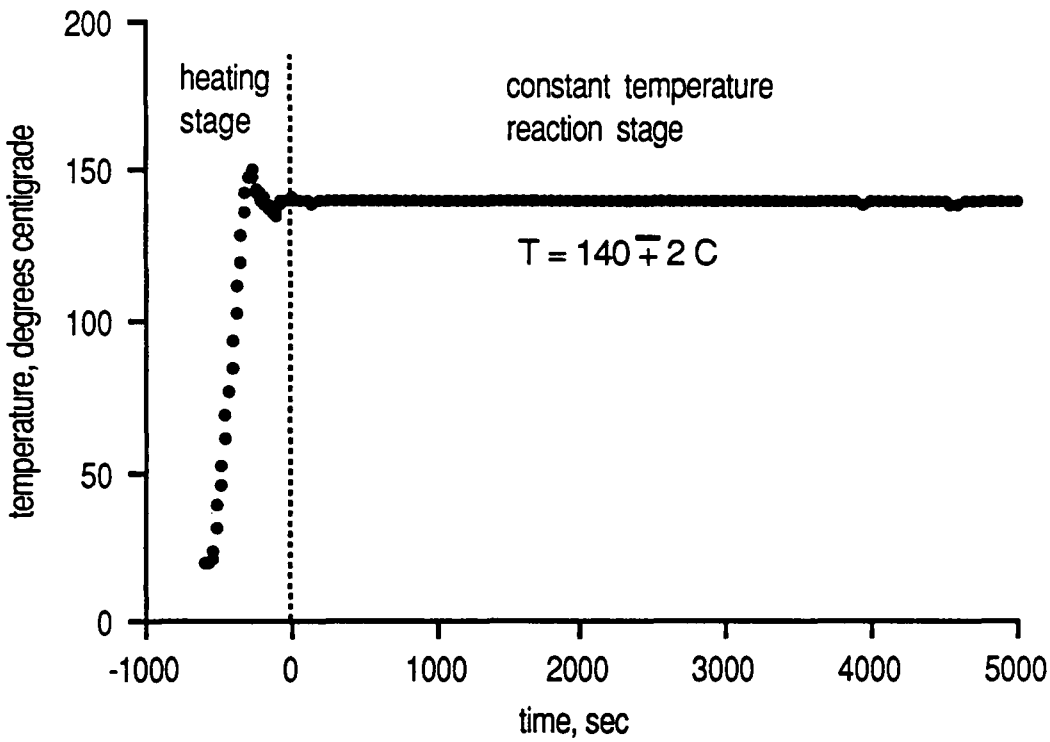

Figure 5-13b: Temperature-time profile for pulse microwave imidization of BTDA/BAP based poly(amic acid) at 140°C

respectively. In general, the reaction cell was heated with a heat gun to the desired reaction temperature of 140 degrees centigrade in less than 500 seconds, and then controlled at this temperature to within ±2°C with microwave energy. The kinetic study was initiated immediately after the heating period by withdrawing aliquots from the reaction cell as a function of time. The reactions were generally followed as a function of time for up to two hours with microwave radiation. In this section, there is not sufficient data to support that the temperature inside the sample cell was uniform and homogeneous during the course of reaction with microwave energy. In the next section, the solution is agitated to eliminate any temperature gradient in the cell.

Figure 5-14 displays the FTIR spectra of BTDA/BAP poly(amic acid) immediately after the heating period. There was less than one percent conversion during the heating period, as shown in Figure 5-14. Figure 5-15 displays a plot of reaction rate versus time for curing of poly(amic acids) with thermal energy and continuous microwave radiation. The ordinate in Figure 5-15 is the negative of natural logarithm of one minus α_a, where α_a is the conversion of amic acid, and the abscissa is time in seconds. The slope of the plot in Figure 5-15 is the rate constant for the imidization reaction as was derived in the theory chapter in section 3.3.

According to Figure 5-15, the rate of imidization of BTDA/BAP based poly(amic acid), at constant temperature of 140 degrees centigrade, was identical for thermal energy and continuous microwave radiation. The same experiment was repeated with a different type of poly(amic acid) based on BTDA as the dianhydride but para-diaminodiphenyl sulfone (pDDS) as the diamine. Table 5-8 compares the imidization rate constant for two different types of poly(amic acids) with thermal energy as well as continuous microwave radiation. According to Table 5-8, the rate of imidization was identical, within experimental error (see measurement errors in Table 5-8), using

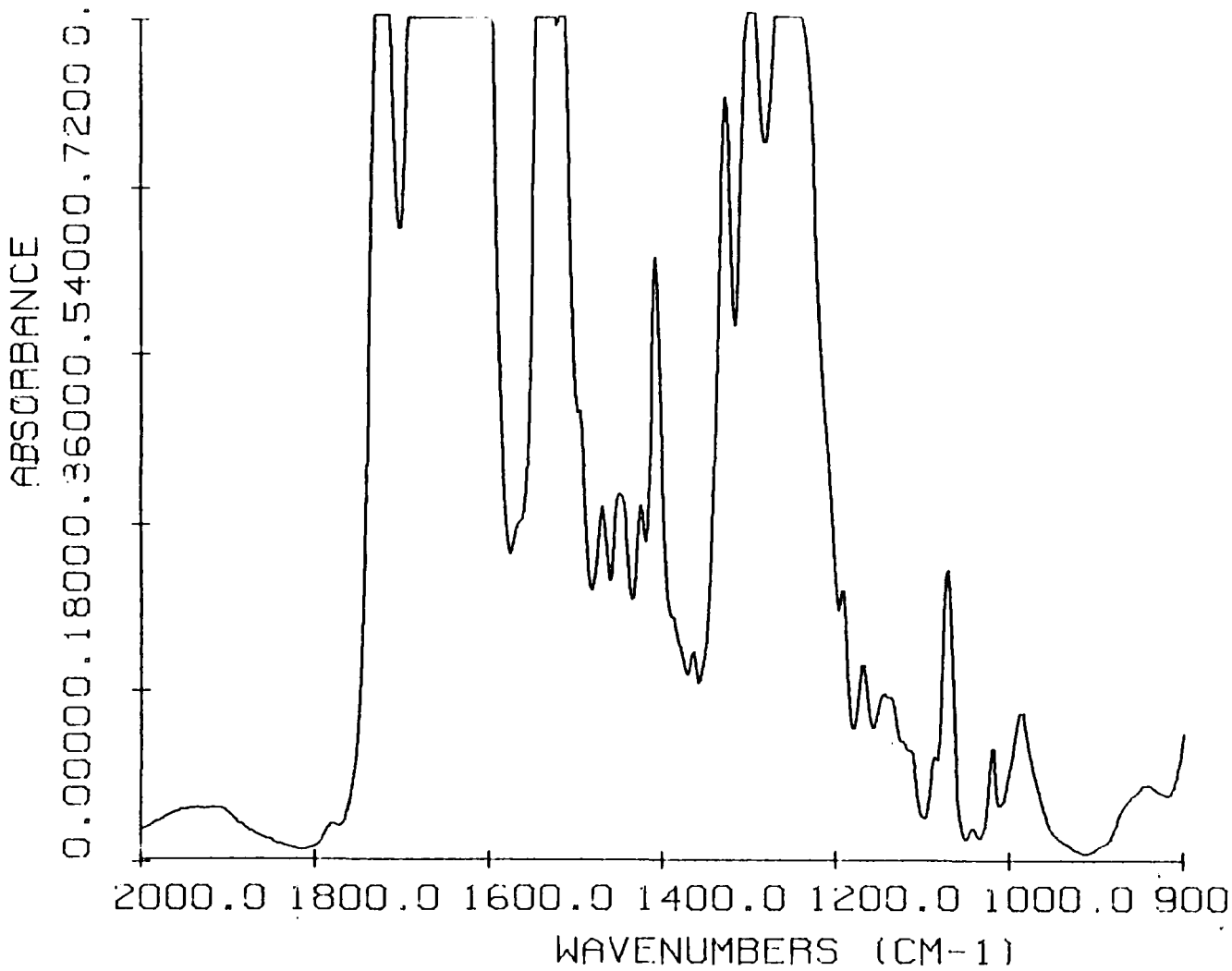

Figure 5-14: FTIR spectra of BTDA/BAP poly(amic acid) after the heating period

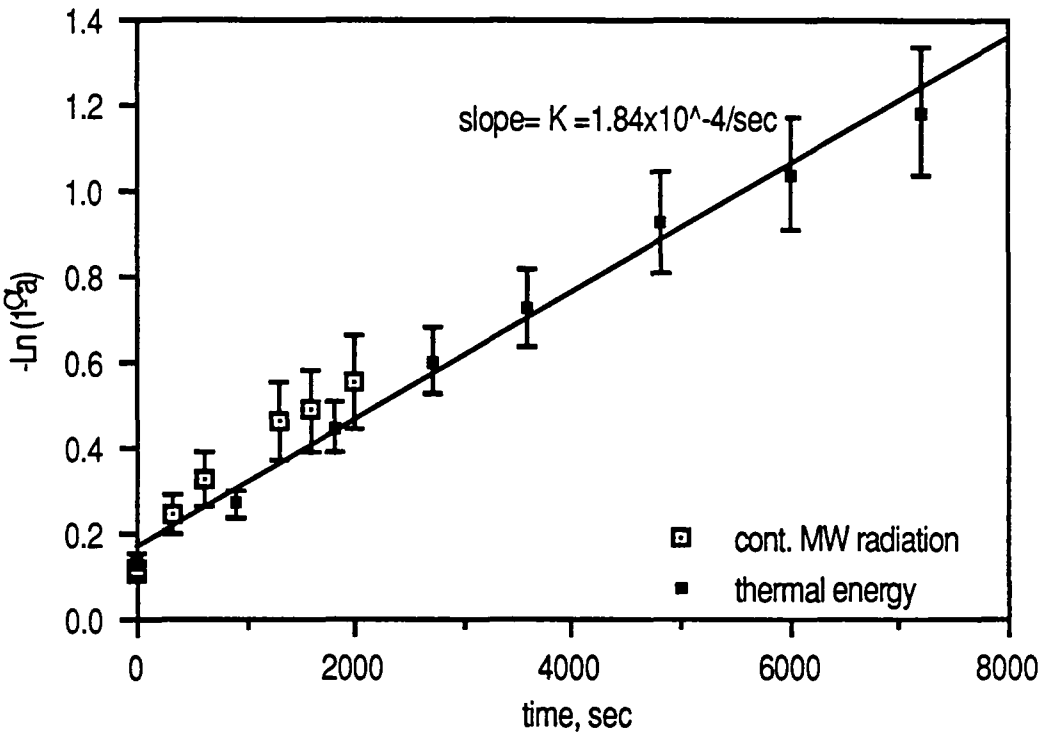

Figure 5-15: Extent of reaction versus time for imidization of BTDA/BAP poly(amic acid) with thermal energy and continuous microwave radiation at 140°C

Table 5-8 : Rate constant versus imide type for thermal energy and continuous microwave radiation at 140 C.

imide system / heating source	rate constant, K (10^-5)/ sec	
	BTDA/BAP	BTDA/pDDS
thermal energy	14.8± 1.8 †	2.61± 0.31
continuous microwave radiation	21.0± 4.0	4.08± 0.78

† error of measurement

thermal energy or continuous microwave radiation for both types of poly(amic acids). This apparent contradiction between our results and the previously reported results by Lewis et. al. will be investigated in more detail in the next section where we study the effect of agitation rate at constant temperature on the rate of imidization of poly(amic acids).

Figure 5-16 displays a plot of reaction rate versus time for imidization of BTDA/BAP based poly(amic acid) with pulse microwave radiation for repetition rates ranging from 50 to 30,000 Hertz. The pulse repetition rate was varied at constant average power by varying the pulse width from 0.5 to 50 microseconds, respectively. According to Figure 5-16, the rate of imidization of poly(amic acid), at constant temperature of 140 degrees centigrade, remained the same, within experimental error, as the pulse repetition rate was varied from 50 to 30,000 Hertz.

The data in Figures 5-15 and 5-16 are combined and plotted once more in Figure 5-17 to compare the rate of thermal, continuous , and pulsed microwave curing of poly(amic acids) side by side. Figure 5-17 demonstrates that the imidization rate of poly(amic acids), at constant temperature of 140 degrees centigrade, is identical, within experimental error, for thermal energy, continuous, and pulse microwave radiation. The numerical values of the reaction rate constants for imidization of BTDA/BAP based poly(amic acids) at 140 degrees centigrade, with their corresponding measurement error, are also listed in Table 5-9.

Based on the results of this section, not only pulsed microwave radiation has no special effect on the imidization rate of poly(amic acid) at constant temperature, but also continuous microwave energy has no special effect. Also, comparison of the results in the previous section of this chapter and this section indicates that the increase in the maximum temperature observed by Jullien and co-workers [14] for

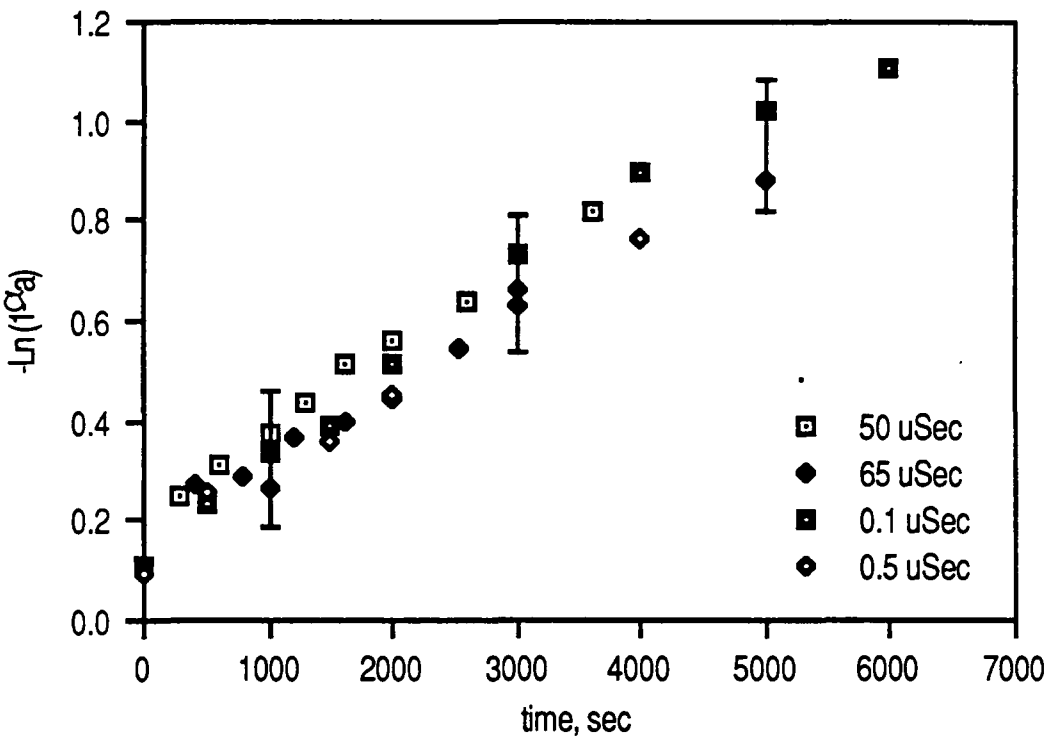

Figure 5-16: Extent of reaction versus time for imidization of BTDA/BAP with pulsed microwave radiation at 140°C

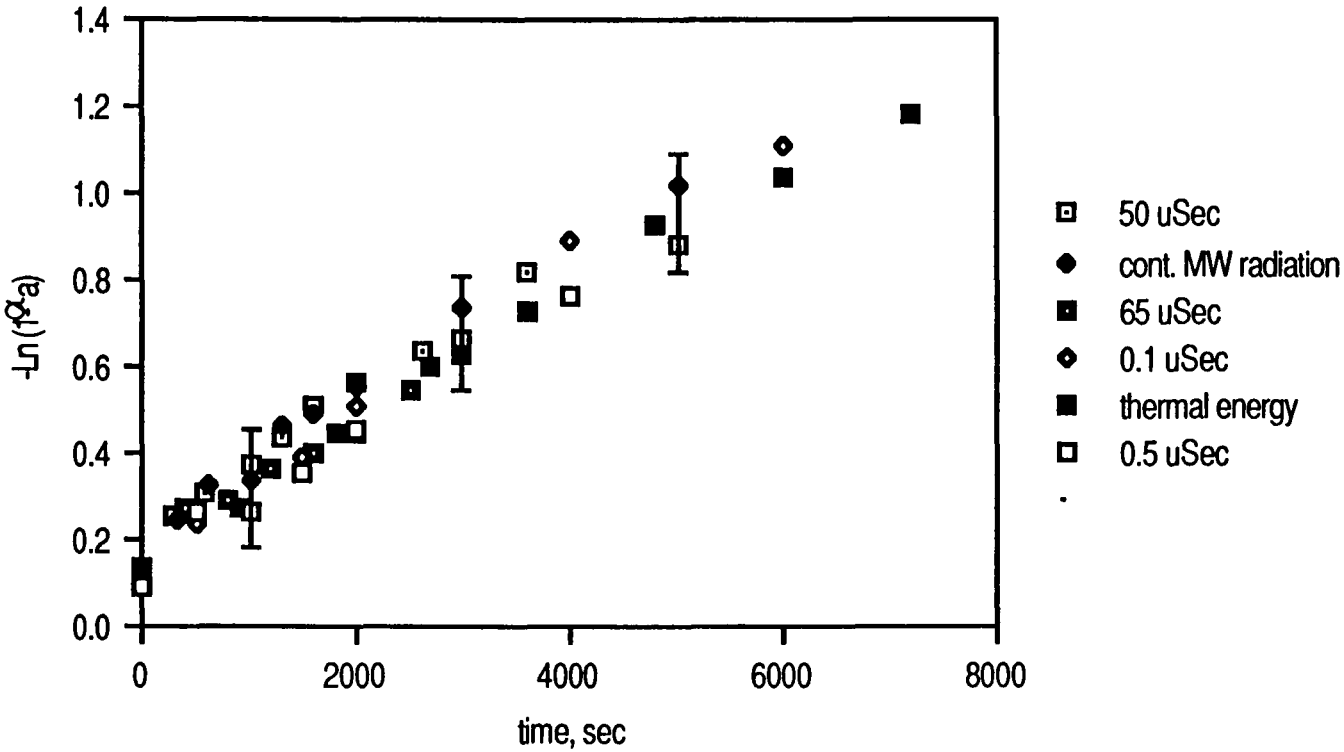

Figure 5-17: Extent of reaction versus time for imidization of BTDA/BAP poly(amic acid) with thermal energy, continuous, and pulsed microwave radiation at 140°C

Table 5-9: Rate constant for imidization of BTDA/BAP based poly(amic acid) with thermal energy, continuous, and pulse microwave radiation at 140°C

type of heating source	rate constant, K (10^-4)/ sec
thermal energy	1.48 ± 0.18 †
continuous microwave radiation	2.10 ± 0.40
pulse microwave radiation PW = 65 usec; PRF = 50 Hz	1.54 ± 0.29
pulse microwave radiation PW = 50 usec; PRF = 70 Hz	1.83 ± 0.35
pulse microwave radiation PW = 0.5 usec; PRF = 10,000 Hz	1.57 ± 0.30
pulse microwave radiation PW = 0.1 usec; PRF = 30,000 Hz	1.71 ± 0.32

PW [=] pulse width

PRF [=] pulse repetition frequency

† error of measurement

curing of poly(urethanes) may be attributed to higher heating rate of the poly(urethane) sample with pulsed microwave as compared to continuous microwave radiation.

5.2. Effect of Microwave Power and Agitation Rate at Constant Temperature on the Curing Rate of Polymers

The objective of this set of experiments was to determine whether microwave radiation has any special effect on the curing rate of polymers at constant temperature as compared to thermal energy. Based on theoretical analysis for an empty, completely closed, hollow cylindrical cavity (e.g., see chapter III), there may exist significant power distribution or temperature gradients along the length of a sample with height greater than two millimeters. In this set of experiments, the experimental apparatus was modified in order to agitate the reaction mixture to eliminate any temperature gradients in the cell. Also, the sample was cooled, simultaneously, as it was irradiated with higher microwave power to intensify any special effect of microwave radiation as compared to thermal energy.

The reaction for imidization of BTDA/pDDS based poly(amic acid) in solution is presented in Figure 5-18. For all of the experiments in this section, poly(amic acid) based on BTDA/pDDS was imidized at the "measured" temperature of 140 degrees centigrade. Figure 5-19 displays the superimposed FTIR spectra of BTDA/pDDS based poly(amic acid) reaction mixture before imidization and after 90 percent imidized by bulk thermal imidization method in an oven. The peaks of interest in the FTIR spectra are marked in Figure 5-19 and are also listed in Table 5-10. The imide peak at 1371±1.3, the amic acid peak at 1405±2.8, and the reference peak at

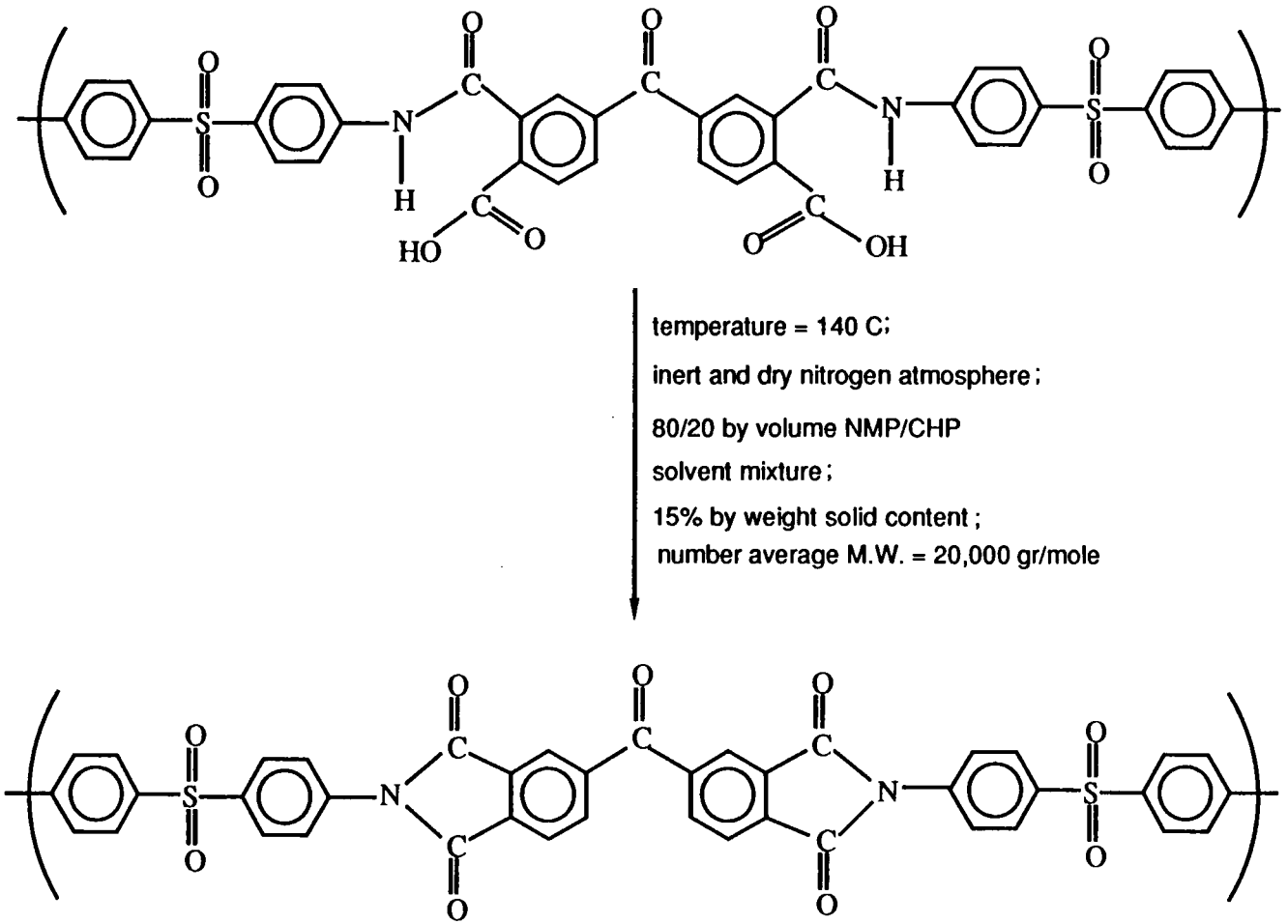

Figure 5-18: Reaction scheme for imidization of BTDA/pDDS poly(amic acid)

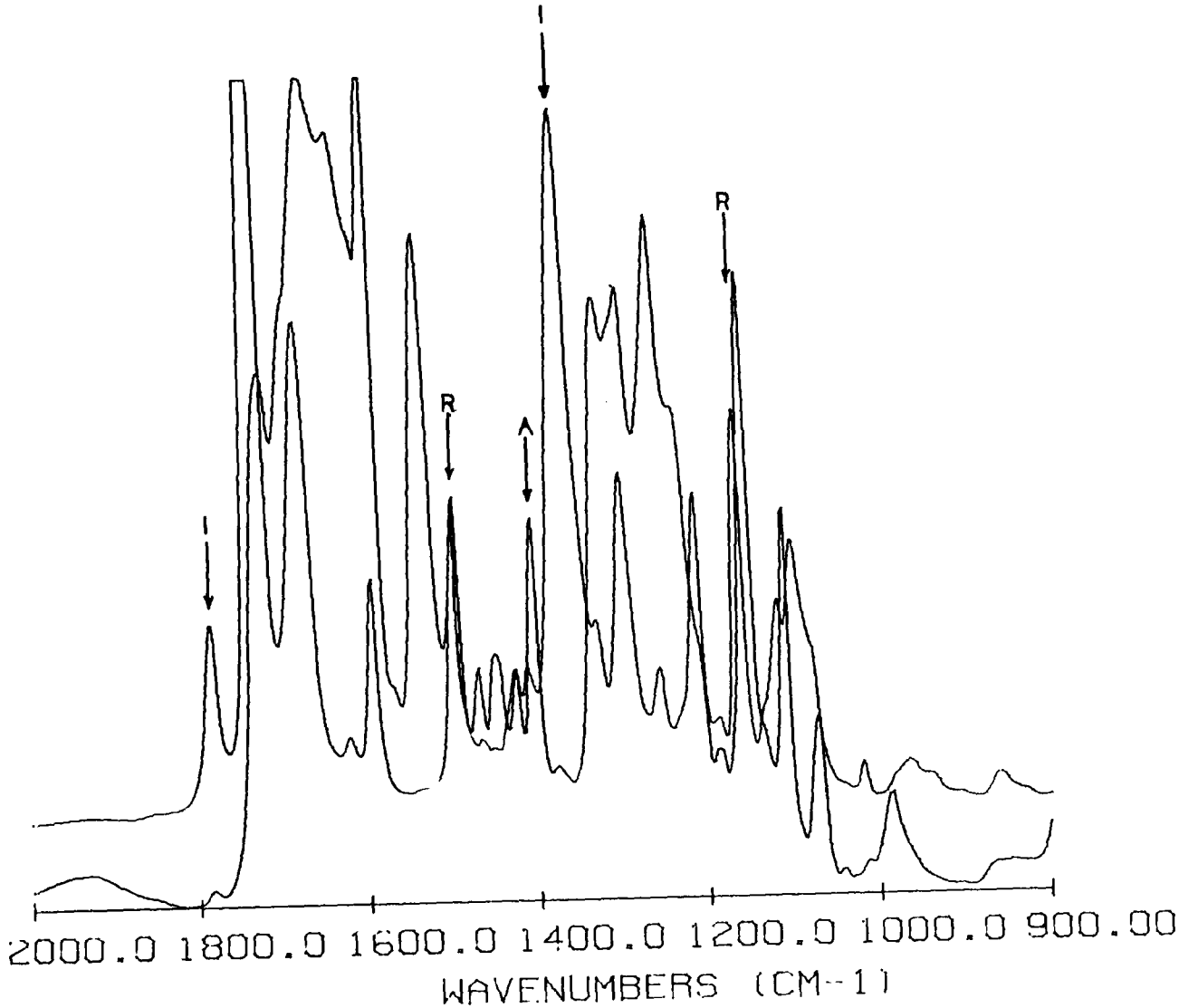

Figure 5-19: FTIR spectra of BTDA/pDDS poly(amic acid) reaction mixture before imidization and after it is 90% imidized thermally in an oven

Table 5-10: Useful peaks in the FTIR spectra of BTDA/pDDS based poly(amic acid) for studying the kinetics of imidization

FTIR peak, wavenumbers	description of the peak
1781.3-1783.1	imide peak
1495.8-1497.0	reference peak due to vibrations of the benzene ring
1403.3-1407.8	amic acid peak
1369.8-1372.3	imide peak, more intense than the peak at 1778
1153.5-1157.4	reference peak due to vibrations of the sulfone group

1156±2.5 wavenumbers were used to determine the extent of reaction, because the baseline was very well defined for these peaks.

Figure 5-20 is a plot of reaction rate versus time for thermal solution imidization of BTDA/pDDS based poly(amic acid) at 140 degrees centigrade. The rate constant for the imidization of BTDA/pDDS based poly(amic acid) was 2.6×10^{-5} per second at 140 degrees centigrade with an excellent correlation coefficient. The temperature-time profiles for the imidization of poly(amic acid) with continuous microwave radiation without agitation, slow agitation, and fast agitation are displayed in Figures 5-21a, 5-21b, and 5-21c, respectively. The reaction mixture was heated with microwave energy from room temperature to the desired reaction temperature of 140 degrees centigrade in approximately forty seconds. During the heating period, less than one percent of the poly(amic acid) was imidized, as shown in Figure 5-22. Figure 5-22 is the FTIR spectra of BTDA/pDDS poly(amic acid) immediately after the heating period. Then the temperature was controlled at 140 degrees centigrade for 1200 seconds to within ±2°C, 5±°C, and ±3°C for experiments with no agitation, slow, and fast agitation, respectively, by adjusting the incident microwave power on the sample. For experiments with slow agitation, it was more difficult to control the temperature , because temperature was very sensitive to the level of power. Since the volume of the sample was relatively small (i.e., two cubic centimeters), it was possible to withdraw only one 0.2 milliliter aliquot from the reaction mixture at 1200 seconds for microwave experiments, without changing the solution volume significantly.

Figure 5-23 displays the effect of agitation rate on the normalized conversion at 140 degrees centigrade, after 1200 seconds, and at average microwave power between 40-45 watts. Note that higher microwave power was used, as compared to the experiments in the previous section, to intensify any special effect of microwave

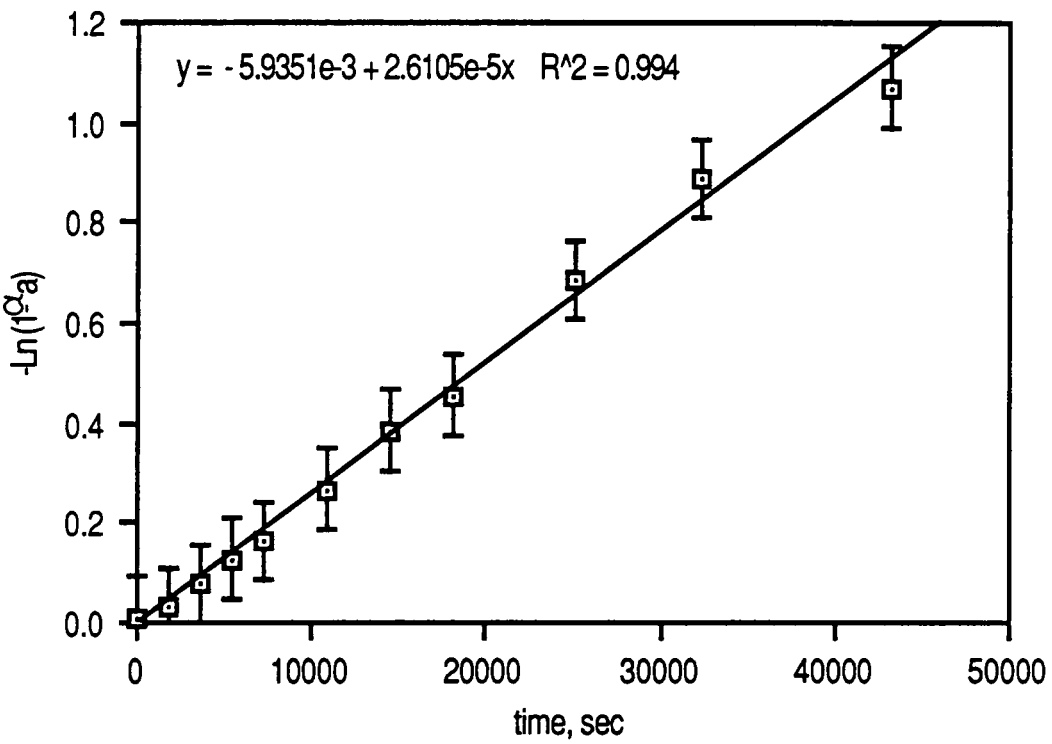

Figure 5-20: Extent of reaction versus time for thermal solution imidization of BTDA/pDDS based poly(amic acid) at 140°C

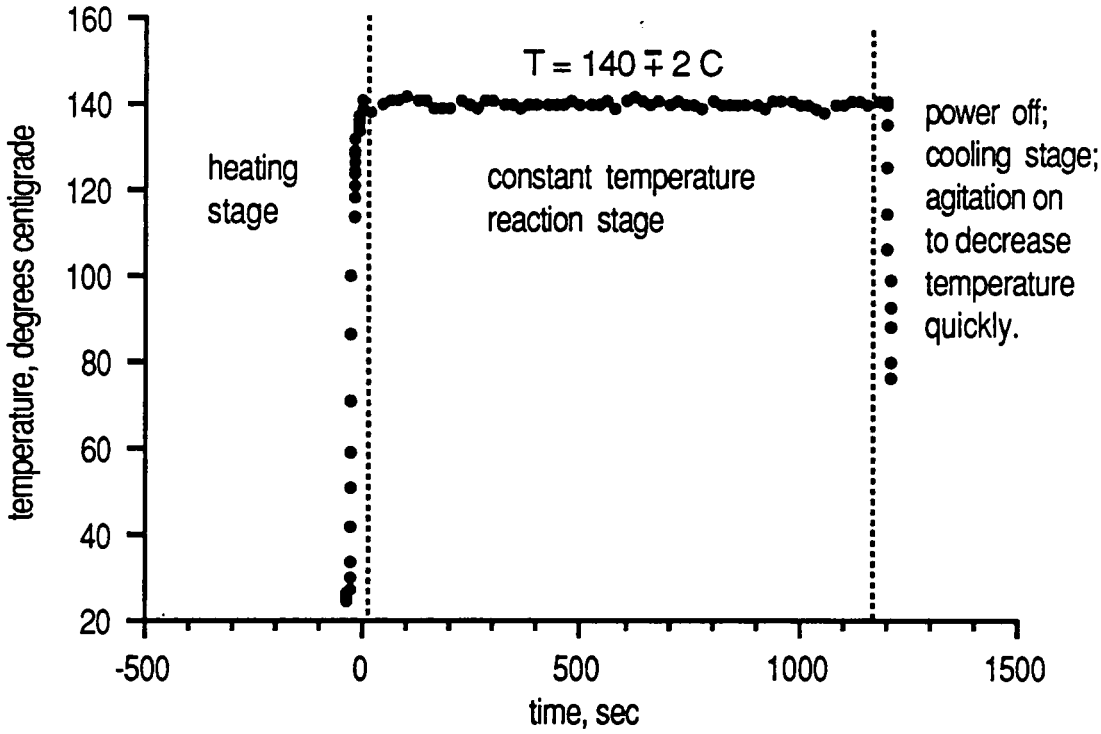

Figure 5-21a: Temperature-time profile for imidization of BTDA/pDDS poly(amic acid) at 140°C with cooling but no agitation

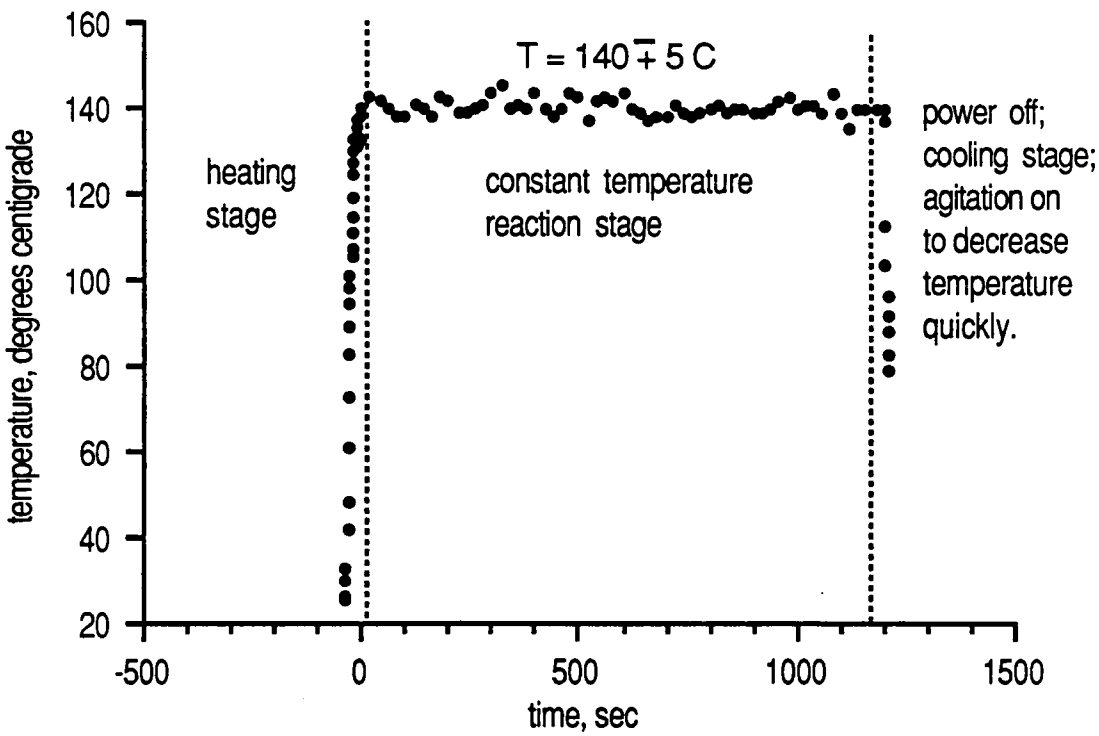

Figure 5-21b: Temperature-time profile for imidizaion of BTDA/pDDS poly(amic acid) at 140°C with cooling but slow agitation

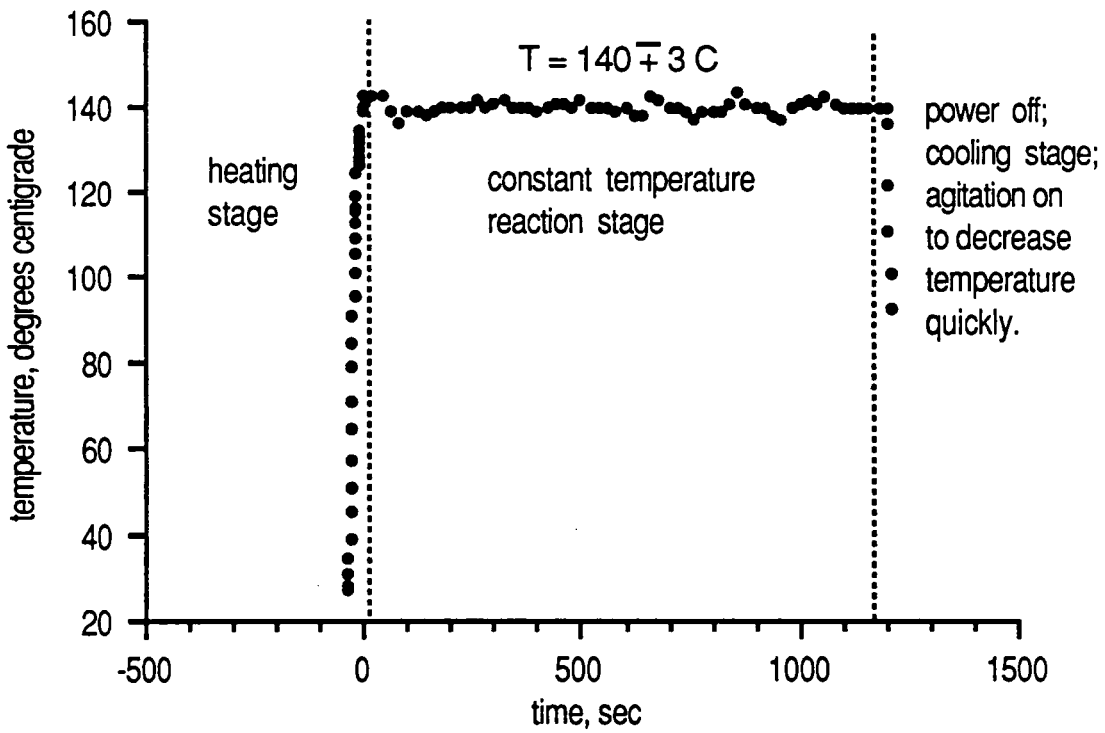

Figure 5-21c: Temperature-time profile for imidizaion of BTDA/pDDS poly(amic acid) at 140°C with cooling and fast agitation

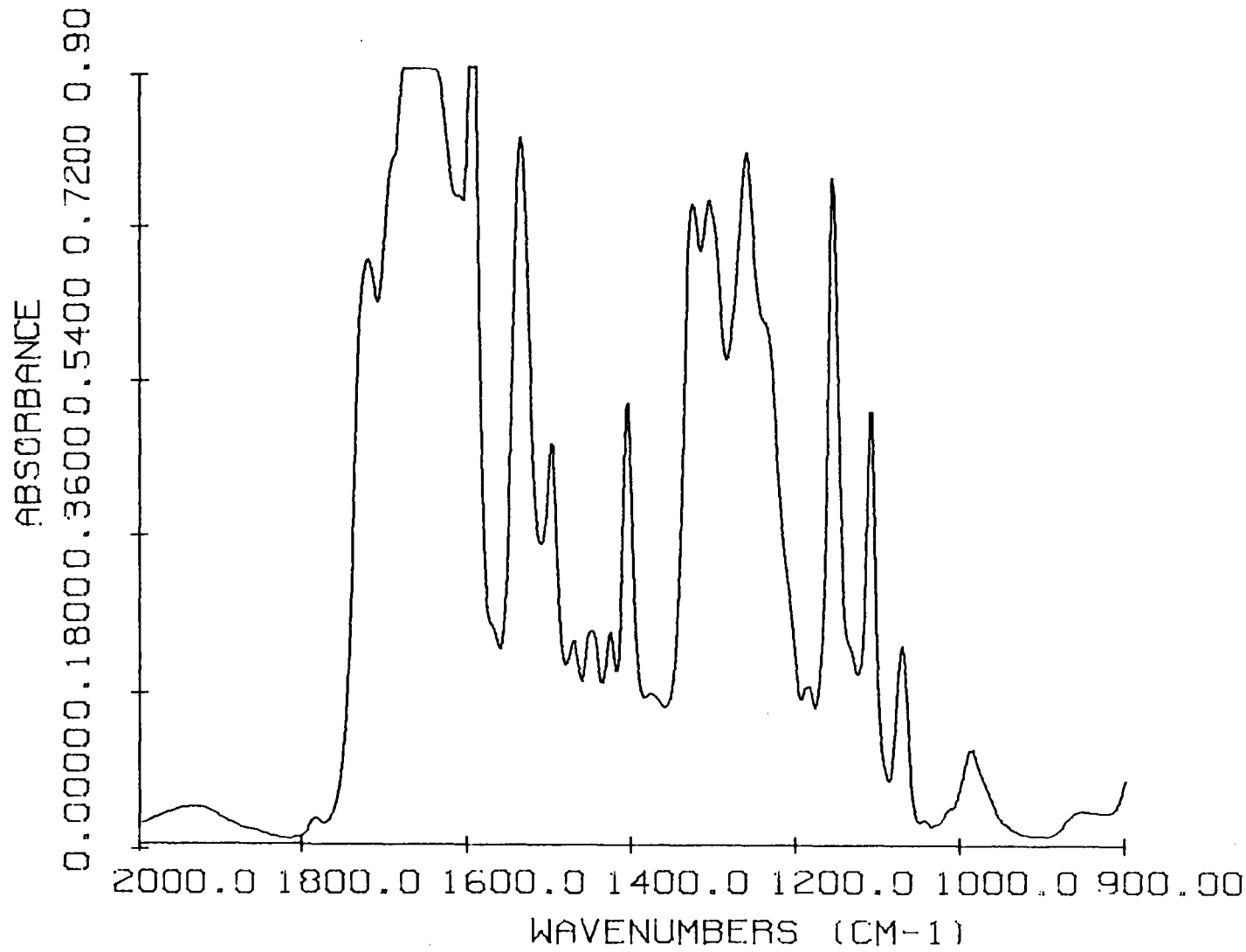

Figure 5-22: FTIR spectra of BTDA/pDDS poly(amic acid) after the heating period

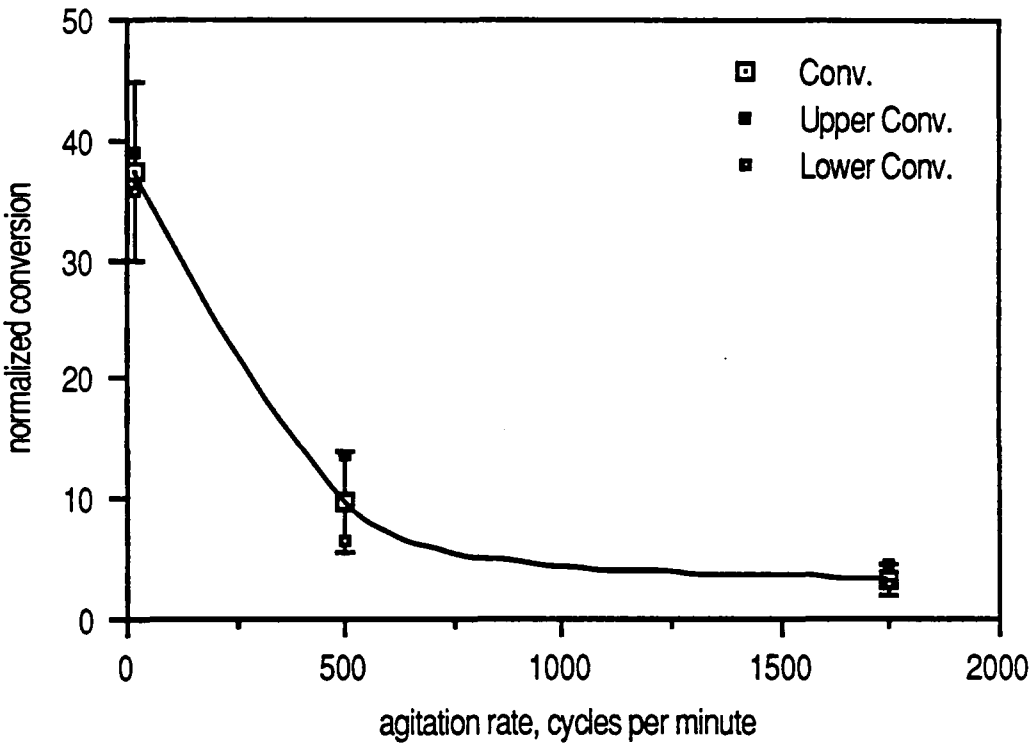

Figure 5-23: Normalized conversion versus agitation rate for BTDA/pDDS poly(amic acid) at 140°C and 40-45 watts

energy. The normalized conversion in Figure 5-23 is defined as conversion with microwave radiation at 140 degrees centigrade after 1200 seconds divided by conversion with thermal solution imidization at 140 degrees after 1200 seconds. The conversion after 1200 seconds with thermal solution imidization was calculated from the rate constant obtained from Figure 5-20. Therefore, the ordinate in Figure 5-23 may be regarded as the enhancement in the rate of imidization with microwave radiation as compared to thermal energy.

According to Figure 5-23, as the agitation rate increased from zero to 1700 cycles per second, the enhancement in the rate of imidization decreased from 39 times faster to three times faster. Therefore, as the agitation rate increased, the microwave conversion approached the thermal solution conversion. The numerical values for conversions in Figure 5-23 are listed in Table 5-11, with their corresponding measurement error. Also, typical FTIR spectrums for imidization of BTDA/pDDS based poly(amic acid), at 140 degrees centigrade, after 1200 seconds, at average power between 40-45 watts, with agitation rate of 1700 Hertz and without agitation are displayed in Figures 5-24a and 5-24b, respectively.

A small volume of the BTDA/pDDS poly(amic acid) sample (e.g., 0.5 milliliter to reduce dimensions of the sample so that temperature gradients are reduced) was imidized with continuous microwave energy at 140 degrees centigrade for 1200 seconds. Figure 5-25 displays the FTIR spectra of this sample after 1200 seconds. The level of microwave energy needed to maintain the sample at 140 degrees was 8-10 watts. The amount of poly(amic acid) imidized after 1200 seconds was 3%, as shown in Figure 5-25, which was the same as thermal solution imidization after 1200 seconds (e.g., 2.5%), within the experimental error which was 6%.

Table 5-11: Conversion for BTDA/pDDS based poly(amic acid) after 1200 seconds at 140 C without agitation and with fast agitation

conversion / experiment	with no agitation		with fast agitation	
	percent conversion	normalized† conversion	percent conversion	normalized† conversion
trial 1	89.2 ± 16.9	36 ± 6.8	7.8 ± 1.5‡	3 ± 0.8
trial 2	97.0 ± 18.4	39 ± 7.4	7.2 ± 1.9	3 ± 0.8
trial 3	——	——	11.4 ± 3.1	4.6 ± 1.2
trial 4	——	——	6.3 ± 1.7	2.5 ± 0.7
average	93.1 ± 18.4	38 ± 7.4	8.2 ± 3.1	3.3 ± 1.2

† Normalized conversion = microwave conversion / thermal conversion

‡ Thermal conversion after 1200 seconds at 140 C = 2.5 %

‡ Error of measurement

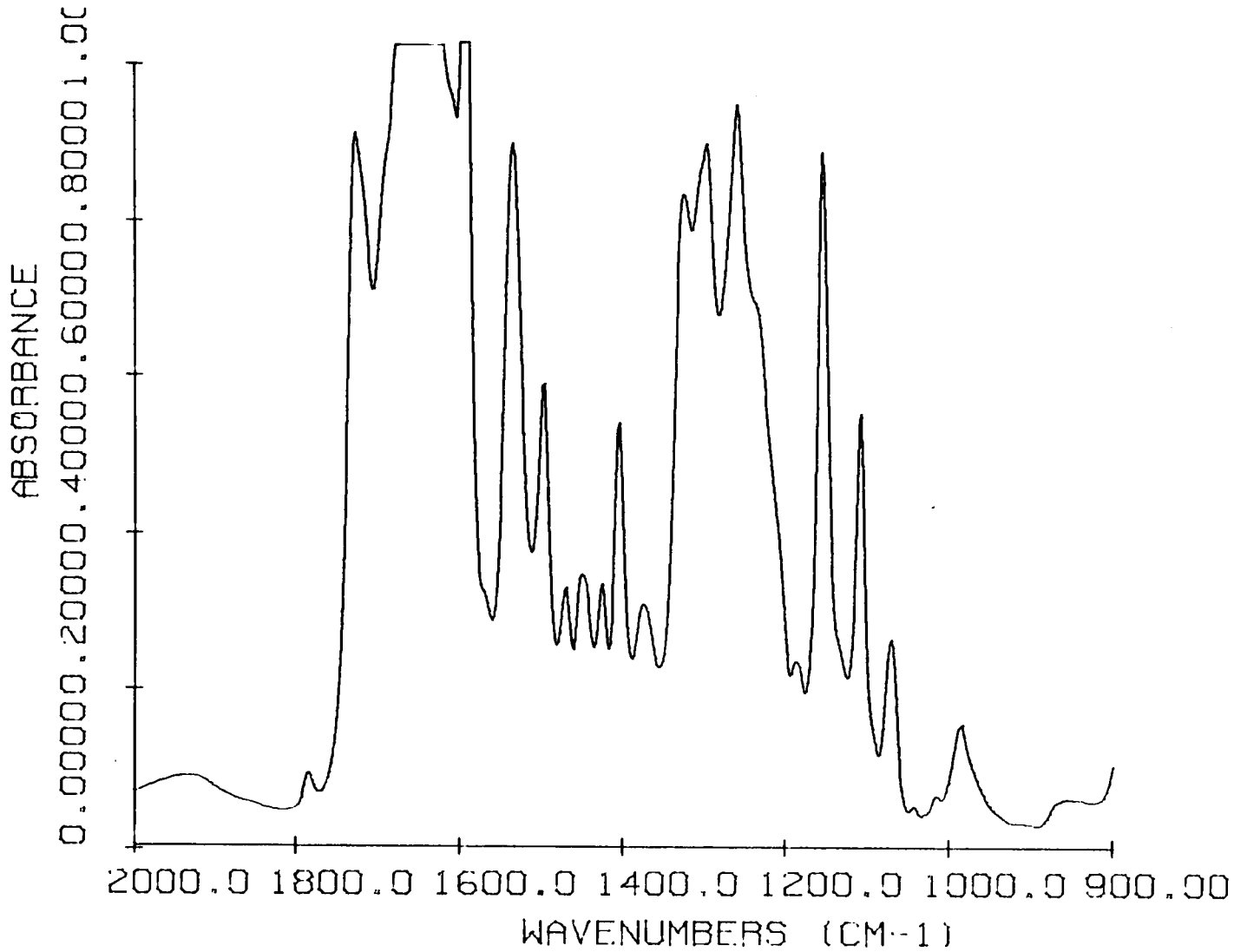

Figure 5-24a: FTIR spectra of BTDA/pDDS poly(amic acid) after 1200 seconds at 140°C, at average microwave power of 40-45 watts, and with fast agitation

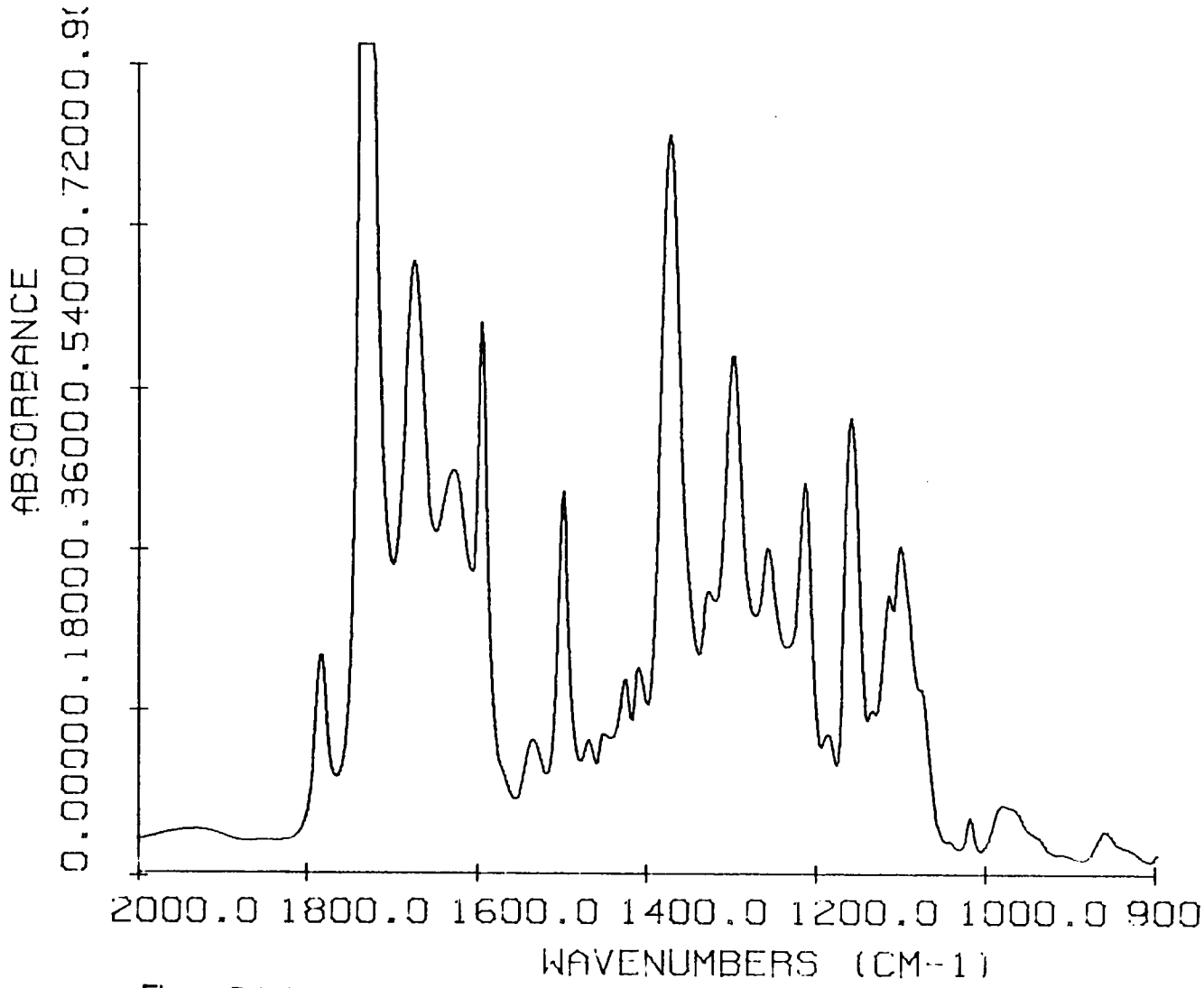

Figure 5-24b: FTIR spectra of BTDA/pDDS poly(amic acid) after 1200 seconds at 140°C, at average microwave power of 40-45 watts, and without agitation

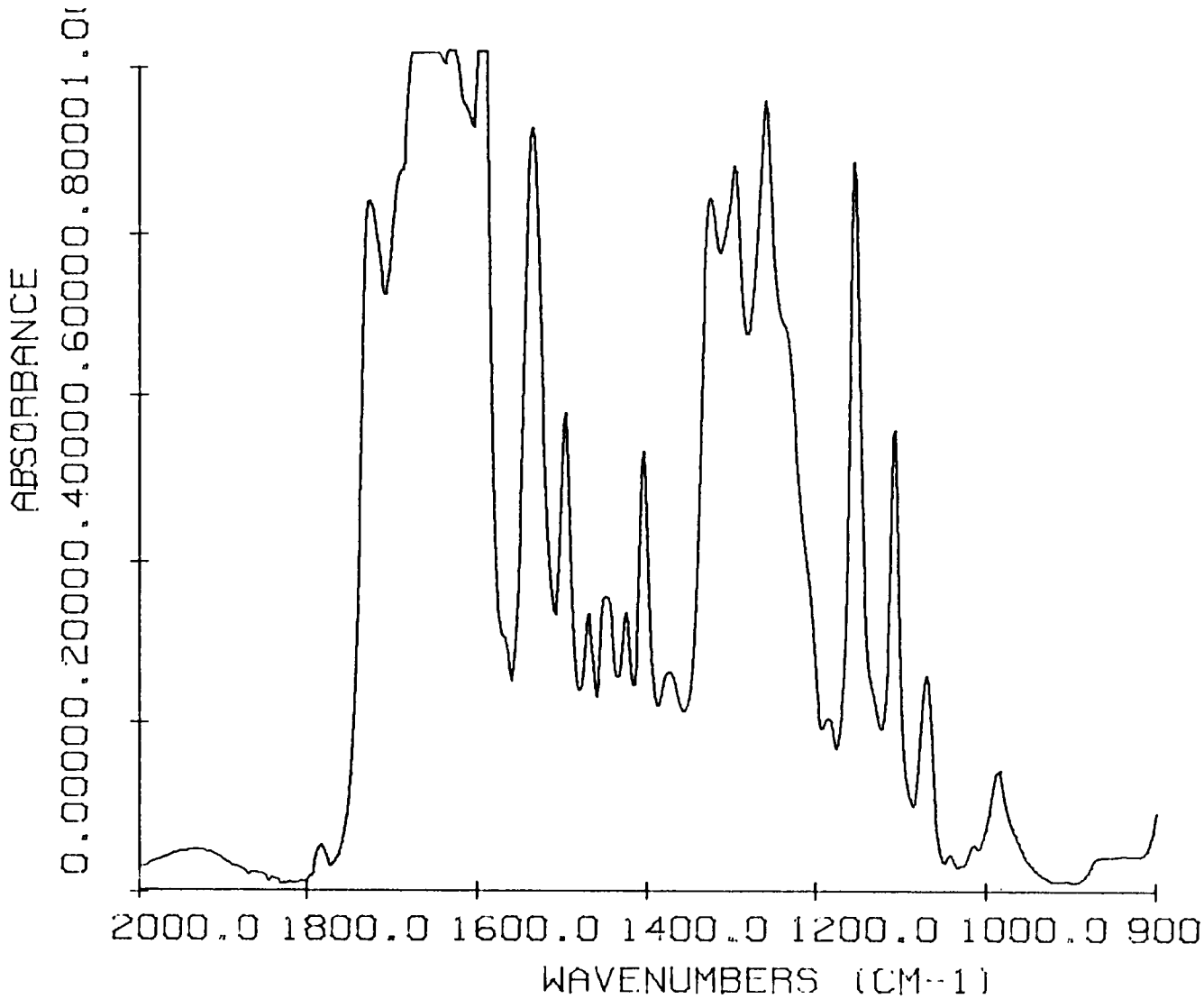

Figure 5-25: FTIR spectra of a 0.5 milliliter BTDA/pDDS poly(amic acid) sample after 1200 seconds at 140°C, at average microwave power of 8-10 watts, and without agitation

To present experimental evidence that there exist temperature gradients in the sample, the heating rate of 1-methyl-2-pyrrolidinone (NMP), which was the solvent for solution imidization of poly(amic acid), was measured at 80 degrees centigrade for two different locations in the cell, using only one temperature probe, as a function of microwave power. Figure 5-27 displays the heating rate of NMP as a function of power for two different locations in the cavity which was determined from the slope of temperature-time profile. The temperature-time profile for 40 watts of microwave power is displayed in Figure 5-26. The two locations in the sample were 0.5 centimeter (e.g., the lower line in Figure 5-27) and three centimeters (e.g., the upper line in Figure 5-27) above the bottom surface of the cavity, respectively.

According to Figure 5-27, at 40 watts of microwave power, the heating rate of NMP at three centimeters above the bottom surface of the cavity was 240 degrees per minute while the heating rate at 0.5 centimeter was 110 degrees per minute. This means if the sample, initially at room temperature (e.g., 25 degrees centigrade), is heated with microwave radiation, the temperature at the top of the cell would be 205 degrees whereas the temperature at the bottom would be 110 degrees centigrade, after 45 seconds at 40 watts. In fact, while we were measuring a temperature of 120 degrees centigrade at the bottom of the cell, the NMP which has a boiling point of 202 degrees centigrade was evaporating at the top. Therefore, there is indeed significant temperature gradients in the axial direction of the sample due to the distribution of microwave power, as predicted theoretically in chapter III.

The data in Figure 5-27 was obtained using one temperature probe positioned at two different locations inside the sample cell. Figure 5-28 displays the temperature-time profile for NMP at two different locations measured by two different probes one at 0.5 centimeter and the other at three centimeters above the bottom surface of the

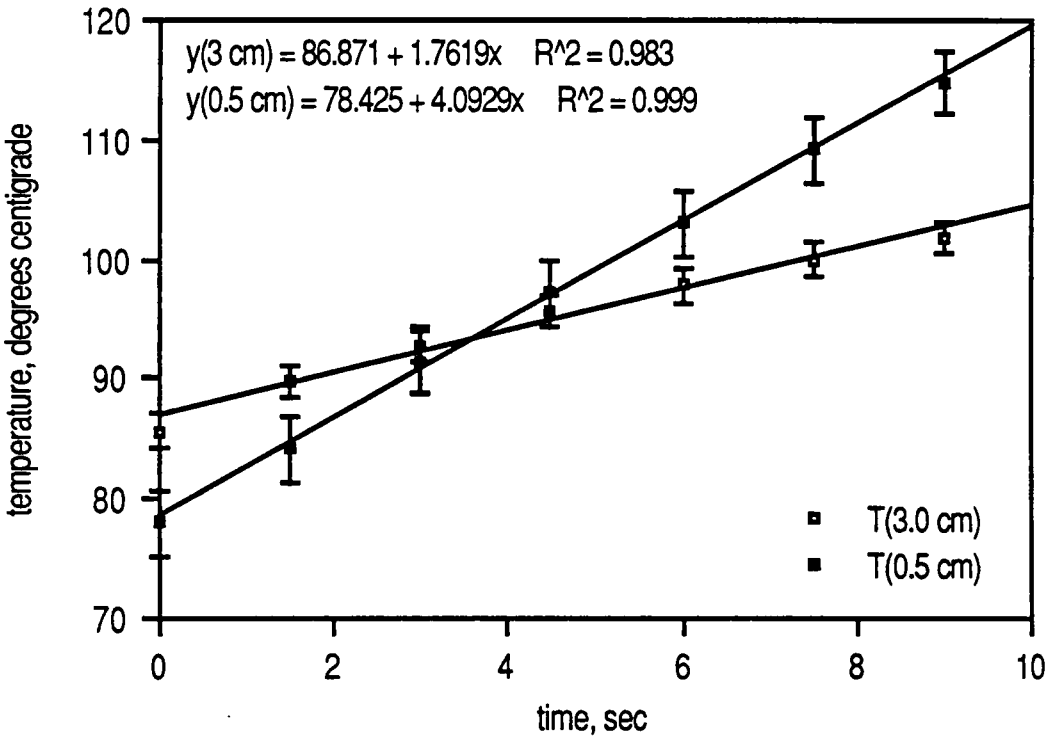

Figure 5-26: Temperature-time profile for NMP at 40 watts and 80°C

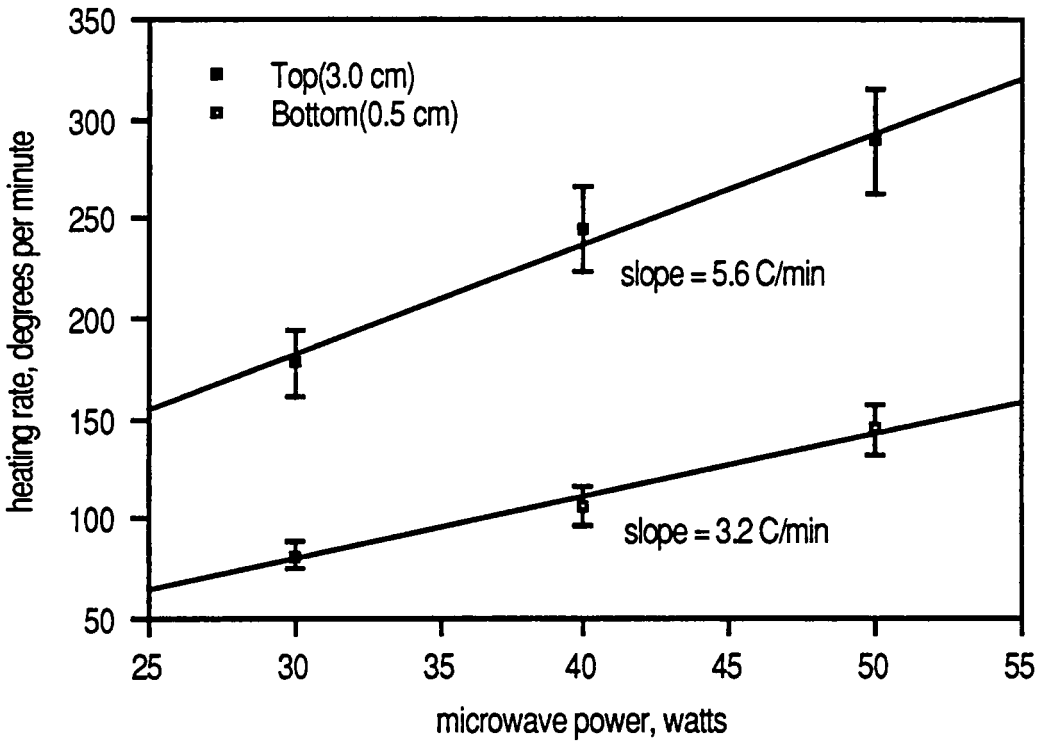

Figure 5-27: Heating rate versus microwave power for NMP at 80°C

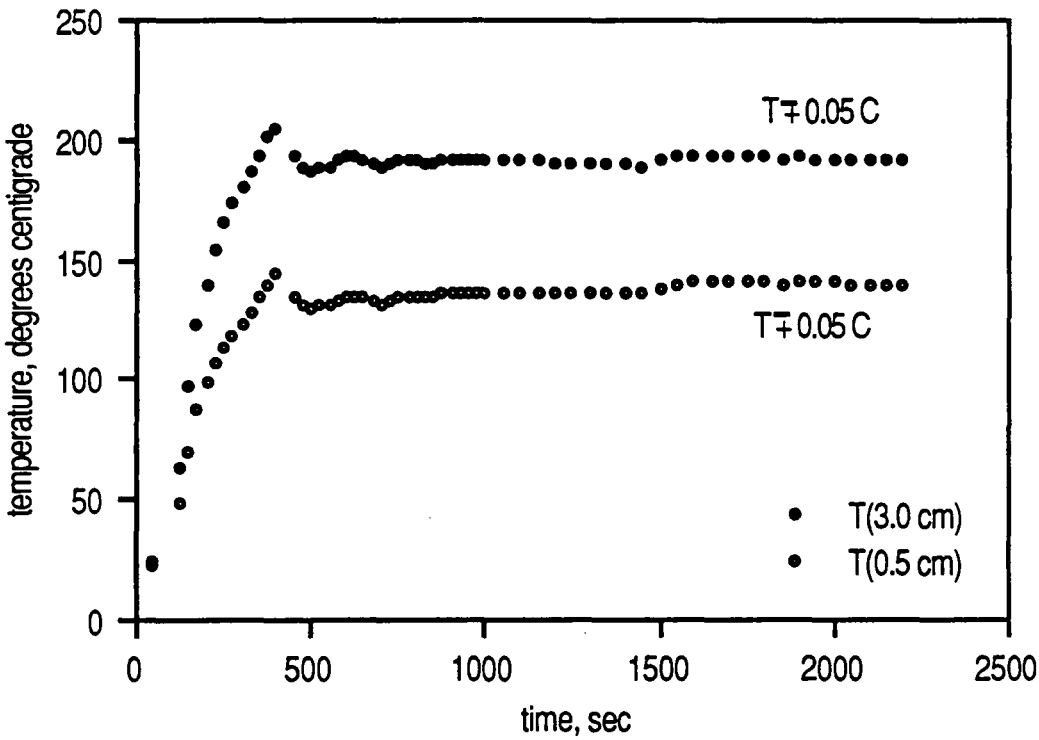

Figure 5-28: Temperature-time profile for NMP at two different locations in the sample cell measured with two probes

cavity. Figure 5-28 indicates that these temperature gradients, along the length of the sample cell, do not equilibrate or do not become uniform even after an extended period of thirty minutes. Also, the non-linearity of heating rate of polymers near their glass transition temperature, predicted theoretically in chapter three, supports our idea that the temperature distribution inside the reaction cell can be highly non-uniform.

Figure 5-29 displays the temperature-time profile for NMP at two different locations measured by two different probes, one at 0.5 centimeter and the other at three centimeters above the bottom surface of the cavity, without and with fast agitation. According to Figure 5-29, the temperature of the two locations in the cell become identical as the solution is agitated, and the solution temperature becomes uniform. As the agitation is terminated, the solution temperature becomes non-uniform again, as displayed in Figure 5-30. Figure 5-31 shows the temperature-time profile for NMP at two different locations and different agitation rates. According to Figure 5-31, temperature gradient for the two locations depends on the rate of agitation. The temperature gradient was 40°C, 22°C, 8°C, 3°C, and 0.5°C for no agitation, slow (100<rate<500 cycles per minute), medium (500<rate<1000), fast (1000<rate<1500), and very fast agitation (1500<rate<2000), respectively.

The results suggest that the kinetics of imidization of poly(amic acids) is identical for thermal energy and microwave radiation, at constant temperature. Also, the enhancement in curing rate observed in samples cured by microwave radiation as opposed to those thermally cured arise from the microwave power distribution in the cavity.

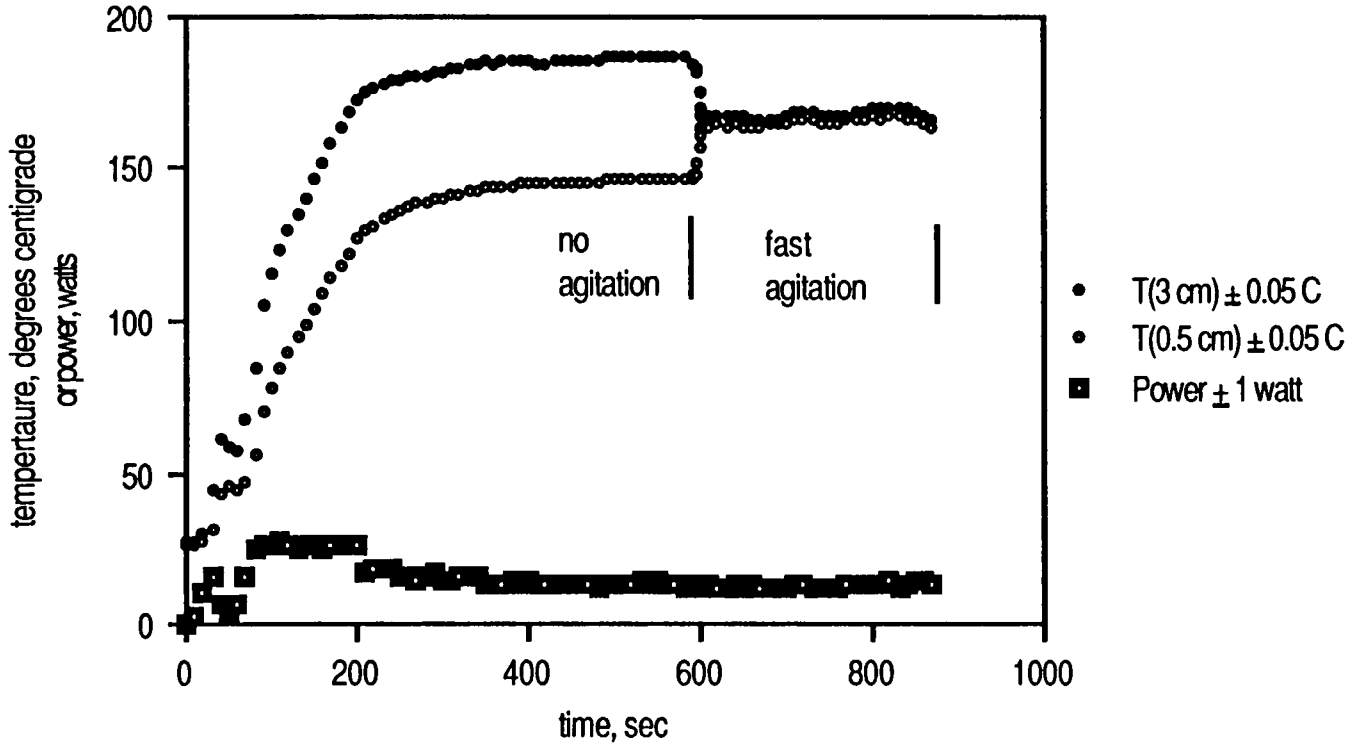

Figure 5-29: Temperature and power-time profile for NMP with fast agitation and no agitation

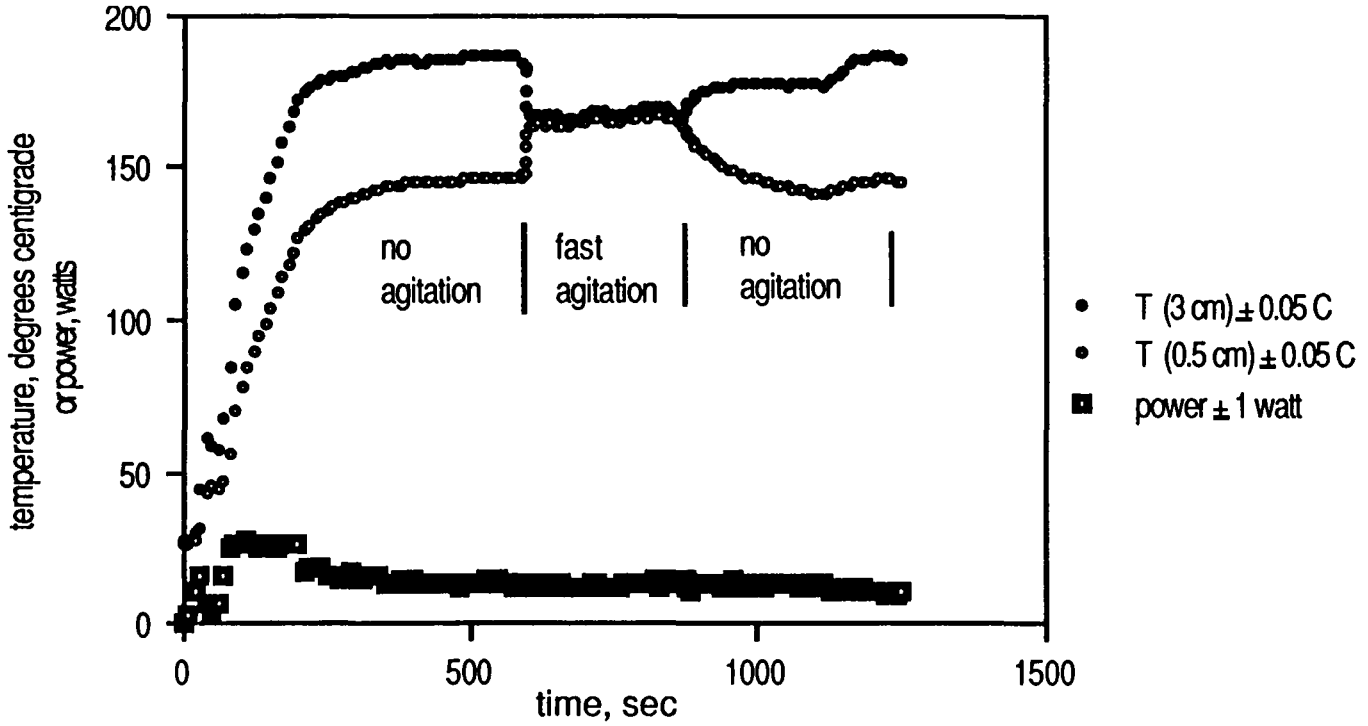

Figure 5-30: Temperature and power-time profile for NMP with fast agitation and no agitation

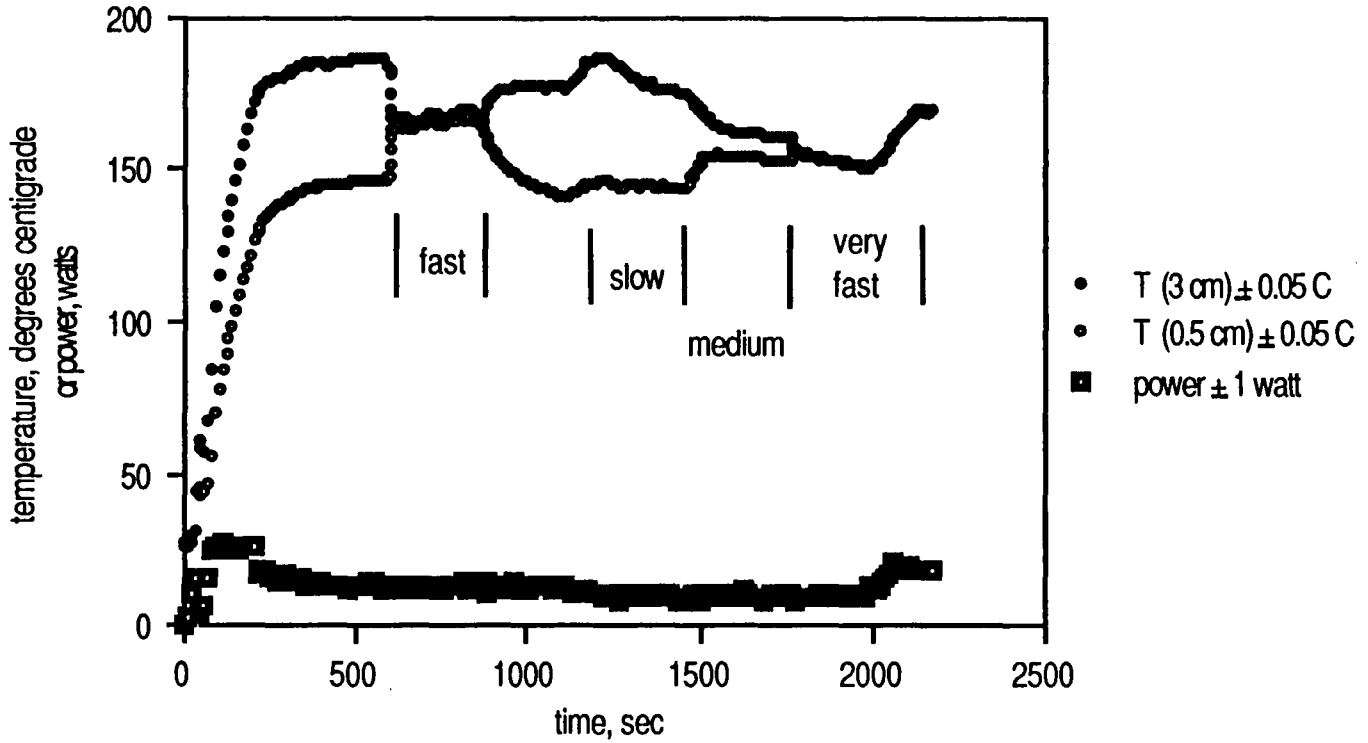

Figure 5-31: Temperature and power-time profile for NMP with slow, medium, fast, and very fast agitation

VI. Conclusions, Recommendations and Future Work

Conclusions:

1) The enhancement in the curing rate of poly(urethanes) with pulse microwave energy, observed by Jullien and co-workers, was due to the increase in heating rate of the polymer with pulse microwave as opposed to continuous wave. Furthermore, the enhancement in the rate of heating with pulse microwave radiation depends on the low frequency absorption spectrum (i.e., less than 10,000 Hertz) of the polymer. According to the results, the heating rate of poly(propylene glycol), which has a low frequency absorption, was enhanced by pulsing the microwave energy, whereas the heating rate of poly(ethylene glycol), which does not have a low frequency absorption, remained the same as compared to continuous wave.

2) The enhancement in the rate of imidization of poly(amic acids) at constant temperature, reported by Lewis et. al., was caused by temperature gradients along the length of the reaction cell and was not due to localized hot spots. This has been confirmed experimentally by agitating the reaction cell to eliminate the temperature gradients. According to the experimental results, as the agitation rate was increased, the rate of imidization of poly(amic acids) with microwave radiation approached the rate of thermal imidization, at constant temperature.

Recommendation:

3) Microwave radiation enhances the heating rate of polymers as compared to conventional thermal heating. Therefore, the use of microwave radiation in applications that require high heating rate is recommended. The

enhancement in the drying rate of wet solids with microwave radiation, the increase in density of ceramic materials sintered with microwave energy, and the variations in morphology observed in microwave cured two phase polymers, are a direct consequence of high heating rate of materials with microwave radiation, as opposed to conventional thermal heating.

Future Work:

4) The other contribution to the enhanced heating rate observed by pulsing the microwave radiation may be due to a more efficient absorption of microwave energy at very high peak microwave power. This hypothesis is depicted schematically in Figure 6-1 which is a plot of heating rate per unit power versus peak microwave power. Curves a,b, and c in Figure 6-1 depict more efficient, no change, and less efficient absorption of microwave energy, respectively, as the power is increased. The effect of peak microwave power on the heating rate of polymeric materials should be investigated in the future.

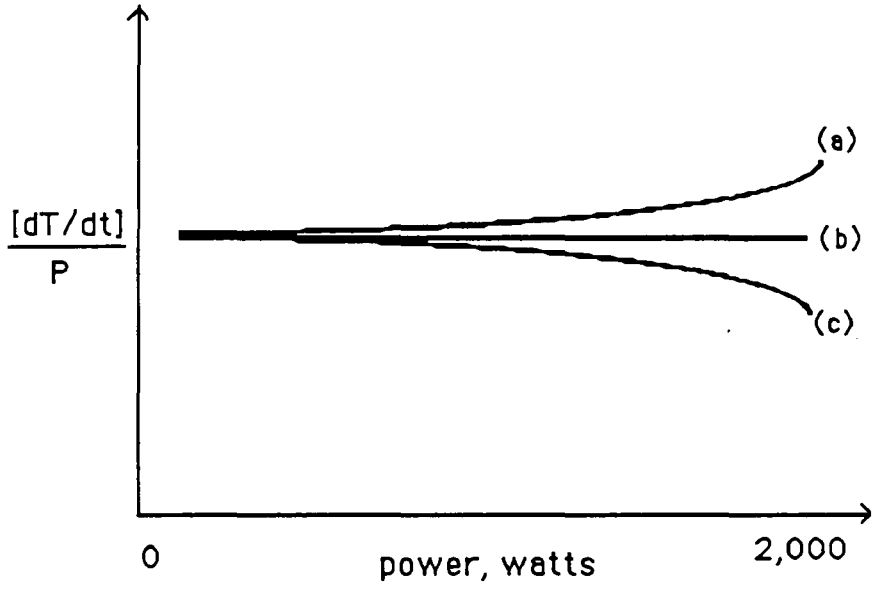

Figure 6-1: An idealized plot of normalized heating rate versus microwave power

VII. References

1. A. Bouazizi and A. Gourdenne, European polymer Journal, 24(9), 1988, pp. 889-893.

2. Y. Baziard and A. Gourdenne, European Polymer Journal, 24(9), 1988, pp. 881-888.

3. Y. Baziard and A. Gourdenne, European Polymer Journal, 24(9), 1988, pp. 873-880.

4. N. Beldjoudi, A. Bouazizi, D. Douibi, and A. Gourdenne, European Polymer Journal, 24(1), 1988, pp. 49-52.

5. N. Beldjoudi and A. Gourdenne, European Polymer Journal, 24(3), 1988, pp. 265-270.

6. N. Beldjoudi and A. Gourdenne, European Polymer Journal, 24(1), 1988, pp. 53-59.

7. J. C. Hedrick, D. A. Lewis, T. C. Ward, and J. E. McGrath, Polym. Prepr., 29(1), 1988, pp. 363-365.

8. D. A. Lewis, T. C. Ward, J. D. Summers, and J. E. McGrath, Polym. Prepr., 29(1), 1988, pp. 174-175.

9. L. M. Sheppard, Ceramic Bulletin, 67(10), 1988, pp. 1656-61.

10. A. L. Bement, Materials And Processing Report, 3(4), 1988, pp. 1-6.

11. Q. Le Van and A. Gourdenne, European Polymer Journal, 23(10), 1987, pp. 777-780.

12. B. Silinski, C. Kuzmycz, and A. Gourdenne, European Polymer Journal, 23(4), 1987, pp. 273-277.

13. A. Gourdenne, D. Le Pen, and D. Doiuibi, Polym. Prepr., 27(2), 1986, pp. 401-402.

14. H. Jullien and H. Valot, Polymer, 26(4), 1985, pp. 506-510.

15. M. Teffal and A. Gourdenne, European Polymer Journal, 19(6), 1983, pp. 543-549.

16. A. Endo, M. Takado, H. Takasao, T. Sugiura, T. Yada, and Y. Onishi, Proc. Electrochem. Soc., 87(4), 1987, pp. 78-91.

17. X. Wu, J. Dong, and M. Tang, Cem. Concr. Res., 17(2), 1987, pp. 205-210.

18. D. A. Lewis, J. C. Hedrick, J. C. McGrath, and T. C. Ward, Polym. Prepr., 28(2), 1987, pp. 330-331.

19. F. M. Thuillier, H. Jullien, and M. F. Grenier-Loustalot, Polym. Commun., 27(7), 1986, pp. 206-208.

20. H. Kimura, F. Teraoka, H. Ohnishi, T. Saito, and M. Yato, J. Osaka. Univ. Dent. Sch., 23, 1983, pp. 43-49.

21. A. Gourdenne, 2nd Proc. Int. Conf. React. Process. Polym., 1982, pp. 23-30.

22. P. Heintz and A. Gourdenne, Proc. Symp. on Macromolecules IUPAC, 28, 1982, p. 486.

23. A. Gourdenne and Q. Le Van, Polym. Prepr., 22(2), 1981, pp. 125-127.

24. A. Gourdenne, A. Maassarani, P. Monchaux, S. Aussudre, and L. Thourel, Polym. Prepr., 20(2), 1979, pp. 471-474.

25. R. H. Kottke, Trans. Am. Foundrymen's Soc., 89, 1981, pp. 251-260.

26. N. S. Strand, Soc. Manuf. Eng., Tech. Pap. Ser., EM79-368, 1979, 14 pp.

27. M. Furuya, Senshoku Kogyo, 28(7), 1980, pp. 346-352.

28. W. A. Smith, Org. Coat. Plast. Chem., 39, 1978, pp. 324-328.

29. J. Ippen, Plastichem, 9, 1979, pp. 93-100.

30. C. L. Lee, ACS Symp. Ser., 107, 1978, pp. 45-50.

31. H. F. Schwarz, R. G. Bosisio, M. R. Wertheimer, and D. Couderc, Rubber Age, 107(11), 1975, pp. 27-38.

32. M. J. Falconer-Flint, Aust. Plast. Rubber, 24(11), 1973, pp. 33-36.

33. H. F. Schwarz, R. G. Bosisio, M. R. Wertheimer, and D. Couderc, J. Microwave Power, 8(4), 1973, pp. 303-322.

34. R. Rajan, J. Cell. Plast., 4(8), 1968, pp. 304-308.

35. R. N. Gedye, F. E. Smith, and K. C. Westaway, Can. J. Chem., 66, 1988, pp. 17-26.

36. R. N. Gedye, F. E. Smith, K. C. westaway, H. Ali, L. Baldisera, L. Laberge, and J. Rousell, Tetrahedron Letters, 27(3), 1986, pp. 279-282.

37. R. J. Giguere, T. L. Bray, and S. M. Duncan, and G. Majetich, Tetrahedron Letters, 27(41), 1986, pp. 4945-4948.

38. F. Smith, B. Cousins, J. Bozic, and W. Flora, Analytica Chimica Acta, 177, 1985, pp. 243-245.

39. J. K. S. Wan, K. Wolf, and R. D. Heyding, "Catalysis on the energy scene," Edited by S. Kaliaguine and K. Mahay, Elsevier, Amsterdam, 1984, p. 561.

40. R. A. Nadkarni, Anal. Chem. 56, 1984, pp. 2233-2237.

41. M. Bacci, M. Bini, A. Checcucci, A. Ignesti, L. Millanta, N. Rubino, and R. Vanni, J. Chem. Soc., Faraday Trans. 1, 77, 1981, pp. 1503-1509.

42. J. Jow, M. C. Hawley, M. C. Finzel, and J. Asmussen, Rev. Sci. Instrum., 60(1), 1989, pp. 96-103.

43. A. C. Metaxas and R. J. Meredith, "Industrial Microwave Heating," Peter Peregrinus Ltd, London, 1988.

44. G. Roussy, J-M Thiebaut, A. Bennani, and N. Mouhab, Journal of Microwave Power and Electromagnetic Energy, 23(1), 1988, pp. 29-37.

45. C. Gibson, I. Matthews, and A. Samuel, Journal of Microwave Power and Electromagnetic Energy, 23(1), 1988, pp. 17-27.

46. D. Kajfez, P. Guillon, H. A. Auda, A. W. Glisson, D. F. Hanson, A. S. Khanna, and K. A. Michalski, "Dielectric Resonators," Edited by D. Kajfez and P. Guillon, Artech House, Inc., 1986.

47. R. F. Harrington, "Time-Harmonic Electromagnetic Fields," McGraw-Hill Book Company, New York, 1961, pp. 321-326.

48. G. Roussy, J-M Theibaut, M. Charreyre-Neel, Journal of Microwave Power, 19(4), 1984, pp. 243-250.

49. C. De Wagter, Journal of Microwave Power, 19(2), 1984, pp. 97-105.

50. W. I. Lee and G. S. Springer, Journal of Composite Materials, 18(7), 1984, pp. 387-409.

51. W. I. Lee and G. S. Springer, Journal of Composite Materials, 18(7), 1984, pp. 357-386.

52. A. C. Loos and G. S. Springer, Journal of Composite Materials, 17(3), 1983, pp. 135-168.

53. W. I. Lee, A. C. Loos, and G. S. Springer, Journal of Composite Materials, 16(11), 1982, pp. 510-520.

54. G. S. Springer, Journal of Composite Materials, 16(9), 1982, pp. 400-410.

55. A. D. Cross, P. L. Jones, and J. Lawton, Trans. IChemE., 60, 1982, pp. 67-74.

56. A. D. Cross, P. L. Jones, and J. Lawton, Trans. IChemE., 60, 1982, pp. 75-78.

57. R. E. Haven, Ph. D. Thesis, Massachusetts Institute of Technology, 1980.

58. Y. Baziard, S. Breton, S. Toutain, and A. Gourdenne, Eur. Polym. J., 24(7), 1988, pp. 633-638.

59. Y. Baziard, S. Breton, S. Toutain, and A. Gourdenne, Eur. Polym. J., 24(6), 1988, pp. 521-6.

60. F. Legros, A. Fourrier-Lamer, D. Le Pen, and A. Gourdenne, Eur. Polym. J., 22(4), 1986, pp. 335-339.

61. F. Legros, A. Fourrier-Lamer, D. Le Pen, and A. Gourdenne, Eur. Polym. J., 22(4), 1986, pp. 331-334.

62. F. Legros, A. Fourrier-Lamer, D. Le Pen, and A. Gourdenne, Eur. Polym. J., 20(11), 1984, pp. 1057-59.

63. A. J. Bar, Polymer, 26(7), 1985, pp. 963-77.

64. P. C. Bandyopadhyay, T. K. Chaki, S. Srivastava, and G. S. Sanyal, Polymer Engineering and Science, 20(6), 1980, pp. 441-446.

65. R. D. McCammon, R. G. Saba, and R. N. Work, Journal of Polymer Science: Part A-2, 7, 1969, pp. 1721-1733.

66. V. Frosini, E. Butta, and M. Calamia, Journal of Applied polymer Science, 11, 1967, pp. 527-551.

67. J. D. Hoffman, G. Williams, and E. Passaglia, Journal of Polymer Science: Part C, 14, 1966, pp. 173-235.

68. N. Saito, K. Okano, S. Iwayanagi, and T. Hideshima, "Molecular Motion in Solid State Polymers," in 'Solid State Physics,' Academic Press, New York, 14, 1963, pp. 343-502.

69. P. Hedvig, "Dieclectric Spectroscopy of Polymers," John Wiley & Sons, Inc., 1977, Chapter 2.

70. P. Hedvig, "Dieclectric Spectroscopy of Polymers," John Wiley & Sons, Inc., 1977, Chapter 1.

71. R. J. Meakins, "Mechanisms of Dielectric Absorption in Solids," in 'Progress in Dielectrics,' John Wiley & Sons, Inc., 3, 1961, pp. 151-202.

72. J. J. O'Dwyer and E. Harting, "Theories of Dielectric Loss," in 'Progress in Dielectrics,' John Wiley & Sons, Inc, 7(1), 1967, pp. 1-44.

73. K. S. Cole and R. H. Cole, Journal of Chemical Physics, 9(4), 1941, pp. 341-351.

74. R. M. Fuoss and J. G. Kirkwood, Journal of the American Chemical Society, 63(2), 1941, pp. 385-394.

75. G. Williams, Chemical Reviews, 72(1), 1972, pp. 55-69.

76. A. C. Lynch, Proc. IEE, 118(1), 1971, pp. 244-246.

77. J. D. Hoffman and H. G. Pfeiffer, Journal of Chemical Physics, 22(1), 1954, pp. 132-141.

78. J. D. Hoffman, Journal of Chemical Physics, 23(7), 1955, pp. 1331-1339.

79. R. H. Boyd and S. M. Breitling, Macromolecules, 7(6), 1974, pp. 855-862.

80. E.M. Amrhein, "The Vibrational Spectrum of Noncrystalline Solids," in 'Annals of the New York Academy of Sciences,' 196, 1972, pp. 179-194.

81. E. M. Amrhein and H. W. Schulze, Kolloid Z. Z. Polym., 250, 1972, pp. 921-926.

82. A. R. von Hippel, "Dielectric Materials and Applications," The Technology Press of M. I. T. and John Wiley & Sons, Inc., 1954, pp. 294-370.

83. J. D. Summers, Ph. D. thesis, Virginia Polytechnique Institute & S. U., 1988.

84. H. Ishida, S. T. wellinghoff, E. Baer, and J. L. Koenig, Macromolecules, 13, 1980, pp. 826-834.

85. C. E. Sroog, "Polyimides," in 'Journal of Polymer Science: Macromolecular Reviews,' 11, 1976, pp. 161-208.

86. C. S. Marvel, J. Macromol. Sci.- Revs. Macromol. Chem., C13(2), 1975, pp. 219-233.

87. R. A. Dine-Hart and W. W. Wright, Die Makromolekulare Chemie, 143, 1971, pp. 189-206.

88. J. A. Kreuz, A. L. Endrey, F. P. Gay, and C. E. Sroog, Journal of Polymer Science: Part A-1, 4, 1966, pp. 2607-2616.

89. N. L. Alpert, W. E. Keiser, and H. A. Szymonski, "IR-Theory and Practice of Infrared Spectroscopy," Plenum Press, New York, 1970, pp. 303-321.

90. J. E. Mark and D. S. Chiu, Journal of Chemical Physics, 66(5), 1977, pp. 1901-1904.

91. A. Abe and J. E. Mark, Journal of the American Chemical Society, 98(21), 1976, pp.

92. J. E. Mark, Accounts Chem. Res., 7(7), 1974, pp. 218-225.

93. K. Bak, G. Elefante, and J. E. Mark, Journal of Physical Chemistry, 71(12), 1967, pp. 4007-4011.

94. M. E. Baur and W. H. Stockmayer, Journal of Chemical Physics, 43(12), 1965, pp. 4319-4325.

95. T. Uchida, Y. Kurita, and N. Koizumi, Journal of Polymer Science, 21, 1956, pp. 313-321.

96. J. Jow, M. E. Hawley, M. C. Finzel, J. Asmussen, H. H. Lin, and B. Manring, IEEE Transactions on Microwave Theory and Techniques, MTT-35(12), 1987, pp. 1435-43.

97. J. Asmussen, H. H. Lin, B. Manring, and R. Fritz, Rev. Sci. Instrum., 58(8), 1987, pp. 1477-86.

98. J. J. Aklonis and W. J. McKnight, "Introduction to Polymer Viscoelasticity," John Wiley & Sons, 2 ed., 1983, pp. 47-52.

99. M. J. Brekner and C. Feger, J. Polymer Sci: Polym. Chem. Ed., 25, 1987, p. 2005.

100. Luxtron, "The Operator's Guide: Model 750 Fluoroptic Thermometry System," 1986.

101. Epsco, Inc., "Operation and Maintenance Manual: High Power Pulsed Signal Source PG5KB," 1987.

102. Hewlett-Packard Co., "HP Catalog: Measurement, Computation, Systems," 1986, pp. 558-59, 564, 580-81.

103. Narda Microwave Corporation, "Catalog 24," 1986, pp. 142-43.

104. Weinschel Engineering Co., Inc., "Attenuators and Components," 1985.

105. Savillex Corporation, 5325 Hwy 101, Minnetonka, MI, 55343,U. S. A.

106. A. R. Von Hippel, "Dielectrics and Waves," John Wiley & Sons, New York, 1954.

107. C. R. Vail, Electro-Technology Sci. and Eng. Series, No. 38, 1962, pp. 82-98.

108. Nicolet Instrument Corp., "MX-1 FTIR Spectrometer: Operating Manual," 1980.

109. R. H. Perry and C. H. Chilton, "Chemical Engineers' Handbook," McGraw-Hill Book Company, 5th Ed., p. 10-11.

110. R. C. Weast and M. J. Astle, "Handbook of Chemistry and Physics," 63ed Ed., 1982, p. D-179, E-10, F-3.

Appendix 1

a) Estimation of rate of temperature change by conduction

The rate of temperature change by conduction is given by the following equation [109]:

$$(dT/dt)_{cond} = Q/\rho C_p = [K\,\Delta T\,A] / [\Delta L\,\rho\,C_p] \qquad \text{(A-1)}$$

Where Q=rate of heat transfer

C_p=heat capacity of the liquid= 1 Cal/gr °C

ρ=density of the liquid= 1 gr/cm^3

K=conductivity of the liquid= 3×10^{-4} Cal/sec cm °K

A=cross sectional area of the sample cell= 2 cm^2

ΔL=length of the sample= 1 cm

ΔT=temperature difference along the length of the sample= 100°K

The values given above are for liquid water at room temperature from reference [110].

Substitution of these values in Equation A-1 results in the following:

$$(dT/dt)_{cond} = 1.8\ °C/min.$$

b) Estimation of rate of temperature change by convection

The rate of temperature change by convection is given by the following equation [109]:

$$(dT/dt)_{conv} = [h\,A_s\,\Delta T] / [\rho\,C_p] \qquad \text{(A-2)}$$

Where h=convection heat transfer coefficient= 2.0 Btu/hr ft^2 °F

A_s=surface area of the sample cell= 10 cm^2

ΔT=temperature difference between the sample cell and the surrounding= 150°C

ρ=density of the sample= 1 gr/cm^3

C_p=heat capacity of the sample= 1 cal/gr°C

The values given above are for liquid water at room temperature from references [109] and [110]. Substitution of these values in Equation A-2 results in the following:

$$(dT/dt)_{conv} = 3.5\ °C/min$$

Appendix 2

The maximum uncertainty for a dependent variable due to measurement error of some independent variables is given by the following equation:

$$\Delta F = | (\partial F/\partial A)\Delta A | + | (\partial F/\partial B)\Delta B | + | (\partial F/\partial C)\Delta C | + \ldots \qquad \text{(A-3)}$$

In Equation A-3, F is the dependent variable and A, B, and C are the independent or the measured variables.

a) Heating rate studies

For heating rate studies, the dependent variable is the heating rate and the measured variables are temperature, time, and the level of microwave power. The uncertainty in heating rate is given by the following equation:

$$|\Delta F_T| = 2|\Delta T/T| + 2|\Delta t/t| + |\Delta P_I/(P_I - P_R)| + |\Delta P_R/(P_I - P_R)| \qquad \text{(A-4)}$$

Where $F_T=(dT/dt)$ and ΔF_T is the error in heating rate
T=temperature and ΔT is the error in temperature measurement
t=time and Δt is the error in time measurement
P_I=incident power and ΔP_I is the error in incident power
P_R=reflected power and ΔP_R is the error in reflected power

The measurement errors for each variable are given in section 4.8. The error bars for heating rate studies are calculated according to Equation A-4.

b) Kinetic studies

For kinetic studies, the reaction rate constant is the dependent variable and temperature, time, and absorbance values are the measured variables. The uncertainty in the reaction rate constant is given by the following equation:

$$|\Delta K/K| = 4|F(\alpha)\ \Delta A_I/A_I| + |\Delta t/t| + |\Delta E\ \Delta T/RT^2| \qquad \text{(A-5)}$$

Where $F(\alpha) = \alpha / (1-\alpha)\ \mathrm{Ln}(1-\alpha)$

K=reaction rate constant and ΔK is the error

α=conversion at time t

A_I=absorbance of the imide group and ΔA_I is the error

ΔE=activation energy for the reaction

R=gas constant

The measurement error for each variable is given in section 4.8. The error bars for the kinetic studies are calculated according to Equation A-5.

The vita has been removed from the scanned document